2019

Growth of Two-Dimensional Molybdenum Disulfide via Chemical Vapor Deposition

Zachary Durnell Ganger
Wright State University

GROWTH OF TWO-DIMENSIONAL MOLYBDENUM DISULFIDE VIA CHEMICAL VAPOR DEPOSITION

A thesis submitted in partial fulfillment of the
requirements for the degree of
Master of Science in Materials Science and Engineering

By

ZACHARY DURNELL GANGER
B.S.M.S.E. Wright State University, 2015

2019
Wright State University

WRIGHT STATE UNIVERSITY

GRADUATE SCHOOL March 28th, 2019

I HEREBY RECOMMEND THAT THE THESIS PREPARED UNDER MY SUPERVISION BY Zachary Durnell Ganger ENTITLED Growth of Two Dimensional Molybdenum Disulfide via Chemical Vapor Deposition BE ACCEPTED IN PARTIAL FULFILLMENT OF THE REQUIREMENTS FOR THE DEGREE OF Master of Science in Materials Science and Engineering.

Committee on Final Examination

_____

Hong Huang, Ph.D.
Thesis Director

_____

Hong Huang, Ph.D.

_____

Joseph C. Slater, Ph.D., P.E.
Chair, Department of Mechanical and Materials Engineering

_____

Yan Zhuang, Ph.D.

_____

Shin Mou, Ph.D.

_____

Barry Milligan, Ph.D.

Interim Dean of the Graduate School

ABSTRACT

Ganger, Zachary Durnell. M.S.M.S.E., Department of Mechanical and Materials Engineering, Wright State University, 2019. Growth of Two-Dimensional Molybdenum Disulfide via Chemical Vapor Deposition.

Graphene has successfully been a 2D material applied in various fields, but it is not the most appropriate candidate for many electronic devices unless its bandgap structure is tuned through functionalization. Among all other 2D material families, transition metal dichalcogenides (TMDs), represented by molybdenum disulfide (MoS_2), are promising and emerging in power electronics due to their large direct bandgap and other electronic properties. 2D MoS_2 has been fabricated through different approaches such as mechanical exfoliation, chemical etching, and chemical vapor deposition (CVD). The current major challenge in fabricating 2D MoS_2 films is to produce a high-quality large-area monolayer film at a controlled condition.

This thesis study is to grow 2D MoS_2 films by CVD method at various experimental settings and to characterize the size, thickness, and morphology of the films, towards finding an optimal processing condition. Experimental settings for the growth parameters include the precursor amounts and placements, growth time, growth temperature, carrier gas flow rate, substrates, and seeding promoters. The growth films are characterized with the help of optical microscopy, Raman spectroscopy, scanning electron microscopy (SEM), energy dispersive spectroscopy (EDS), and atomic force microscopy (AFM). It is found that 1) MoS_2 growth is sensitive to the carrier flow rate and temperature; and 2) 2D MoS_2 grain size and areal coverage are correlated with grow time as well as the distance from the promoter PTAS (perylene-3,4,9,10-tetracarboxylic acid tetrapotassium salt) resource. Existence of monolayer MoS_2, in the presence of PTAS promotor, is

confirmed with Raman Spectroscopy and AFM. Multilayer MoS_2 films with grains up to several hundreds of micrometers, confirmed with optical microscopy, SEM and Raman, are successfully grown on clean Si/SiO_2 substrate in the presence of PTAS promotor vapor in the vicinity. Growth of monolayer/multilayer MoS_2 on sapphire and graphene was also demonstrated.

TABLE OF CONTENTS

1 INTRODUCTION AND BACKGROUND 1

1.1 Motivation 1

1.2 Different Kinds of 2D Semiconducting Materials 3

1.2.1 First Generation 2D Materials - Graphene 3

1.2.2 Second Generation 2D Materials 5

1.2.3 Third Generation 2D Materials 9

1.3 2D TMDs and Their Emerging Applications 16

1.3.1 Overview of 2D TMDs 16

1.3.2 Structure and Properties of 2D MoS_2 17

1.3.3 Fabrication of 2D MoS_2 20

1.4 Research Objectives and Outline of this Thesis 24

2 CURRENT RESEARCH ON CHEMICAL VAPOR DEPOSITION OF 2D MOLYBDENUM DISULFIDE 26

3 EXPERIMENTAL ASPECTS OF THIS STUDY 44

3.1 CVD Growth 44

3.1.1 The CVD Setup 44

3.1.2 Growth Procedures 44

3.2 Growth Variables 46

3.2.1 Position of Precursors 46

3.2.2 Growth Time 47

3.2.3 Carrier Gas Flow Rate 47

3.2.4 Quench Temperature……...……...47

3.2.5 Substrate……...……..47

3.2.6 Substrate Surface Treatments…...……..48

3.2.7 PTAS Promotors……...…….…….49

3.3 Characterizations 50

3.3.1 Optical Imaging and ImageJ Quantification Analysis.....50

3.3.2 Scanning Electron Microscopy and Energy Dispersive X-Ray Spectroscopy 51

3.3.3 Atomic Force Microscopy.....52

3.3.4 Raman Spectroscopy.....53

4 RESULTS AND DISCUSSION..... 58

4.1 Preliminary Optimization 58

4.1.1 Processing Settings.....58

4.1.2 Sulfur Position……60

4.1.3 MoO_3 Position ……61

4.1.4 Substrate……..62

4.2 Surface Treatments on Sapphire Substrate 62

4.3 With PTAS Applied via Thermal Drying..... 67

4.3.1 Drying Temperature 67

4.3.2 Surface Treatment 68

4.4 With PTAS Applied via Spraying 69

4.4.1 Graphene Substrate with PTAS…..71

4.5 PTAS Seeding Promoter on Separate Upstream Substrate..... 73

4.5.1 Varying Amounts of PTAS.……...……...74

4.5.2 Varying Carrier Gas Flow Rate…….80

4.5.3 Varying Growth Time……81

4.6 Quantitative Analysis……...84

5 CONCLUSION 87

6 BIBLIOGRAPHY 89

LIST OF FIGURES

Figure 1: Graphene flake and atomic sketch [3] *4*

Figure 2: (a) α-, β-, and γ- graphyne, (b) graphdiyne, and (c) f extended graph-n-yne by acetylenic carbon chain length [8] *7*

Figure 3: Graphene (1) and graphene allotropes pentaheptites (2-3), haeckelites (4), graphynes (5-6), 4:8 net (7)[10], C4 squares and C10 decagons (8), distorted hexagons (9) supergraphene (10), polycyclic network of C3 and C12 (11) and squarographenes (12- 13'): [9] *8*

Figure 4: (a) Silicene and (b) Germanene two-dimensional structures. [13] Stanene - two sublattices of tin on a Bi_2Te_3 substrate from (c) a top view and (d) a side view. [14] *10*

Figure 5: Top view of layered structures of (a) black phosphorous and (b) blue phosphorous. (c) A schematic depicting the conversion from black phosphorous to blue phosphorous and (d) a side view of stacked blue phosphorous. [15] *12*

Figure 6: Atomic structure (a) of Bare Ti_2C, (b) Ti_2CO_2, (c) Ti_2CO_2-II, and (d) Ti_2CO_2-III [21] *15*

Figure 7 (a) Top view of monolayer MoS_2, (b) Side view of monolayer MoS_2.[28] *17*

Figure 8: Band structure of MoS_2 for bulk, 4 layer, 2 layer and 1layer [29] *18*

Figure 9: Schematic diagram of MoS_2 photosensor device structure. [33] *19*

Figure 10: MoS_2 Biosensor for DNA sequencing [34] *20*

Figure 11: (Left) Wet chemical thinning process. (Right) Optical image of MoS_2 flake before (a) and (d) with image of MoS_2 flake after etching (b) and (e). [37] *21*

Figure 12: (left) Optical images of growths with varying temperature of (a) 725°C, (b) 750°C, (c) 775°C, and (d) 800°C. SEM image of growth at (e)750°C and (f) 800°C. (right) Optical images of growths with varying carrier gas flow rates of (a) 15sccm, (b) 25sccm, (c) 30sccm, (d) 35sccm, (e) 40sccm, and (f) 50sccm. [41] *23*

Figure 13: Seed promoter and growth processes for creating MoS_2 nanosheets. (a) thermal evaporation, (b) metalation process, (c) growth of MoS_2 sheets, (d) transfer of MoS_2 sheets, and (d) fabrication of MoS_2 device. [42] *24*

Figure 14: (Left) Graphic depicting typical layering of MoS_2. (Right) Optical image of MoS_2 grown on SiO_2/Si. [40] *26*

Figure 15: Optical micrographs of MoS_2 synthesized with rGO seeders [43].....27

Figure 16: (I) Seeding promoter application. (II) Growth substrate at various distances from promoter substrate. Distances of (a) 60µm, (b) 126µm, (c) 192µm, (d) 258µm, (e) 324µm, (f) 390µm, (g) 456µm, (h) 522µm, (i) 588µm, (j) 654µm, (k) 720µm, (l) 786µm, (m) 852µm, (n) 918µm, (o)984µm, and (p) 1050µm. (the white scale bars for the images are all 20µm) [44].....29

Figure 17: (I) Growth set-up showing substrate, S, and MoO_3 placements. (II) Growth at different durations (a) 5mins, (b) 10mins, (c) 15mins, (d) 20mins, (e)25mins, (f) 30mins, (g)40mins, (h) 50mins, and (i) 60mins [45] 30

Figure 18: (a) Experimental setup of furnace, (b) SEM image of MoO_3 nanoribbon, (c) Optical image of MoS_2 growth [6].....31

Figure 19: (I) (a) Experimental set-up for CVD (b) substrate positioned at 0^o and (c) substrate positioned at 30^o, 45^o, 70^o, and 90^o. (II)SEM images of MoS_2 growth with different substrate angles. (a) 0^o, (b) 30^o, (c) 45^o, (d) 70^o, and (e) 90^o. (f) A wide view of the 90^o substrate. [46] 32

Figure 20: (I) CVD setup for MoS_2 growth. (II) Crystal growth of MoS_2 synthesized at (a) 800^oC, (b) 810^oC, (c) 820^oC, (d) 830^oC, (e) 840^oC, and (f) 850^oC. [47] 34

Figure 21: (I) CVD furnace and sample set up. (II) FESEM images of MoS_2 nanosheets taken (a) closer to S source and (b) closer to MoO_3 source [48].....35

Figure 22: (a) Heating furnace and precursor positioning for CVD growth (b) reaction and nucleation process of MoS_2 thin films [49] 36

Figure 23: (a) CVD set-up for MoS_2 growth (b) SEM imaging of MoS_2 grains [52] 38

Figure 24: Optical image of MoS_2 grown on sapphire substrate. near (a) edge and (b) center of sample. [53] 39

Figure 25: (a) Furnace setup for CVD growth, (b) optical image of MoS_2 grown on SiO_2/Si substrate, (c) optical image of MoS_2 grown on h-BN film, and (d) Raman data comparing MoS_2 growth on SiO_2/Si and h-BN.[56] 41

Figure 26: (a) Furnace setup for CVD growth, (b) optical image of single layer MoS_2-SnS_2 heterostructure (scale bar is 20µm), and (c) SEM image of single layer MoS_2-SnS_2 heterostructure (scale bar is 40µm). [57].....42

Figure 27: Schematic of growth parameters. (Top) Substrate and precursor positions inside furnace tube. (Bottom) Growth substrates and seeding promoter placement. 45

Figure 28: Scratch configuration for 3 and 5 scratch surface treatment.....48

Figure 29: (a) Penetration depth profile of primary electrons on surface (b) spectrum of emitted electrons from surface (c) electron emission effected by surface topography. [39] 52

Figure 30: MoS_2 characteristic peaks of bulk, 1 layer, 2 layers, 3 layers and 4 layers. [64] 56

Figure 31: Typical temperature profile for growth 58

Figure 32: (a) Growth with S position at 3/10 inches and (b) 4/10 inches. 59

Figure 33: Growth with MoO_3 powder distances of (a) 1.25, (b) 1.5, (c) 1.75, and (d) 2 inches 60

Figure 34: Substrates evaluated for growths with S at 4/10 in, MoO_3 at 1.25in and carried out at 650°C for 3mins. (a) sapphire, (b) SiO_2/Si, and (c) HOPG: 62

Figure 35: Growths with S at 4/10 in, MoO_3 at 1.25in and carried out at 650°C for 3mins (a) Sample with 3 scratch surface treatment on sapphire at 100x near the center of the sample and (b) Sample with 5 scratch surface treatment on sapphire at 100x at the upstream edge 63

Figure 36: Raman Spectroscopy for sample (a) with 3 scratches and a peak separation of 18 and (b) with 5 scratches and a peak separation of 19, both indicating monolayer film. 64

Figure 37: Growth on substrate treated with O_2 plasma etcher at (a) 50 watts for 3 minutes at 100x near the center of the sample and at (b) 50 watts for 5 minutes at 100x near the middle of the substrate 66

Figure 38: Growth on substrate treated with O_2 plasma etcher at 100 watts for 1 minute at 100x (a) near the center of the sample and (b) near the downstream edge 66

Figure 39: Growth on substrate treated with O_2 plasma etcher at 100 watts for 5 minutes at (a) 100x at the upstream edge and (b) 50x at the downstream edge 66

Figure 40: Sample with PTAS dried on a hotplate at a temperature of 50°C at (a) 1.25x and (b) 100x and sample with PTAS dried at 100°C at (c) 1.25x and (d) 100x. Growth settings of S at 4/10 in, MoO_3 at 1.25in and carried out at 650°C for 3mins 68

Figure 41: Growth on hydrophobic substrate at (a) 1.25x and (b) 100x and growth on hydrophilic substrate at (c) 1.25 x and (d) 100x. Growth S at 4/10 in, MoO_3 at 1.25in and carried out at 650°C for 3mins. 69

Figure 42: Optical images (100x) of growth with (a) 5 sprays, (b) 10 sprays, (c) 15 sprays, and (d) 20 sprays. Growths settings of S at 4/10 in, MoO_3 at 1.25in and carried out at 650°C for 3mins 70

Figure 43: Sample graphene as sole seeding promoter at (a) 1.25x (b) 50x 72

Figure 44: Sample with graphene and PTAS (a) upstream edge of sample at 100x, (b) upstream edge of graphene at 100x, and (c) Raman data growth near the graphene. *72*

Figure 45: (a) Raman on graphene showing MoS_2 peaks, (b) extended Raman on graphene showing MoS_2 and graphene peaks, and (c) Raman of thicker growth next to graphene *73*

Figure 46: Large MoS_2 growth on SiO_2/Si substrate with PTAS on a separate substrate in the upper stream. (a) 1 PTAS droplet, (b) 2PTAS droplets, and (c) 3PTAS droplets *74*

Figure 47: SEM images across the entire bare substrate in the presence of a separate PTAS substrate (2 droplet concentration) in the upper stream. *75*

Figure 48: (a) SEM Image of star-like shape MoS_2 grain, showing the difference between thicker film (dark gray) at the center of the grain and the thinner film (light gray) near the edges. (b)Thin triangular growth, with smaller triangles and nucleating points *76*

Figure 49: (a) Image from Raman and (b) Raman data for sample with a 2-droplet concentration. *77*

Figure 50: SEM image of continuous downstream area at (a) 7.25kX, (b) 23.63kX; *77*

Figure 51: EDX (a) analysis of star, (b) triangular area, and (c) downstream area (0138) *78*

Figure 52: SEM images across the entire bare substrate in the presence of a separate PTAS substrate (3 droplet concentration) in the upper stream. *78*

Figure 53: SEM imagines of large star/triangles in center of substrate. At (a)790X, (b) 19.42kX, (c) 4.57kX, (d) 16.10kX, (e) EDX on grain, and (f) bright substrate area (0136) *79*

Figure 54: (a) SEM image of continuous area with (b) EDX measurement (0136) *80*

Figure 55: Optical images of MoS_2 growth with Ar flow rate of (a) 100sccm, (b) 200 sccm, (c)400 sccm, and (d) 500 sccm *81*

Figure 56: (a) 1 minute, (b) 3 minutes, and (c) 5 minutes with other growth settings being S at 4/10 in, MoO_3 at 1.25in and carried out at *82*

Figure 57: (a) AFM image of 1 min growth, (b) topography measurement for 1 min growth, (c) AFM image for 3 min growth, (d) topography measurement of 3 min growth. *83*

Figure 58: ImageJ Analysis of 1-minute growth (0153). (a) Original microscope picture, (b) edited picture for measurement, (c) digital picture from thresholding measurement; ImageJ output measurement (0153) (d) the percentage of grains at different sizes, and (e) the total coverage by the grains of different sizes.....84

Figure 59: ImageJ Analysis and measurements of 3-minute growth (0151). (a) Original microscope picture, (b) edited picture for measurement, and (c) digital picture from thresholding measurement. (d) The percentage of grains at different sizes and (e) the total coverage by the grains of different sizes. 85

Figure 60: ImageJ Analysis and measurement of 5-minute growth (0154). (a) Original microscope picture, (b) edited picture for measurement and (c) digital picture from thresholding measurement. (d) The percentage of grains at different sizes and (e) the total coverage by the grains of different sizes. 85

LIST OF TABLES

Table 1: Characteristic E2g1 and A1g peaks of monolayer MoS2 excited by lasers of different wavelengths.[65] 57

Table 2: Summary of the quantitative analytical results showing the percentage of smaller grains (<100 µm2), the percentage of larger grains (>100 µm2), the largest size of the grain, and the total coverage of larger grains within the image.....86

1 Introduction and Background

1.1 Motivation

Electronics and computing technologies have been a convenience for many decades but continue to become an increasingly integral part of how society functions. As the technological achievements increase, so does society's dependence and reliance on its electronic devices. Therefore, it is necessary to devote time and research towards the improvement of electronics, both in form and function.

Semiconductors, as opposed to metals and insulators, usually have a band gap in the range up 0.1 - 4eV, which electrons can overcome to contributing the conduction. [1] The discovery of semiconductors has shaped the field of electronics and their applications. Semiconductors have many applications including diodes, transistors, integrated circuits, and light emitting devices and detectors.

Properties of semiconductors, such as photoconductivity was initially discovered and noted in the 1870's by Willoughby Smith while studying selenium for use in visual image transport by telegraph. Semiconductor technology was brought attention as J. C. Bose studied and successfully produced electromagnetic wave detectors using silicon and galenite. In the late 1920's when Grondahl and Geiger designed and manufactured their own rectifier based on a cuprous oxide. At the onset of WWII, it became a necessity to begin studying semiconducting crystals which allowed devices to be designed smaller. High quality, single crystal, silicon and germanium semiconductors were able to be reliably and repeatedly fabricated. Upon this success, many devices were built and researched using silicon and germanium. [1] In the later 1940's research conducted by

the Bell Telephone Laboratories led to the discovery of the amplification effect and, ultimately, to the invention of the transistor.

Silicon has long been established as a good semiconductor and continues to be a widely used material due to perfected fabrication and well understood properties. As research has progressed many compounds have been determined to be promising semiconductors. GaAs is a common III-V compound. other binary compounds exist such as II-VI and IV-VI compounds, along with ternary and quaternary compounds as well. [1]

Depending on the desired results the semiconductor may be constructed differently and may be doped with other elements to alter properties of the semiconductor. One common construction is to place oppositely doped materials into contact with each other creating a p-n junction. P-n junctions create a buildup of internal charge where the p and n regions meet, which serves as a barrier that requires an extra energy for charge to flow across the region. The barrier serves to assist flow of charge in one direction and deter flow in the other direction, allowing the charge to be better controlled; this can be either forward biased or reverse biased. [2] Devices such as diodes and transistors are built on these principles, and can be used as current control switches and amplifiers in microelectronics or optoelectronic devices used in photonics. A couple commonly used transistors are bipolar junction transistors (BJTs) and field effect transistors (FETs). Transistors are often used in electronics because they can operate as fast on-off switches, and can be used to amplify the current or voltage. BJTs are comprised of two p-n junctions in a back to back setup, this creates a three-terminal carrying device. The band gap in semiconductors also allows for the emission of light. Using a p-n junction semiconductor diode, light can be emitted by radiative recombination of injected minority carriers into

the majority carriers, causing light emission from a forward biased diode; this device is commonly referred to as a light emitting diode (LED). The extra energy from the electrons injected into the conduction band which fall into the valence band, is converted into photon emission. Reverse biased p-n junction diodes can be used for the detection of light, this device is called a photodiode. Light is detected in a photodiode due to the generation of electron-hole pairs from the presence of a light source. These charge carriers affect the current through the device, allowing for detection when a change is measured. [2]

Typical semiconductor materials, such as the aforementioned silicon and germanium, have been and will continue to play an important role in electronic applications and research. However, as electronics research continues there is an interest to create smaller devices with higher processing speeds. As a result, typical semiconductor materials begin to run into limitations creating a need to study alternative semiconducting materials. This has led many researchers to investigating two-dimensional (2D) materials.

1.2 Different Kinds of 2D Semiconducting Materials

1.2.1 First Generation 2D Materials - Graphene

Interest in monolayer materials dates back to the mid-1900s when scientists argued that strictly two-dimensional (monolayer) materials would be thermodynamically unstable. It was theoretically determined that thermal fluctuations in such low dimensional lattices would cause such large atomic displacements that the lattice would no longer hold its structure. A thin film's melting temperature decreases with a decreasing thickness, so it

was assumed that a monolayer film would not be able to exist apart from a three-dimensional structure. [3]

In 2004 scientists (Sir Andre Geim and Sir Kostya Novoselov) at the University of Manchester separated graphene flakes from a piece of bulk graphite (see Figure 1) using adhesive tape (referred to as the scotch tape method), and noticed interesting electronic differences as a flake of one atom thick had been obtained. [4] While there had been many attempts from other scientists to grow graphene on other surfaces, this was the first time that graphene had been isolated. Upon later research, it was found that the two-dimensional material was both continuous and had high crystal quality. The existence of these materials could be justified by the fact that two-dimensional materials are essentially quenched in a meta-stable state having been removed from a three-dimensional crystal and the strong interatomic bonds paired with the small size prevents thermal fluctuations that could cause dislocations or defects in the lattice. [3]

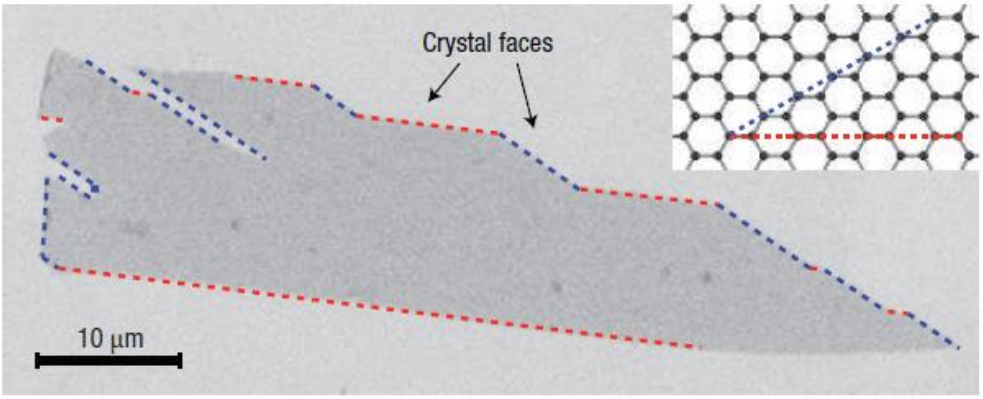

Figure 1: Graphene flake and atomic sketch [3]

Since its discovery, graphene has been a well-researched and used material in nanotechnology due to its many very unique characteristic as a semiconducting material. It was believed that graphene would be able to replace the conventional semiconductors

in uses such as metal-oxide field effect transistors (MOSFETs). However, as a result of its zero-band gap, graphene MOSFETs cannot be switched off, a necessity for digital logic usage, and have low radio frequency performance. [5] Graphene's zero-band gap also limits its uses in electronics and optoelectronics due to high leakage current. [6] This has led to an increased interest in other two-dimensional semiconducting materials to be used for electronics in nanotechnology.

1.2.2 Second Generation 2D Materials

With the discovery of graphene, various two-dimensional materials have emerged. The second generation 2D materials include layered van der Waals solids, layered ionic solids, 2D nonlayered materials and other carbon-based 2D materials. The most common class is layered van der Waals solids represented by metal dichalcogenides.

1.2.2.1 Layered van der Waals Solids

Layered van der Waals solids are the more common class of two-dimensional materials having a crystal structure with neutral single atom thick, or polyhedral thick, layers of atoms. These atoms are held together by typical ionic or covalent bonding within the plane, however, the layers are held together by van der Waals bonds along the third axis. [7] Single layer or few layer films of these materials are often acquired via mechanical exfoliation and chemical exfoliation. Mechanical exfoliation is the act of removing a layer of material from the bulk by some mechanical action such as the "scotch tape" method. Similarly, chemical exfoliation is the act of removing a layer from the bulk material with the aid of some solvent. The most commonly used method is mechanical exfoliation due to the fact that it does little damage to the bulk material during

exfoliation. The most widely studied family within van der Waals solids is the layered transition metal dichalcogenides (TMDs), which will be described in detail in section 1.3.

1.2.2.2 Layered Ionic Solids

Rather than van der Waals bonds, the materials in this class are often held together by either strongly electronegative anions or strongly electropositive cations. [7] A typical structure for layered ionic solids is a polyhedral layer that has been sandwiched between either hydroxide or halide layers. [8] Layers are held together due to the electrostatic forces between the anions and cations. To create the layers of ionic solids, via exfoliation, or as it is more commonly referred to as intercalation, the cations and anions are exchanged with larger organic cations and anions, then dispersed onto a substrate. [7] It is also possible to get single layers by exfoliating the bulk material via ion exchanges. Perovskite type oxides are a common example of such layered ionic solids exfoliated by this method. [8]

1.2.2.3 2D Nonlayered Materials

Materials in this class exhibit similar properties as the other two-dimensional materials, however, their crystal structure has chemical bonding in three dimensions making it difficult to exfoliate to atomic thicknesses like the layered solids. There are many dangling bonds on the surfaces of these materials leading them to become chemically active in catalysis, sensing, and electronic transport. Due to the challenges of isolating layers, few exfoliation methods with surface modification were successful. Common examples of 2D nonlayered materials would be group III-V semiconductors, with a high carrier mobility and direct bandgap. [8]

1.2.2.4 Other Carbon-Based 2D Materials

In attempts to circumvent issues that arise from graphene's lack of a bandgap, other carbon-based materials have been explored. These materials are similar to graphene given that they have the same honeycomb lattice, however, the carbon atoms are replaced with sp- and sp^2- hybridized carbon atoms. This allotrope is called graphyne, and the carbon bonds are replaced by acetylenic bonds. By varying the length of the acetylene chains a variety of derivatives can be formed such as graphdiyne, graphtriyne, and graphtetrayne (see Figure 2). [8]

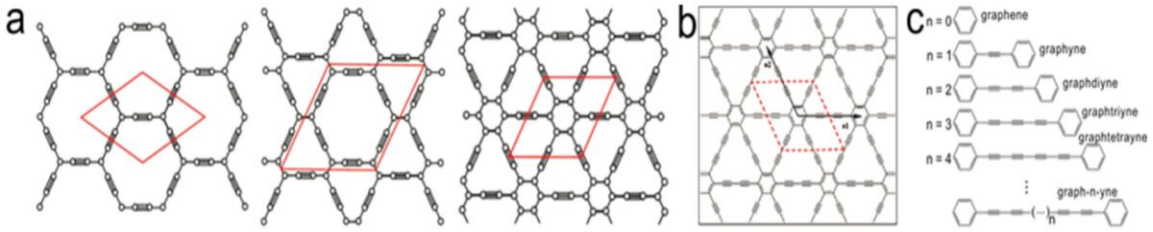

Figure 2: (a) α-, β-, and γ- graphyne, (b) graphdiyne, and (c) f extended graph-n-yne by acetylenic carbon chain length [8]

Additionally, much research has been done to functionalize graphene via doping and introducing different defects into the lattice. For instance, a particular family of graphene allotropes called pentaheptites make use of a pentagonal (C_5) or heptagonal (C_7) structure of carbon atoms rather than graphene's typical hexagonal structure (C_6). Constructing a sheet of carbon with C_5 or C_7 bonds will create stone Wales defects. Stone Wales defects are characterized by an in plane 90-degree rotation of two carbon atoms causing a change in the lattice structure. What would normally be an all hexagonal structure becomes a combination of heptagons and pentagons (see Figure 3). [9]

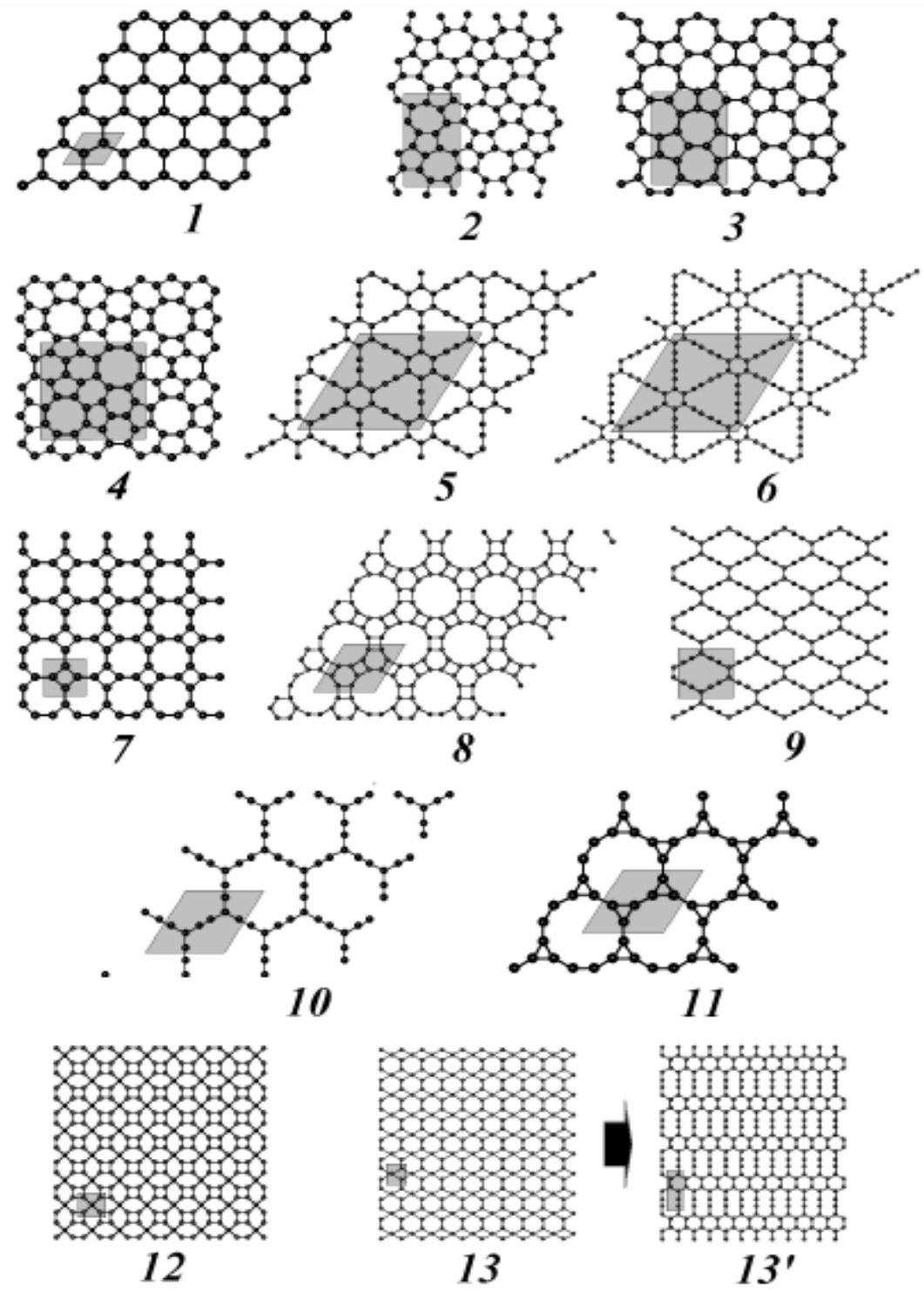

Figure 3: Graphene (1) and graphene allotropes pentaheptites (2-3), haeckelites (4), graphynes (5-6), 4:8 net (7)[10], C4 squares and C10 decagons (8), distorted hexagons (9) supergraphene (10), polycyclic network of C3 and C12 (11) and squarographenes (12- 13'): [9]

1.2.3 Third Generation 2D Materials

The more recently studied materials are known as third-generation two dimensional materials. The majority of these third-generation materials fall under the classification of van der Waals solids. Many of these materials were theorized and predicted by computer simulations among which most still have not been successfully isolated yet. A few of the successfully isolated materials were silicene, germanene, and stanene.

1.2.3.1 Silicene, Germanene, and Stanene

Since silicon, germanium and tin are in the same column of the periodic table as carbon (group IV), it was theorized that they might be able to provide similar structures. However, unlike graphene, these are 2D nonlayered materials which makes isolating them a challenge. Despite the fact that the ground state structure of these particular third generation materials show signs of buckling, due to the tendency to favor a sp^3 bond rather than an sp^2 bond, they are still believed to be tunable for use as topological insulators. [11] Silicene was proven to be dynamically stable and has an increased band structure tunability when compared to graphene.

Silicene was not successfully experimentally synthesized until 2012. Silicene was often synthesized using either chemical exfoliation or vacuum deposition. A layer of silicene can be removed from a piece of calcium silicide ($CaSi_2$). By chemically etching away Ca atoms using hydrochloric acid (HCl) and magnesium (Mg), a layer of interconnected Si_6 rings were revealed. Silicene can also be deposited under vacuum conditions on various substrates such as Ag(111), Ag(110), Au(110), Ir(111), MoS_2, ZrB_2, and h-$MoSi_2$. Using similar exfoliation of $CaGe_2$ or vacuum deposition, a layer of germanene can be separated from the bulk state. [8] The overall structures of silicene and germanene are very

comparable and similar to graphene (see Figure 4 (a) and (b)), however, they have slight structural differences in bonding angles and distances.

Silicene and germanene exhibit many unique properties that make them materials of interest. For instance, silicene shows levels of ferromagnetism, quantum spin Hall effect, and tunable thermal conductivity through doping. Like silicene, germanene has half-metallic characteristic with photonic properties in its ground state, structural stability, controllable magnetic properties, and large carrier mobility. [8] Materials that exhibit half-metallic properties are particularly interesting. With electrons of one spin orientation, the material acts as a conductor of electrons, however with electrons of the opposite spin orientation, act as an electronic insulator. [12]

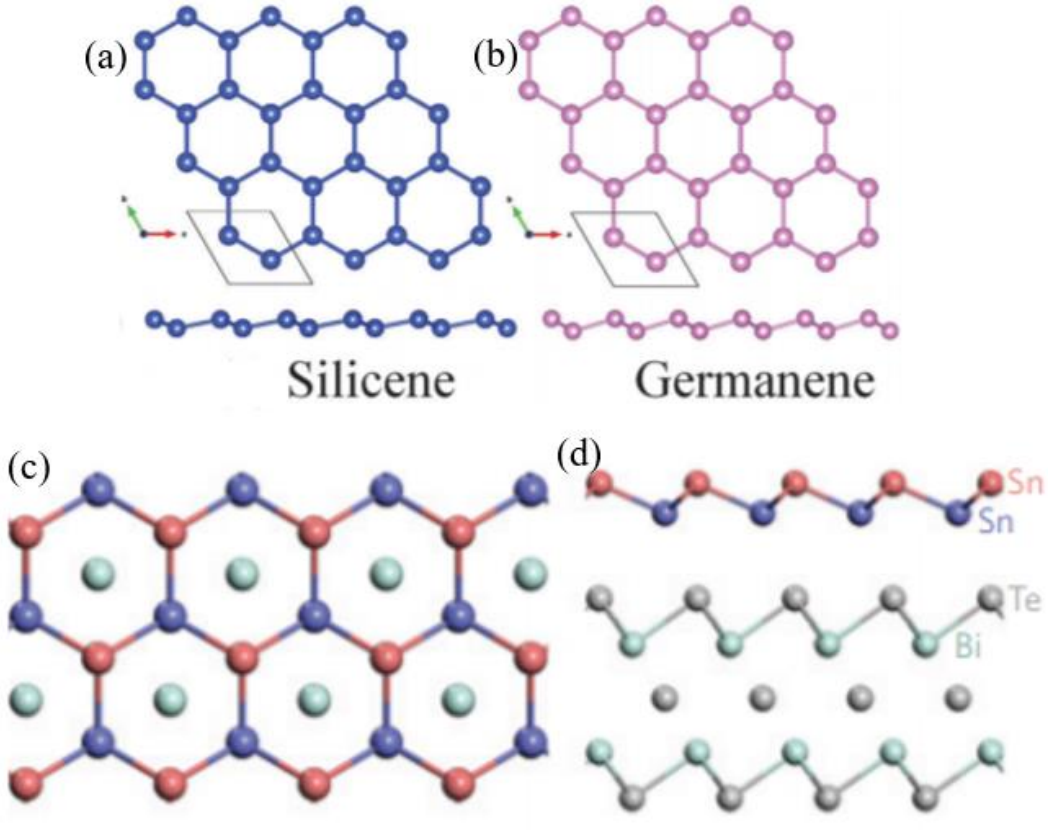

Figure 4: (a) Silicene and (b) Germanene two-dimensional structures. [13] Stanene - two sublattices of tin on a Bi_2Te_3 substrate from (c) a top view and (d) a side view. [14]

The two-dimensional lattice of tin is called stanene (less commonly referred to as tinene). Stanene is formed by stacking two triangular sublattices of tin in the (111) plane. The stacking of these sublattices creates a buckled honeycomb structure. Unlike silicene and germanene, stanene is not easily formed via exfoliation. It is more commonly fabricated through molecular beam epitaxy (MBE). For instance, processed tin atoms were evaporated and deposited onto a Bi_2Te_3(111) (Bismuth Telluride) substrate (see Figure 4 (c) and (d)). Stanene also has many interesting properties such as the quantum spin Hall effect, low thermal conductivity, and superconductivity. [8]

1.2.3.2 Group V Two-Dimensional Materials

Group V semiconducting elements have been explored as two-dimensional materials. This includes black phosphorous (BP), blue phosphorous, arsenene, antimonene, and bismuthine. [8] Black, white, red, blue and violet phosphorous are all allotropes of phosphorous, deriving their names from their fundamental bandgap, among which BP is the most stable phase. [15] In BP each phosphorous atom is covalently bonded to three other phosphorous atoms; this creates a puckered honeycomb structure as a monolayer lattice. As the thickness of BP decreases to a single layer, the band gap increases from nearly no band gap, about 0.3 electron volts (eV), to 1.5eV. It shows great potential for electronics and photonics as it exhibits a large carrier mobility at room temperature around 1000 $cm^2\ V^{-1}\ s^{-1}$ in few layers. The most widely used method of fabrication for BP is mechanical exfoliation. Chemical exfoliation and CVD have also been used in various research efforts. The electronic structure of BP is dependent on the stacking order and the lattice strain, so definitive values are varied; they indicate that BP is a viable option for photoelectronics. [8] The blue phosphorous phase has the honeycomb structure

seen in graphene, when compared to the other phosphorous allotropes. Blue phosphorous shares BP's high stability and layered structure. It is more analogous to graphite, however it can be exfoliated to a quasi-two-dimensional state and demonstrates a wider fundamental band gap than both BP and graphite. [15]

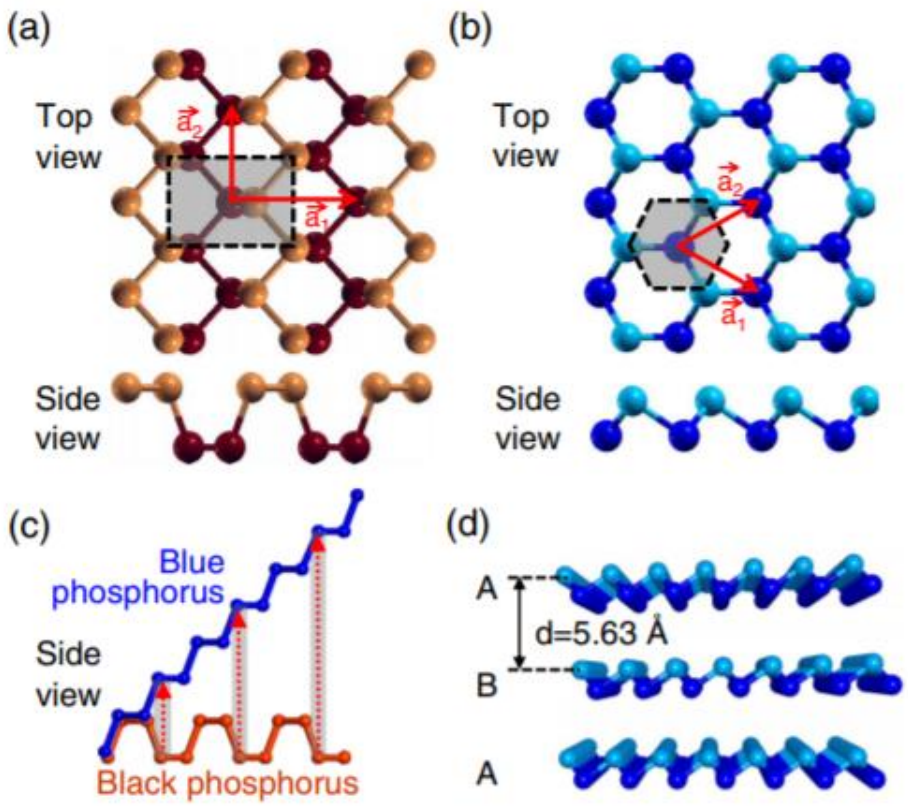

Figure 5: Top view of layered structures of (a) black phosphorous and (b) blue phosphorous. (c) A schematic depicting the conversion from black phosphorous to blue phosphorous and (d) a side view of stacked blue phosphorous. [15]

Arsenene is a single layer of gray arsenic atoms arranged in a rhombohedral structure. It is most commonly fabricated using a plasma assisted ablation onto an indium arsenide (InAs) substrate with a thickness of 14 nm. A couple notable properties are high thermal conductivity and topological phase transitions from strain modulation. [8]

Similarly, the most stable allotrope of antimonene is comprised of a monolayer of gray antimony atoms. In the monolayer state antimonene maintains semiconductor properties with a theoretical indirect bandgap of 2.28eV. Through theoretical calculations it has been found that antimonene presents an array of interesting properties such as ultraviolet light absorption, spin-orbit coupling effect, and electronic properties that are affected by stone-Wales defects. Antimonene's band gap can be shifted from indirect to direct by applying a strain to the monolayer structure. There are many fabrication processes used to develop the monolayer film, such as CVD, MBE, and both mechanical and chemical exfoliation. [8]

The two-dimensional allotrope of bismuth, bismuthene, transitions from semimetal to a semiconductor when thinned to a monolayer film. Bismuthene was first synthesized via deposition on a silicon substrate. The most notably unique characteristics of bismuthene are its ability to remain stable against long wave vibrations, and its thermal excitations at high temperatures. [8]

1.2.3.4 Group III and Transition Metal Elements

Additional elemental two-dimensional materials are group III and transition group materials. The only group III two-dimensional material is currently borophene which derives from boron as a quasi-planar structure. Using additional calculations, it was determined that borophene has a high work function, high magnetic properties, and an ultrahigh hydrogen storage capacity. This makes borophene an ideal candidate for power generation, electricity transmittance and energy storage. [8]

Many of transition metal elements have been successfully fabricated into two-dimensional lattices including Fe, Co, Ni, Cu, Ru, Rh, Pd, Ag, Pt, and Au. The most

suitable method of fabrication differs from material to material. One of the most common methods for the synthesis of the monolayer films is solvent thermal method. Transition metals are thought to be good materials for electrocatalysis applications as a result of their optical absorption and photothermal properties. [8]

1.2.3.5 2D Compounds: h-BN

Hexagonal boron nitride (h-BN) is compound with a structure similar to graphene. Due to the stronger bonding between boron and nitride its chemical and thermal stability is greater than graphene's. h-BN has a high thermal conductivity, and the bending elastic modulus is several hundred of gigapascals (GPa). There is also a large charge transfer from boron to nitrogen atoms that helps to distinguish h-BN from graphene when considering optical and electrical properties. h-BN is white with a band gap of about 5.5eV, making it very useful in dielectric applications. When graphene is placed on top of the h-BN, a band gap can be created due to BN's ability of enhancing carrier mobility. [16] The most prominent method of synthesis for this material is MBE. [17]

1.2.3.6 Transition Metal Oxides

Oxygen is highly polarizable which create non-linear and non-uniform distribution of charges across the surface of the TMO film. Properties of TMOs are affected by the cations and their ability to change oxidation states. Having oxygen ions on the surface in the transition metal oxides (TMOs) opens up many possibilities to the functionalization of the films. Tunability of the nanostructure is primarily controlled by the oxygen vacancies and reduction-oxidation reactions. [18]

1.2.3.7 MXenes

MXenes is the two-dimensional transition metal carbides or nitrides, derived from MAX phase ceramics by etching out the A group elements. MAX are a group of layered structure ceramics in which M is an early transition metal, A is an A-group element (mostly IIIA and IVA), and X is either carbon, nitrogen, or both. [19] Once A group elements are etched out, the material is left with a general chemical formula of $M_{N+1}X_N$. Each layer is created by bonding alternating hexagonal planes of M and X. A few examples are Ti_2C, Ti_2CO_2, and the Cu_2X family. The general structure of MXenes can be seen in the image of Ti_2C and Ti_2CO_2 (see Figure 6). Cu_2S, well studied in its bulk form, has recently been isolated as a two-dimensional layer.[11] Interesting properties of MXenes are their hardness, wear resistant capabilities, metallic conductivity, and thermal stability. [20]

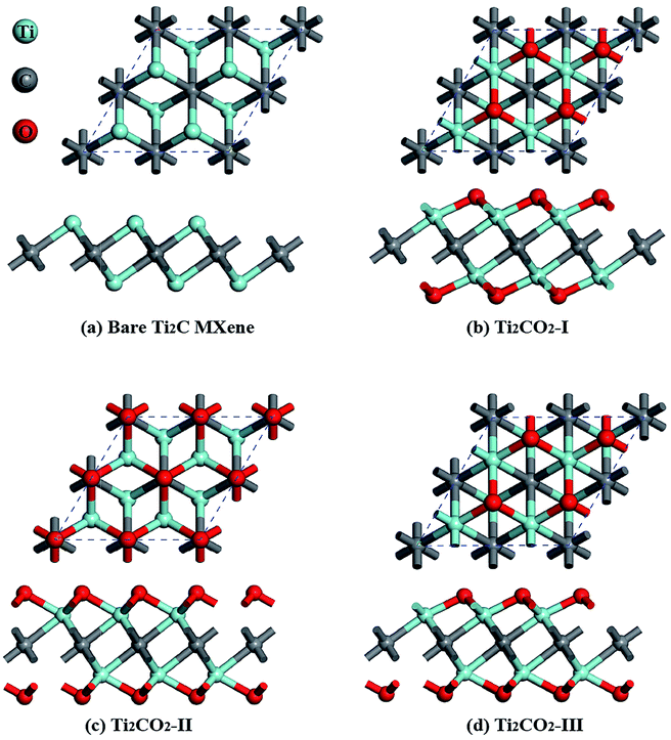

Figure 6: Atomic structure (a) of Bare Ti_2C, (b) Ti_2CO_2, (c) Ti_2CO_2-II, and (d) Ti_2CO_2-III [21]

1.3 2D TMDs and Their Emerging Applications

1.3.1 Overview of 2D TMDs

Third-generation two-dimensional materials have a promising future, but there are extensive developments that can be accomplished within the first and second-generation materials. A large focus has been put on the study and development of transition metal dichalcogenides (TMDs).

TMDs have a chemical formula MX_2 and a layered structure of X-M-X. [22] TMDs can be semiconductors, semi-metals, true metals, or super conductors depending on their composition. [23] A larger focus is on the semiconducting TMDs, where M represents a transition metal and X represents a chalcogen element. [22] A monolayer TMD is defined as two layers of chalcogen atoms in hexagonal planes sandwiched around a hexagonal layer of metallic atoms. [24] Like graphene, TMDs possess weak non-covalent bonds between layers, but strong in-plane covalent bonds.

As a result of quantum confinement, the monolayer TMDs have electronic properties that do not exist in their bulk form. For example, some bulk semiconducting TMDs have an indirect band gap, however the single layer form has a direct band gap. [23] An indirect band gap is one in which the maximum energy of the valence band occurs at a different value of momentum then the minimum energy of the conduction band, while a direct band gap has both the valence maximum and conduction minimum occurring at the same value of momentum. [25] Due to their shift from indirect to direct band gap from bulk to single layer, these TMDs make good candidates for electronic devices like transistors and photodetectors. TMDs also have found applications in photovoltaics, lithium ion batteries, and ultrasensitive biosensors just to name a few.

The most studied TMDs are molybdenum disulfide (MoS_2), molybdenum diselenide ($MoSe_2$), tungsten disulfide (WS_2) and tungsten diselenide (WSe_2). Other notable TMDs are in the form of NbX_2 and TaX_2, where X is a chalcogen atom. In general, MoX_2 and WX_2 will be semiconducting, while NbX_2 and TaX_2 will be metallic. [26][27]

1.3.2 Structure and Properties of 2D MoS_2

MoS_2 is a TMD with an X-M-X structure as discussed in the previous section. From a top down view, the structure is similar in appearance to the honeycomb structure of graphene, however the side view shows that the S atoms sit in an offset plane from the Mo atoms as seen in Figure 7.

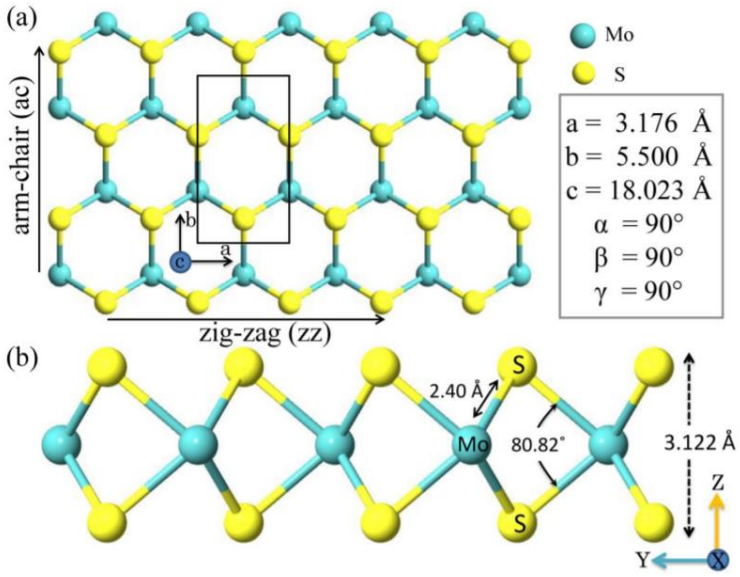

Figure 7 (a) Top view of monolayer MoS_2, (b) Side view of monolayer MoS_2.[28]

In bulk MoS_2 the valence band maximum occurs at the Brillouin zone Γ point while the conduction band minimum occurs at the Brillouin zone K point. The conduction band minimum has a strong dependence on the d orbitals of Mo and the p_z orbitals of S, which causes a dependence in the interlayer coupling. As the number of layers decreases to

one, the K point of both the valence and conduction band remains nearly constant, while the other points reduce or increase, respectively, leaving both the valence band maximum and conduction band minimum at the K point state, seen in Figure 8. [29] The resulting direct band gap is 1.3eV which is larger than the indirect band gap of 1.2 eV. [27]

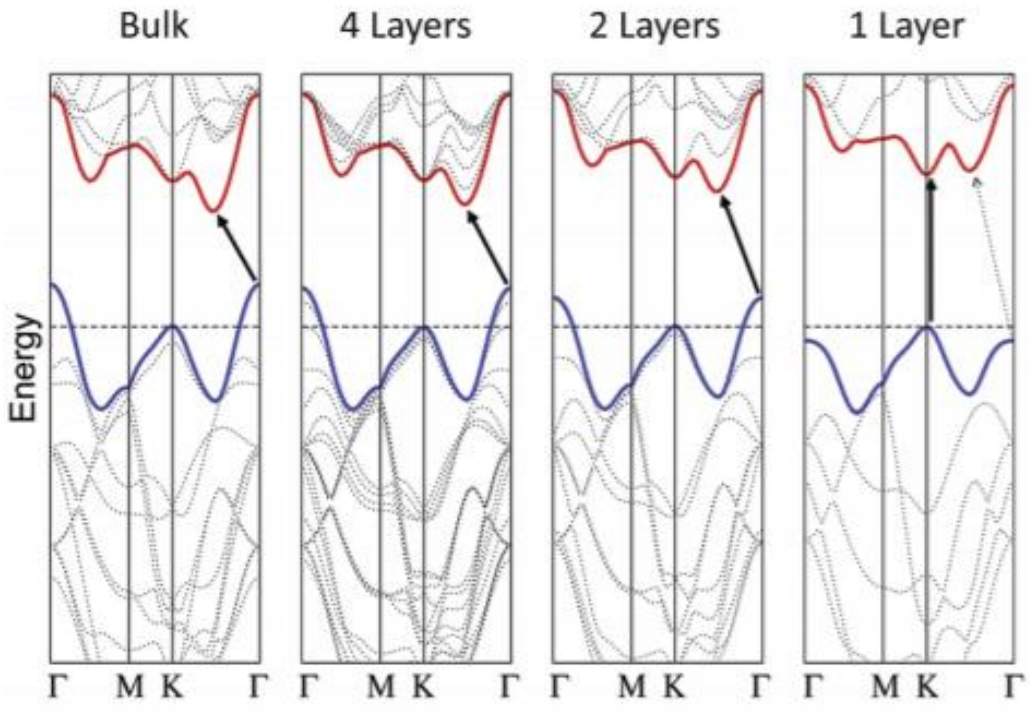

Figure 8: Band structure of MoS_2 for bulk, 4 layer, 2 layer and 1layer [29]

Molybdenum disulfide in its single layer form allows valley polarization. [30] Valley polarization is a smaller part of "valleytronics", a technique that uses the electrical charge of an electron to hold information, rather than the wave quantum number typically used in crystalline materials. [31] It is also noteworthy that MoS_2 has a high on/off ratio ($\sim 10^8$) and a relatively high mobility ($\sim 17 cm^2 V^{-1} S^{-1}$). This is due to the band gap, which is not present in graphene and makes MoS_2 a promising material in electronics, especially in semiconductor applications. [32] There is an increasing demand for flexible devices,

and MoS_2 is one of the materials that can help to pave the way in this direction. It is a practical option for transistors, touch screen devices and even batteries. [5] Applications such as photosensors make use of MoS_2's optical properties (see Figure 9). It has been reported that the gas adsorption on MoS_2 is closely related to the photoresponse. Likewise, the photoluminescence has been noticeably increased by the adsorption of oxygen or water molecules. A photodetector with a two-step response, fast and a slow response, was developed. It was determined that the fast response was due to the electron-hole pair generation from the primary beam of light and the slow response is because of the gas desorption. As a result, the photoresponse is noted to be dependent on wavelength and a shorter wavelength will induce a longer slow response. [33]

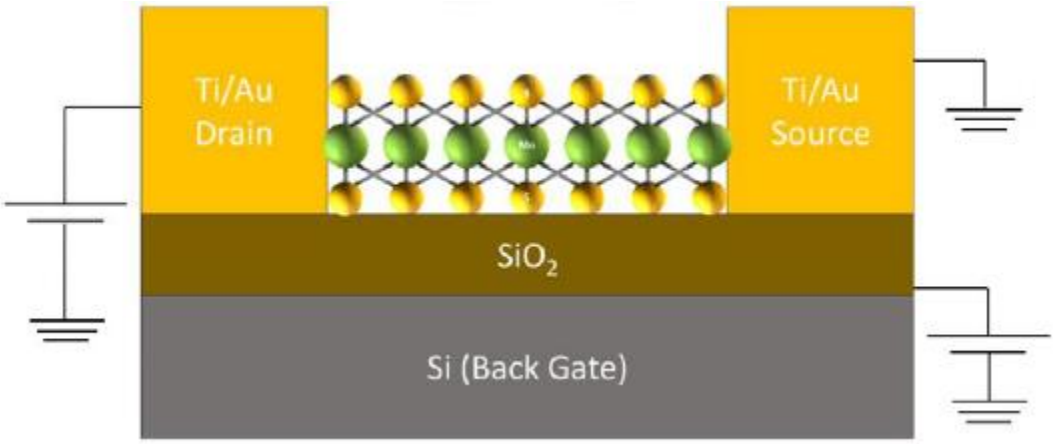

Figure 9: Schematic diagram of MoS_2 photosensor device structure. [33]

In the biomedical field research to use MoS_2 in solid-state nanopores for DNA sequencing has been conducted (see Figure 10). Current efforts are using solid-state nanopores to replace biopores. Biopores have been constructed of a membrane protein complex, used for sequencing a single DNA molecule by allowing each of the four nucleotides to pass through the pore. Each nucleotide has a characteristic change in

current as it passes through the pore. Efforts to make a solid-state nanopore prior to use of MoS_2 were deterred by the inability to create nanopores in SiN_x that could differentiate the nucleotide charges. A solution using MoS_2 was to suspend a few layers of MoS_2, with holes drilled using an electron microscope, on the SiN_x membrane. This solution increased the resolution of the membrane from 20nm to 1nm. [34]

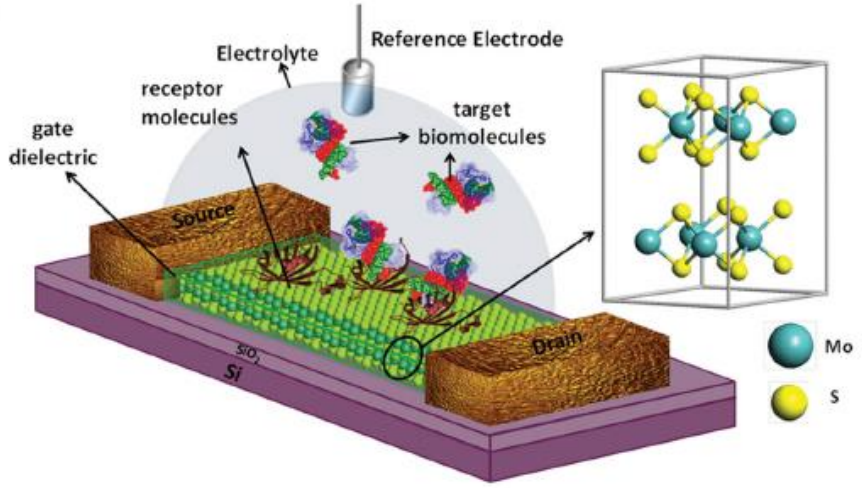

Figure 10: MoS_2 Biosensor for DNA sequencing [34]

1.3.3 Fabrication of 2D MoS_2

As early as the 1950s Robert Frindt attempted to created single layers of molybdenum disulfide by using an adhesive tape and synthesize the monolayers with lithium intercalation, it did not prove to be successful. [23] Since then, multiple other methods have been explored for fabricating 2D molybdenum disulfide.

One method is micromechanical exfoliation, much like Geim and Novoselov's isolation of graphene. Flakes of molybdenum disulfide are removed from the bulk material by sticky tape which is then pressed to a substrate. Some of the flakes will stick to the substrate because of the weak Van der Waals forces between layers, these become the

isolated single layer pieces of molybdenum disulfide. Using this technique can provide both single and multi-layer MoS_2 films. [35] By using this method the film retains the highest crystalline quality which allows its use in ultrasensitive photodetectors and digital circuits. [36]

Another method that has been explored is wet chemical thinning shown in Figure 11. During this process, a thin multilayer film of MoS_2 on SiO_2/Si was put in contact with a nitric acid (HNO_3). When heat is provided the HNO_3 reacts with the MoS_2 at the edges and creates MoO_3. MoO_3 further reacts with the HNO_3 to form H_2MoO_4 which is soluble in the acid. [37]

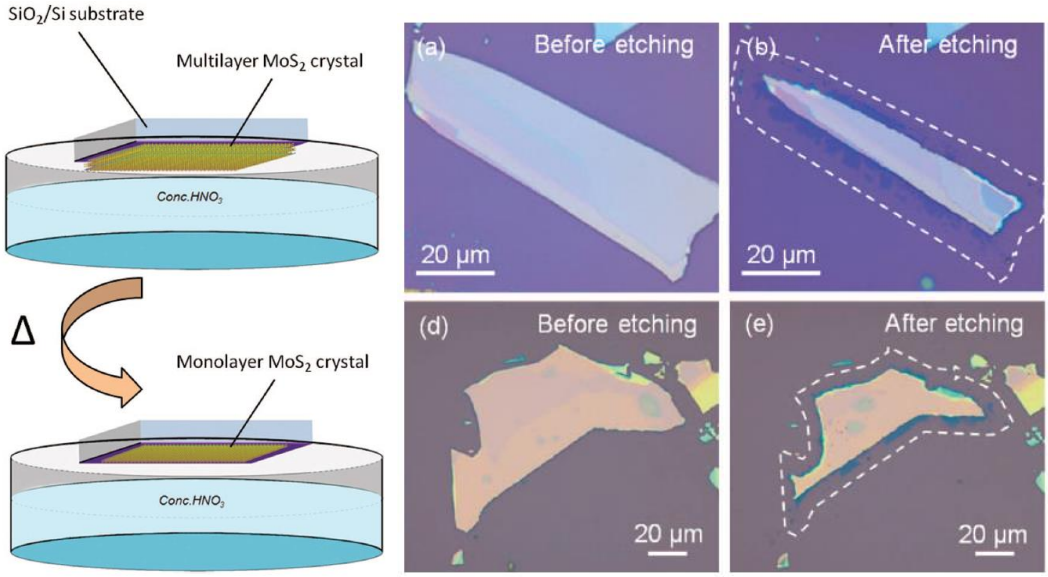

Figure 11: (Left) Wet chemical thinning process. (Right) Optical image of MoS_2 flake before (a) and (d) with image of MoS_2 flake after etching (b) and (e). [37]

There is an approach for fabricating molybdenum disulfide nanosheets from a bulk source with the help of various etching solutions. The bulk molybdenum disulfide is immersed in an etchant such as butyllithium solution for a period of time followed by

ultrasonicating the Li_xMoS_2. The excess lithium is removed, and the thin films are created by filtering a diluted suspension through a membrane. [38]

One of the more popular methods for synthesizing molybdenum disulfide is a modified form of chemical vapor deposition (CVD). A typical chemical vapor deposition process introduces vapors with a non-reactive gas into a chamber, often a furnace, to react and deposit onto a substrate. [39] Due to the complexity of getting molybdenum in a gaseous state, the CVD process most often placed molybdenum oxide ($MoO_{3)}$ and sulfur (S) powders in the furnace and a non-reactive gas flowed through the furnace to carry the evaporated precursors downstream to the substrate on which they will deposit. [40]

Two mechanisms have been proposed to describe the reactions of MoO_3 and S during nucleation. One suggests that the initial reaction between S and MoO_3 creates a volatile compound $MoO_{3-x}S_y$ on the substrate. The complete sulfuration and reaction of this compound leads to a conversion into MoS_2. The other proposed mechanism states that the MoO_3 and S react in the vapor phase and then deposit onto the substrate as MoS_2. The nucleation occurs in the form of either planar nucleation or self-seeding nucleation, depending on the reactant concentrations, carrier gas flow rate, and growth temperature. Planar nucleation, creates a flat even layer flake, while, self-seeding nucleation, produces flakes with a nanoparticle at the center of the triangle. In self-seeding nucleation, these thick center spots serve as a nucleation point for the growth process and can be seen and identified as thicker during characterization after the growth. It was determined that higher temperatures, higher carrier gas flow rates, and higher reactant concentrations tends to lead to self-seeding nucleation. Planar nucleation was usually a result of lower temperatures, flow rates and reactant concentrations.

The above phenomenon can be seen in Figure 12; the set of growths with temperature as the varying factor depict planar growth at the lower growth temperatures (725^{o}C. 750^{o}C, and 775^{o}C), while the higher temperatures (800^{o}C) demonstrates self-seeding growth as exemplified by the white dots in the images. Similar results are obtained in the set of growths with varying carrier gas flow rate. At lower flow rates (15sccm, 25sccm, and 30sccm) planar seeding is observed as seen by the flat triangular growth. Self-seeding growth is seen at higher flow rates (35sccm, 40sccm and 50sccm), characterized by the white/dark blue nucleation points in the center of the triangular grain. [41]

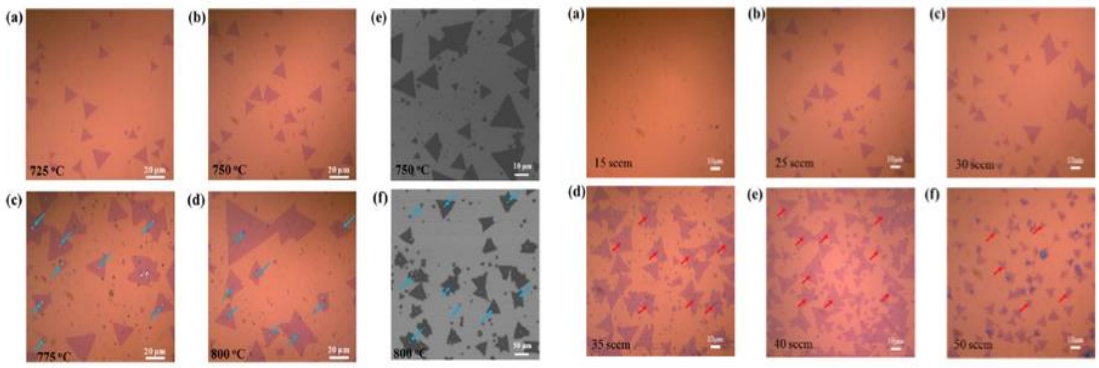

Figure 12: (left) Optical images of growths with varying temperature of (a) 725^{o}C, (b) 750^{o}C, (c) 775^{o}C, and (d) 800^{o}C. SEM image of growth at (e)750^{o}C and (f) 800^{o}C. (right) Optical images of growths with varying carrier gas flow rates of (a) 15sccm, (b) 25sccm, (c) 30sccm, (d) 35sccm, (e) 40sccm, and (f) 50sccm. [41]

MoS_2 sheets can also be fabricated using a combined method of thermal evaporation and atomic layer deposition (ALD) with the help of metalloporphyrin as a growth promoter. The Mo solution, prepared by dissolving 0.1M ammonium heptamolybdate in distilled water, was deposited onto a UV treated SiO_2/Si substrate by spin coating. Sulfur was placed upstream and growth took place at 600˚C for 5 minutes with pressure of about 1 Torr and 500sccm of Ar. The seeding promoter (metalloporphyrin) is deposited on the

growth substrate first (see Figure 13 (b)), then the Mo solution is applied along with the sulfurization seen as a condensed process in Figure 13 (c). The growth on this seeding promoter also allows for doping of the film for use as an MoS_2 based device as seen in Figure 13 (e). [42]

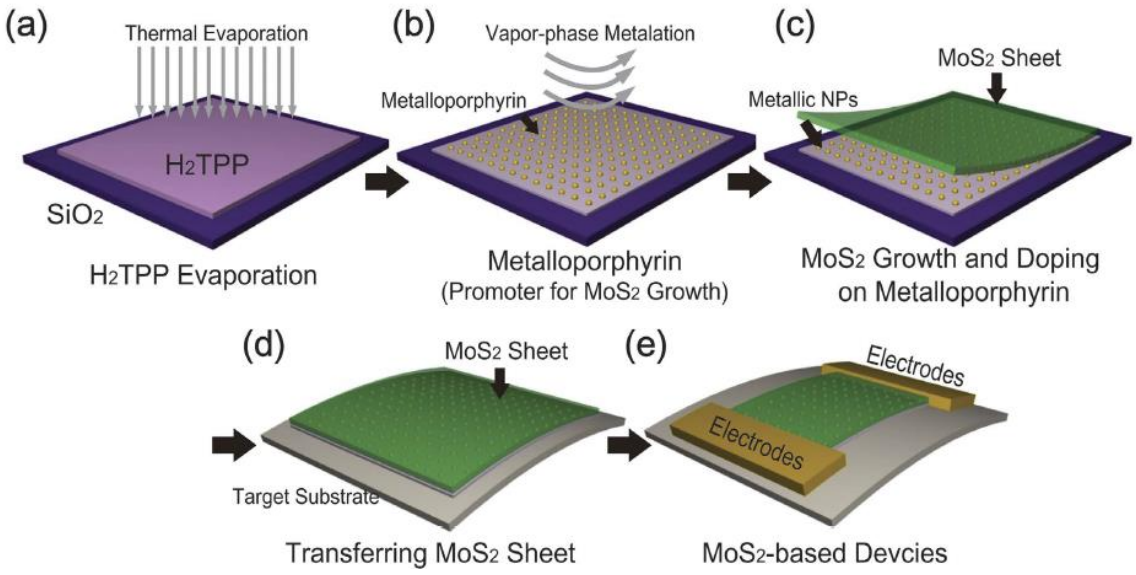

Figure 13: Seed promoter and growth processes for creating MoS_2 nanosheets. (a) thermal evaporation, (b) metalation process, (c) growth of MoS_2 sheets, (d) transfer of MoS_2 sheets, and (d) fabrication of MoS_2 device. [42]

1.4 Research Objectives and Outline of this Thesis

While there are various new generation two-dimensional materials, 2D molybdenum disulfide has great potentials for practical applications in the near future. The big challenge is the capability of producing high quality, large area, monolayer molybdenum disulfide. Density and structural disorders, such as grain boundaries, vacancies and dislocations limit the performance of the material resulting in a lower quality film. The objective of this research is to study and identify key growth parameters towards fabricating large area, monolayer films of MoS_2 in our CVD facility.

In chapter 2, previous research on CVD growth of MoS_2 has been reviewed. The experimental aspects and characterizations used in this study will be presented in chapter 3. Results will be presented and discussed in chapter 4 and concluded in chapter 5.

2 Current Research on Chemical Vapor Deposition of 2D Molybdenum Disulfide

Bilgin et al [40] synthesized monolayer MoS_2 at a growth temperature of 750˚C. The growth took place in a tube furnace, with a 1inch quartz tube at atmospheric pressure. An SiO_2/Si substrate with a thickness of 300nm serves as the growth substrate, which was first cleaned by acetone, isopropyl alcohol (IPA) and deionized water (DI) before being placed faced down in an alumina (Al_2O_3) boat holding 10mg of molybdenum oxide (MoO_2) powder. For the growth, the boat was placed at the center of the tube furnace, while 20mg of sulfur (S) powder was placed upstream at the edge of the furnace. Before starting the growth process the tube was flushed three times with argon (Ar) carrier gas. The tube furnace was then brought to 300˚C for an hour with 100sccm of Ar before being ramped up to 750˚C, at a rate of 3˚/min, held for 15 minutes and then allowed to cool back down to room temperature. The optical images of the obtained MoS2 films are shown in Figure 14.

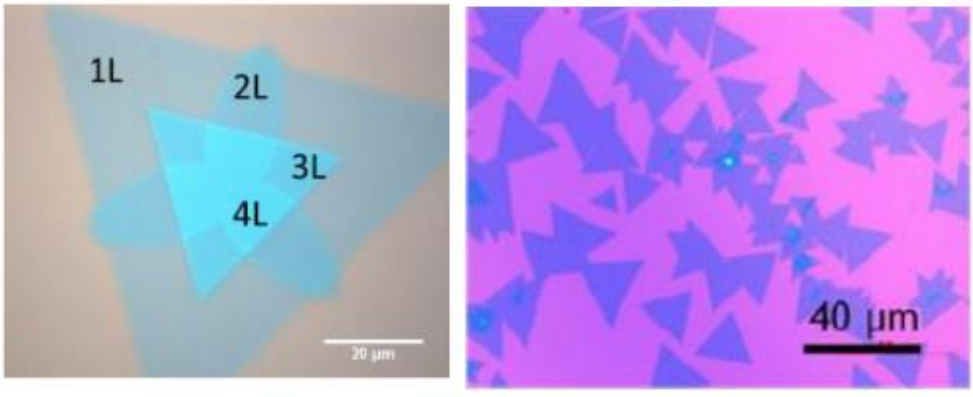

Figure 14: (Left) Graphic depicting typical layering of MoS_2. (Right) Optical image of MoS_2 grown on SiO_2/Si. [40]

Typical grain edge lengths, for this study, ranged between 10 and 50μm. Using atomic force microscope (AFM) near the edge of a multilayer grain, the MoS_2 thickness was found to be 0.5-0.8nm, indicating that the edge of the sample was a monolayer film. Raman spectroscopy was performed on the same grain and used to determine the presence of 1, 2, 3, and 4 layer MoS_2. [40]

A similar experiment was conducted by Dr. Y.-H. Lee et al [43] using various seeding promoters, including reduced graphene oxide (rGO), PTAS (perylene-3,4,9,10-tetracarboxylic acid tetrapotassium salt), and PTCDA (perylene-3,4,9,10-tetracarboxylic dianhydride). The synthesis took place in a hot wall furnace on SiO_2/Si substrates. Before the growth began, a drop of seeding promoter was placed on the substrate. The substrate was placed face down on top of an Al_2O_3 crucible containing MoO_3 powder, with S powder in another Al_2O_3 crucible. Growth temperature was brought to 650˚C at a rate of 15˚/minute then held at that temperature for 15 minutes with a flow of nitrogen of 1sccm.

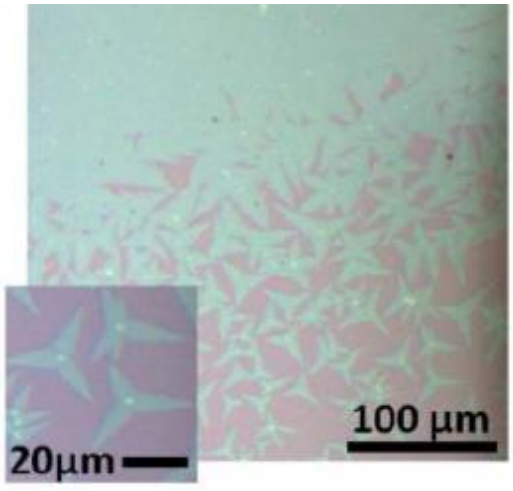

Figure 15: Optical micrographs of MoS_2 synthesized with rGO seeders [43]

Thickness of the film was determined, by AFM, to be approximately 0.72nm; and confirmed by photoluminescence (PL) and Raman spectroscopy to be monolayer. Edge lengths of the grains were determined to be less than 5μm for monolayer triangular grains, and approximately 20μm for three pointed stars (Figure 15) formed using an rGO seeding promoter. A nucleation point can be seen at the center of the stars as well. [43] Ling et al [44] studied PTAS's role as a seeding promoter in a similar synthesis method. First a 300nm SiO_2/Si substrate was cleaned with a piranha solution (H_2O:HCL:H_2O_2-2:1:1). Then PTAS and crystal violet (CV) were dissolved in water, applied to the substrate and spread evenly across the surface using a micropipette tip; the droplet was then dried by N_2 flow. For other seeding promoters used such as, F_{16}CuPc, PTCDA and TCTA (tris(4-carbazoyl-9-ylphenyl) amine) the promoter was placed on an upstream substrate then thermally evaporated onto the growth substrate. The substrate was placed face down on an alumina crucible containing MoO_3 powder, at the center of the quartz tube, while another crucible containing sulfur was placed upstream. After purging the system for 3 minutes with 500sccm of Ar, 5sccm of Ar was flowed through as a carrying gas. Growth took place after heating the furnace to 650˚C at a rate of 15˚/min and held for 3 minutes at atmospheric pressure; as a result, the sulfur temperature during the growth was about 180˚C. Once the growth was complete, the system was cooled quickly by opening the furnace and removing the quarts tube. The reactants were then removed by flowing 500sccm of Ar through the tube. Shown in Figure 16 the grains were measured to be about 50μm in length. Using Raman spectroscopy characteristic peaks were measured between the ranges of 380-382cm^{-1} for the E_{2g} peak and 403-405cm^{-1} for the A_{1g} peak, indicating a range of thicknesses from monolayer to multilayer. [44]

(I)

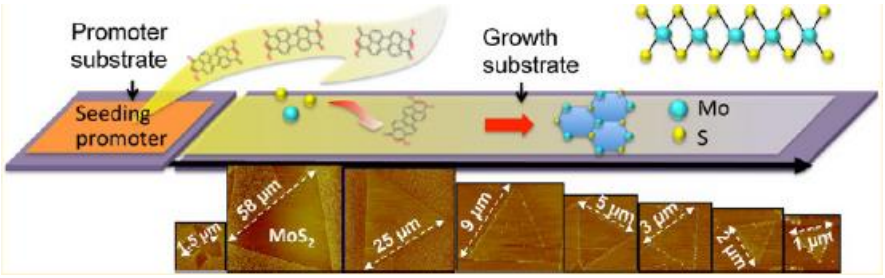

(II)

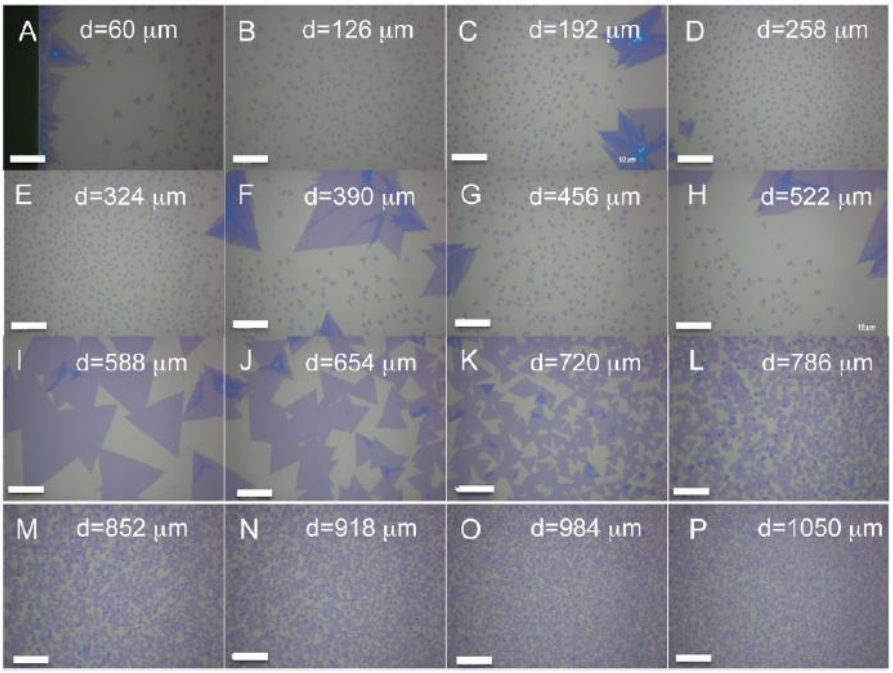

Figure 16: (I) Seeding promoter application. (II) Growth substrate at various distances from promoter substrate. Distances of (a) 60µm, (b) 126µm, (c) 192µm, (d) 258µm, (e) 324µm, (f) 390µm, (g) 456µm, (h) 522µm, (i) 588µm, (j) 654µm, (k) 720µm, (l) 786µm, (m) 852µm, (n) 918µm, (o)984µm, and (p) 1050µm. (the white scale bars for the images are all 20µm) [44]

Chen et al [45] introduced oxygen during the growth to prevent poisoning the precursors and eliminate defects in the growth. MoO_3 and S were loaded, in separate mini quarts tubes (about 10mm in diameter), into a three-zone furnace. The S was placed in the first zone, the MoO_3 was placed in the second and a sapphire (Al_2O_3) substrate was placed in the third zone about 16-18cm away from the second zone. To clean the substrate the third zone was heated to 1000˚C for three hours with an Ar flow at atmospheric pressure.

The three zones were heated to their specified temperatures at a rate of 25˚/min, 115˚C for zone 1, 530˚C for zone 2, 850˚C for zone 3 and stabilized at these temperatures for 20 minutes before growth. Growth took place for 30 minutes with Ar and an O_2 flow varying between 0 and 2sccm. Edge length of the growth was measured with a few grains as large 350µm with a growth time of 40 mins as seen in Figure 17. Raman spectroscopy providing measurements of the thickness; the distance between the characteristic peaks was measured to be 20cm^{-1} indicating that monolayer MoS_2 was present. [45]

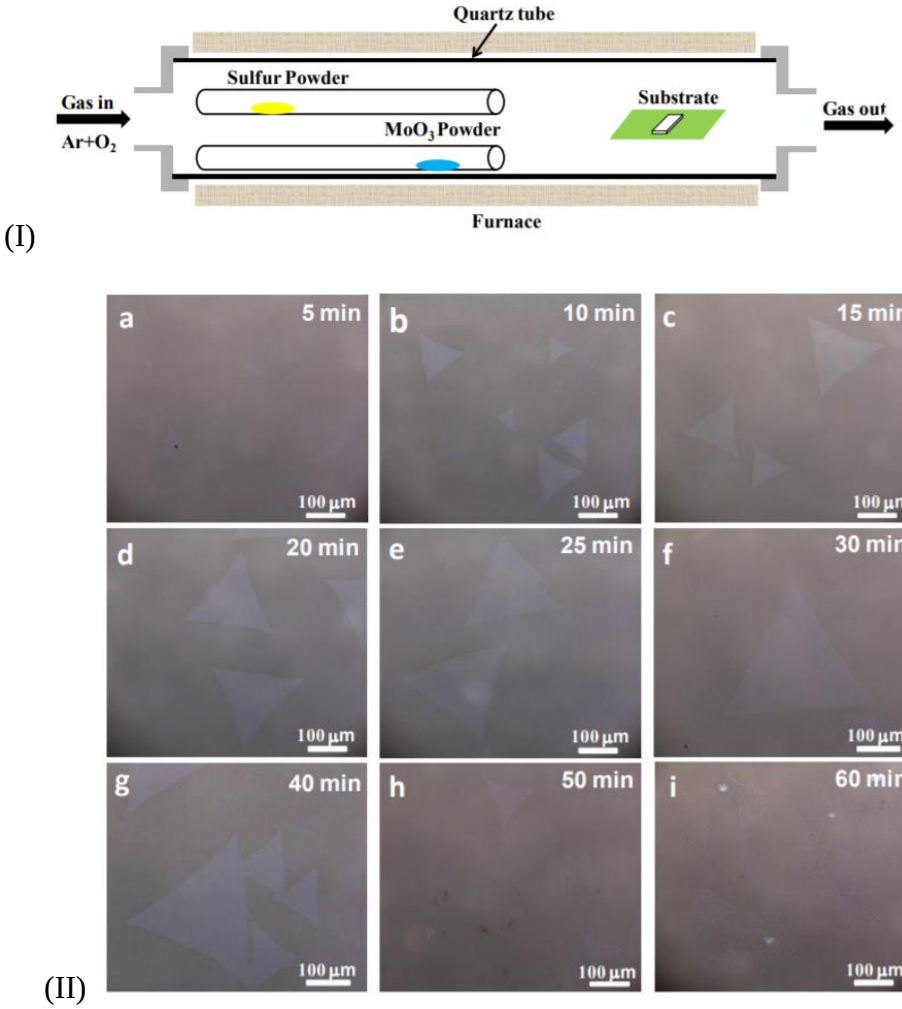

Figure 17: (I) Growth set-up showing substrate, S, and MoO_3 placements. (II) Growth at different durations (a) 5mins, (b) 10mins, (c) 15mins, (d) 20mins, (e)25mins, (f) 30mins, (g)40mins, (h) 50mins, and (i) 60mins [45]

Sina Najmaei et al [6] made an effort to produce monolayer MoS_2 using MoO_3 nanoribbons as a precursor for the CVD process. MoO_3 nanoribbons were placed on a silicon substrate with bare silicon substrates next to it at the center of a tube furnace. At the end of the furnace 0.8-1.2g of sulfur was placed where the temperature was 600˚C. AFM was performed to determine a thickness of about 0.7nm indicating monolayer growth, which was confirmed using Raman spectroscopy to determine the characteristic peak spacing. As seen in Figure 18 (c) MoS_2 growth was measured to have edge lengths of approximately 10μm. [6]

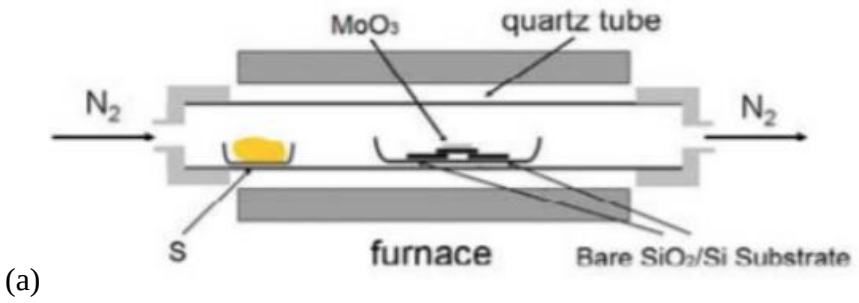

(a)

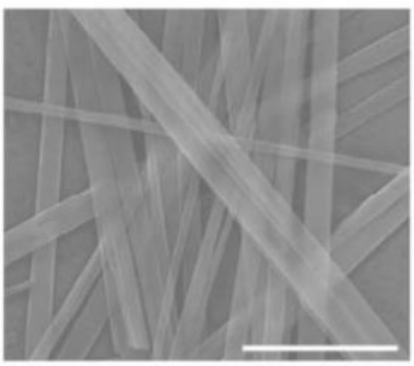

(b)

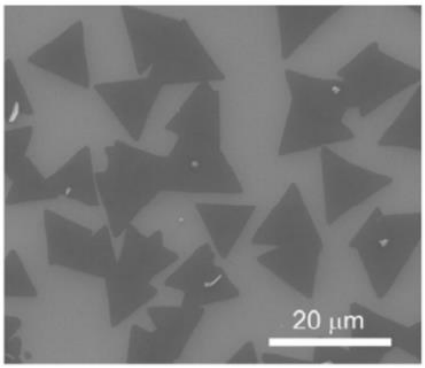

(c)

Figure 18: (a) Experimental setup of furnace, (b) SEM image of MoO_3 nanoribbon, (c) Optical image of MoS_2 growth [6]

S. Inguva et al [46] focused on the angle of the substrate during the growth. SiO_2/Si substrates were held at specific angles between 0^o and 90^o, with 0^o being flat and 90^o standing vertically. The sample was first extensively cleaned via ultrasonication for 3

minutes each in deionized water, acetone, and isopropyl alcohol. This was followed by an immersion in deionized water and an acid piranha solution at 180°C for 20 minutes. Another ultrasonication for 3 minutes each in deionized water and isopropyl alcohol was carried out. Sulfur was weighed out to 1g and placed 10cm upstream of 250mg of MoO_3 which was placed 10cm upstream of the substrate. The furnace was purged with Ar having a flow rate of 400sccm, after which, the furnace was heated to 900°C at a rate of 15°/C, and then held for the 60-minute growth. During the growth the Ar flow rate was set to 100sccm. The setup for the growth can be seen in the following sketch. [46]

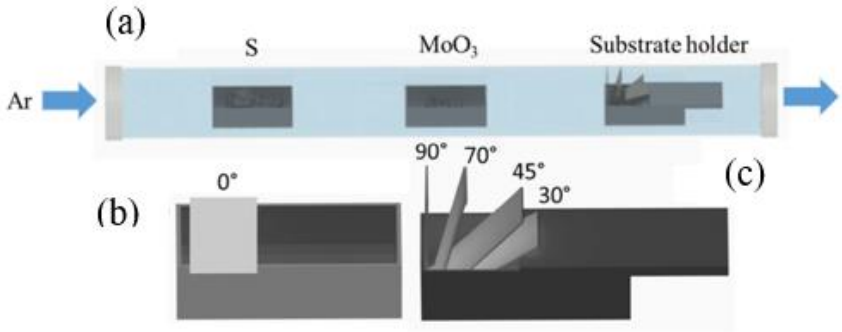

(I)

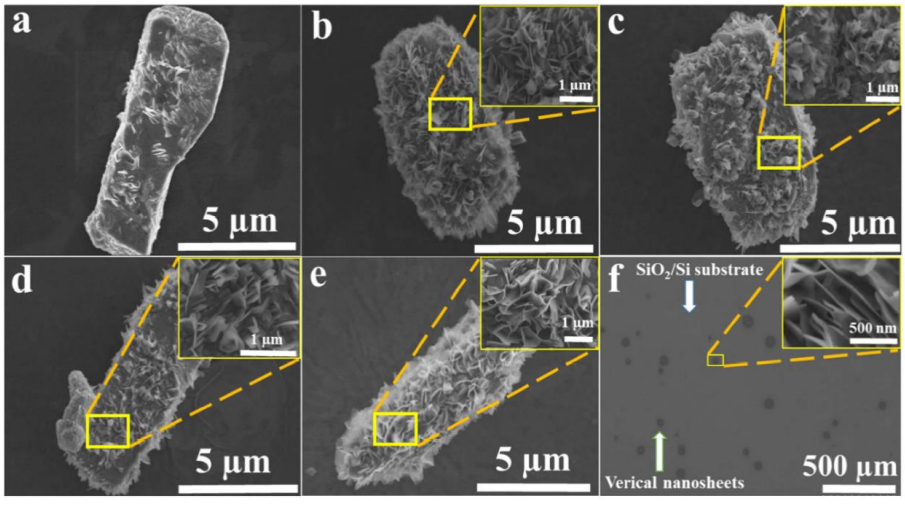

(II)

Figure 19: (I) (a) Experimental set-up for CVD (b) substrate positioned at 0° and (c) substrate positioned at 30°, 45°, 70°, and 90°. (II)SEM images of MoS_2 growth with different substrate angles. (a) 0°, (b) 30°, (c) 45°, (d) 70°, and (e) 90°. (f) A wide view of the 90° substrate. [46]

In this study, as shown in Figure 19 , nanosheets of MoS_2 ranging in thickness from about 1.3~1.5μm. Angle of the deposition substrate affected the length of the microstructure. At an angle of 0^o the average length was approximately 4μm and increased with increasing substrate angle to a length of approximately 8μm at a 90^o angle.

Wang et al [47] examined the effect of growth temperature during the synthesis using a similar single zone CVD furnace. MoO_3 and sulfur powders were used as precursor materials. 3mg of MoO_3 powder was spread out on an SiO_2/Si substrate, with another SiO_2/Si substrate placed face down above the powder as the growth substrate; these were then placed in the center of the furnace. 500mg of S was placed in a Mo boat and placed in the furnace's quartz tube on the upstream side, so as to sit outside of the furnace block. After being flushed with Ar at 100sccm, the furnace was heated at a rate of 18.4^o/min. Once the furnace reached the preset temperature, e.g. 800^oC, 810^oC, 820^oC, 830^oC, 840^oC, and 850^oC, the Mo boat containing S was pushed into the furnace block where the temperature was 200^oC. The furnace was kept at growth temperature for 5 minutes and then allowed to cool down naturally to room temperature. Samples were then studied using Raman spectroscopy, SEM, TEM, and AFM.

Seen in Figure 20, shape of the growth was found to be affected by the temperature of the furnace during the growth. At low (800^oC and 810^oC) as well as high (850^oC) triangular growth was formed, while at temperatures between (820^oC-840^oC) had truncated triangles resulting in hexagons. Throughout the growth temperatures, additional nucleation points appear on the triangles and hexagons. However, grains grown at 810^oC have much less dots on the triangles and even have some without leaving a monolayer growth with an edge length of approximately 5-10μm. AFM was conducted to measure a

thickness of about 6.5μm suggesting monolayer growth, verified by Raman with a characteristic peak difference of 20cm^{-1}. [47]

(I)

(II)

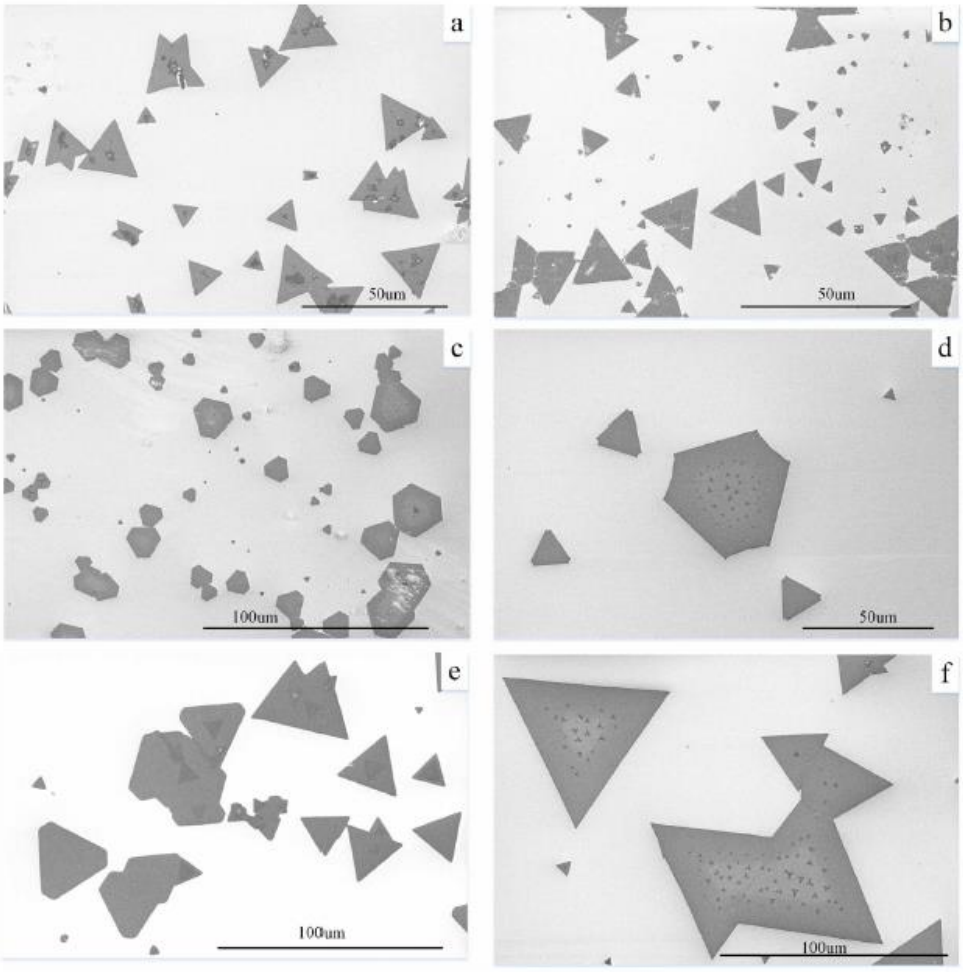

Figure 20: (I) CVD setup for MoS_2 growth. (II) Crystal growth of MoS_2 synthesized at (a) 800°C, (b) 810°C, (c) 820°C, (d) 830°C, (e) 840°C, and (f) 850°C. [47]

A similar MoS_2 growth was conducted by Wang et al [48] by separating S from the MoO_3 and the substrate for sulfur was an insulating plate used to slow the S evaporation so there was enough for the growth. The furnace was heated to 750°C at a rate of

15°/min and held there 30 minutes, after which it was allowed to cool down to room temperature naturally. Pressure inside the chamber was 3.3Pa with an Ar flow of 20sccm. For the precursors, 2g of S was placed upstream near the edge of the furnace block 30cm from the center of the furnace. Si substrates were placed upstream of the 0.1g MoO_3 powder placed at the center of the furnace. Vertical nanosheets were measured to have a thickness of 50-100nm and Raman confirmed the bulk state of MoS_2 with a characteristic peak separation of $25cm^{-1}$. The length of the microstructures was measured to be approximately 1-1.5μm. [48]

(I)

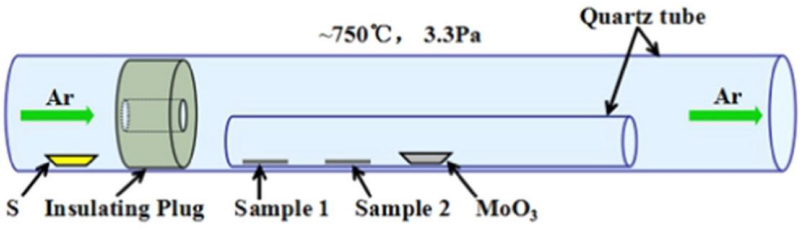

(II)

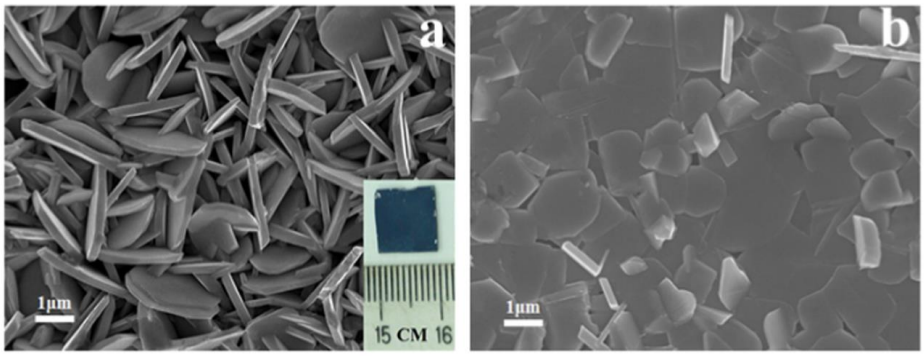

Figure 21: (I) CVD furnace and sample set up. (II) FESEM images of MoS_2 nanosheets taken a) closer to S source and b) closer to MoO_3 source [48]

In another study performed by Wang et al [49], 0.5g of S and 3mg of MoO_3 were used as sulfur and molybdenum sources. MoO_3 was placed at the center of the furnace, sandwiched between two face to face SiO_2/Si substrates, while the S was placed upstream in the cold zone. The furnace was heated to 800°C at a rate of 15°/min and held for the

duration of the growth time with a carrier gas (N_2) flow rate of 80sccm. The setup and reaction mechanism are illustrated in Figure 22. It was determined that the MoO_3 is sulfurated by the S vapor creating a partially sulfurated reactive intermediate. This then becomes sulfurated MoS_2 nanoparticles; the nanoparticles then diffuse to the surface of the substrate to create films of MoS_2. AFM measured a thickness of about 0.71nm, with Raman measuring a characteristic peak difference of 20.7cm^{-1} both of which suggest monolayer growth. The monolayer had edge lengths of around 5-50μm. [49]

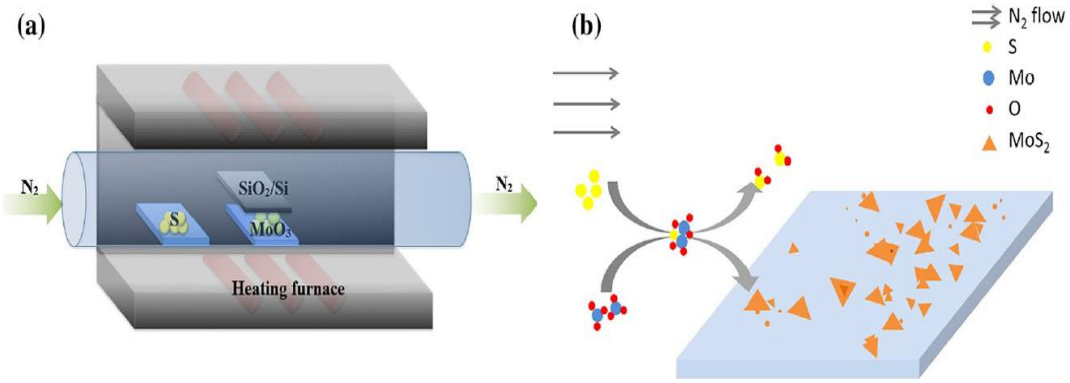

Figure 22: (a) Heating furnace and precursor positioning for CVD growth (b) reaction and nucleation process of MoS_2 thin films [49]

Wang et al [50] thermally evaporated MoO_3 powder and reduced it with S to create MoO_2 microplates on SiO_2/Si substrates. The MoO_2 microplates were then sulfurized during a high temperature (850-950^oC) annealing for 0.5-6 hours creating MoS_2 films. Annealing duration affected the number of layers in the MoS_2 films. AFM was performed to determine the thickness of the MoS_2 film on the MoO_2 microplate. A thickness of about 1.5nm was measured suggesting bilayer film on the microplates; occasionally single layer flakes were detected at about 0.8nm. Grain size was determined

by measuring the edge length of the growth; the largest grains reported were about 10-20μm. [50]

A group of researchers (Zafar et al [51]) studying the intrinsic optical quality of MoS_2 films synthesized their films via a CVD process as well. Growth substrates SiO_2/Si and precursors MoO_3 and S were placed at the center of the furnace and 30cm upstream of the center, respectively. The furnace was prepared for the growth by pumping the pressure down to 10^{-1} Pa and flushed with 200sccm of Ar, the temperature was then raised to 105°C for an hour to remove any water left in the tube. The Ar flow rate was set to 10sccm for the growth, while the furnace was heated to the growth temperature (600-900°C) at a rate of 15°/min; it was then held at the growth temperature for 5 minutes. During the growth the S was kept at 230°C. After the growth, the furnace was allowed to cool down to a specific temperature before being rapidly cooled to room temperature by opening the furnace and increasing the Ar flow rate to 200sccm. Edge length of the samples was measured to be approximately 5-10μm. [51]

One study performed by Zheng et al [52] focused on controlling the growth of six-point star shaped MoS_2 grains also used a single zone furnace with S and MoO_3 powders as precursor sources. SiO_2/Si substrates were prepared by cleaning with acetone, isopropanol alcohol and deionized water. 0.6g of S was placed near the left zone of the furnace, while 30mg of MoO_3 was placed in the right zone of the furnace with the Si/SiO_2 substrates placed 3-4cm downstream of that. The furnace was purged with 1000sccm of Ar for 10 minutes; after purging, the Ar flow rate was reduced to 10-15sccm during the growth. For the growth, the right zone of the furnace (MoO_3) was heated to 680°C at the same time, the left zone of the furnace (S) was heated to 250°C. Once the

right zone reached 680°C the S was pushed into the left zone of the furnace and kept there for the duration of the growth (5-30 minutes). After the growth, the furnace was allowed to cool down to room temperature. The samples were studied using Raman, PL, SEM, and AFM. The experimental setup and SEM image is shown in Figure 23. Thickness of the MoS_2 stars was determined using Raman spectroscopy. The frequency difference between the E_{2g} and A_{1g} peaks was found to be $21cm^{-1}$ indicating that the growth was monolayer. [52]

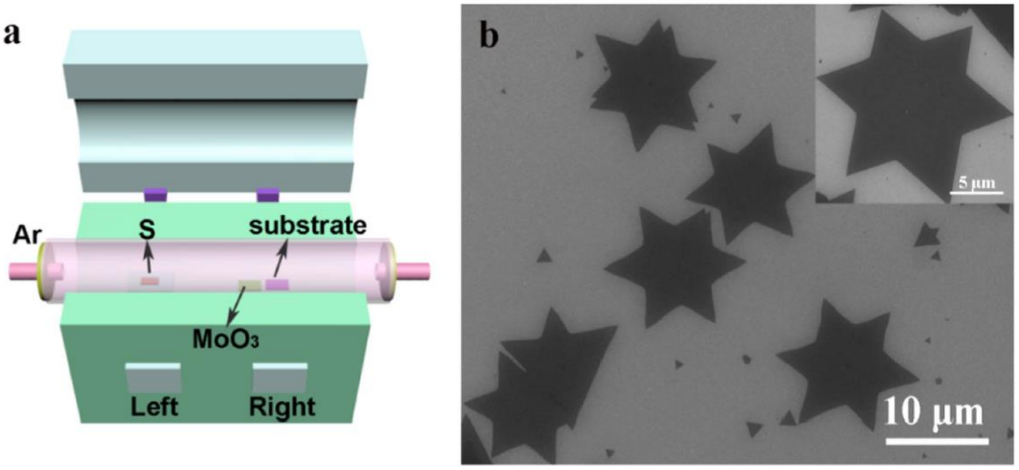

Figure 23: (a) CVD set-up for MoS_2 growth (b) SEM imaging of MoS_2 grains [52]

Dumcenco et al [53] conducted a study to grow MoS_2 films on a sapphire substrate via CVD. Substrates were placed face down above a crucible holding about 5mg of MoO_3 powder; while about 350mg of S was placed upstream from the growth substrate. The furnace was purged at 300°C for 10 minutes with an Ar flow rate of 200sccm; after purging, the furnace was heated to 700°C and held there for 10 minutes with a flow rate of 10sccm. After growth, the furnace was allowed to cool down naturally to 570°C at which point the Ar flow rate was increased to 200sccm and the furnace was opened for rapid cooling of the sample. Using optical microscopy, small grains can be seen near the

edge of the sample (Figure 24 (a)) and can also be seen starting to form together near the center of the sample (Figure 24 (b)). Raman was conducted finding a peak separation of $20cm^{-1}$ suggesting monolayer growth.

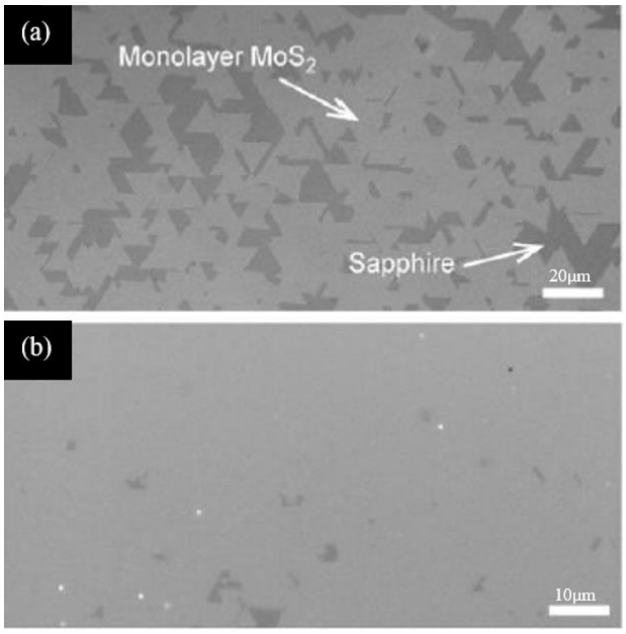

Figure 24: Optical image of MoS_2 grown on sapphire substrate. near (a) edge and (b) center of sample. [53]

Research conducted by Guo et al [54] humidity sensor devices were manufactured on the MoS_2 films via e-beam lithography. The films were prepared using a CVD system. First, 4nm of Mo was deposited onto a sapphire substrate by e-beam deposition. The Mo layer was then sulfurized in a CVD furnace using an H_2S/H_2/Ar gas mixture. Sulfurization was carried out at 1000°C and 1.33kPa, for 20 minutes, after which the substrates were quickly cooled to 500°C. AFM and SEM were performed to determine the quality of the MoS_2 films. Thickness of the film was determined to be 9nm which when considering the measured surface roughness of the film of 3-4nm, it is likely to be monolayer. [54]

Wen et al [55] researched the use of MoS_2 as a transistor was studied with fabrication methods of thermal vapor sulfurization (TVS) and thermal vapor deposition (TVD), both are variants of a CVD process. In a TVS process the growth substrate is first covered with a molybdenum source, either Mo or MoO_3, and then sulfurized by the sulfur vapor. While the TVD process is the same as the CVD growths previously addressed, in which, the sulfur and molybdenum source are both deposited on the surface at the same time. MoO_3 and S precursors are loaded in separate heating zones of the furnace. Growth occurs on a SiO_2/Si substrate under a pressure of 30-Torr, with a carrier gas (Ar) flow rate of 70sccm. The temperature of the heating zone at the MoO_3 is held at 700^oC while the temperature at the S source varies between 140^oC and 152^oC with a step of 3^oC. Raman spectroscopy data was collected with the characteristic peaks difference being measured between 19.7cm^{-1} and 25.5cm^{-1}, which was used to determine that the film varied in thickness between monolayer and bulk. [55]

Wang et al at the University of Oxford [56] studied the growth of MoS_2 on multilayer h-BN compared to growth on SiO_2/Si. This was accomplished by first growing h-BN on a copper foil, via CVD at atmospheric pressure, with ammonia borane as a precursor; after growth, the h-BN film was transferred to a SiO_2/Si substrate. MoS_2 was then grown on either the h-BN film on SiO_2/Si or directly on SiO_2/Si. For the synthesis of the MoS_2 film, MoO_3 and S were used as the Mo and S sources during the CVD growth. Using a two-zone furnace, S was placed in the center of furnace 1, while MoO_3 was placed about 2cm from the upstream opening of furnace 2. The furnaces were then flushed with Ar for 60 minutes, followed by introducing S to the growth region by heating furnace 1 to 180^oC for 15 minutes. Next, furnace 2 was heated to about 800^oC, causing the MoO_3 powder to

heat to about 300ºC and kept at this temperature with an Ar flow rate of 150sccm for 15 minutes; then reducing the flow rate to 10sccm and holding for 25 minutes. After the growth was complete, optical measurements were taken to find the average grain size; while Raman spectroscopy and PL were conducted to determine thickness of the films. Average grain size for both methods was found to be about 3-5μm, and characteristic peaks found via Raman were found to have a frequency difference of about 20.5cm^{-1} indicating monolayer growth. The grain shape, however, was affected by the h-BN film causing truncated triangles (Figure 25 (c)). PL was able to verify monolayer growth by finding MoS_2 peaks at about 625nm and 670nm, matching other reported values for monolayer MoS_2. [56]

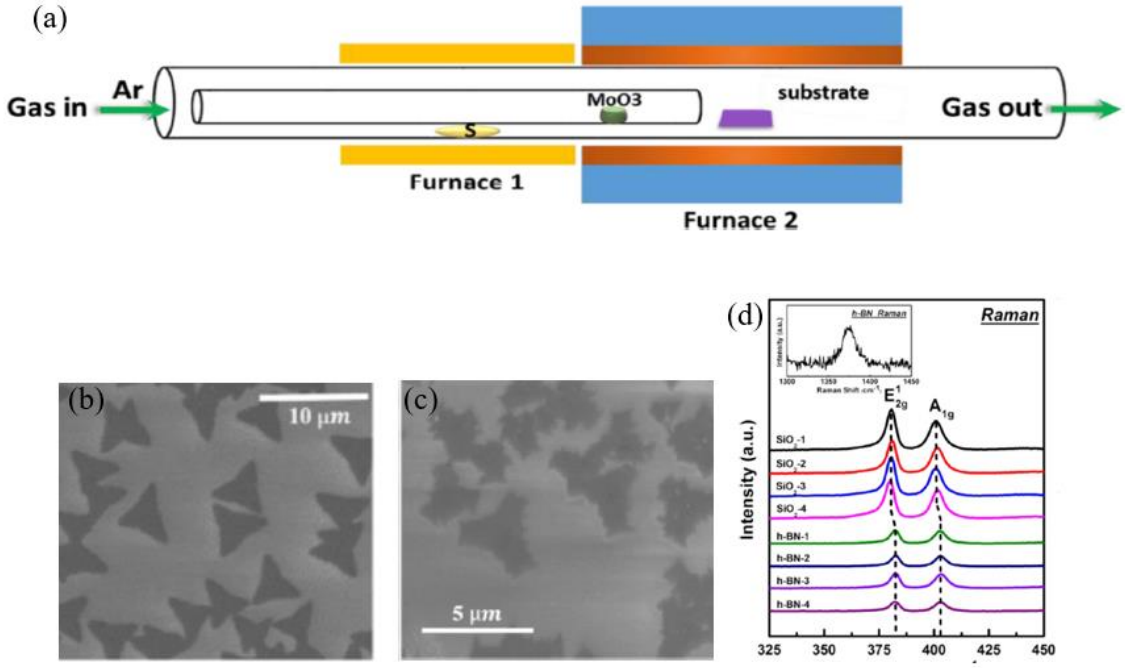

Figure 25: (a) Furnace setup for CVD growth, (b) optical image of MoS_2 grown on SiO_2/Si substrate, (c) optical image of MoS_2 grown on h-BN film, and (d) Raman data comparing MoS_2 growth on SiO_2/Si and h-BN.[56]

Samad et al [57] conducted a similar study of growing MoS_2 on other heterostructural films. First graphene, TaS_2, or SnS_2 was placed on to the growth substrate; then the synthesis of MoS_2 was carried out. $MoCl_5$ and S were used as precursors for the growth. The growth substrates were placed about 1cm away from the center of the furnace and heated to 420°C for a time of 1-2 minutes. Raman, AFM and PL were conducted to characterize the films growth. Raman with a peak separation of $21.5cm^{-1}$ suggested monolayer growth, which was confirmed by PL with the characteristic peaks at 630 and 680nm. AFM was carried out to determine that the film was uniform in thickness. [57]

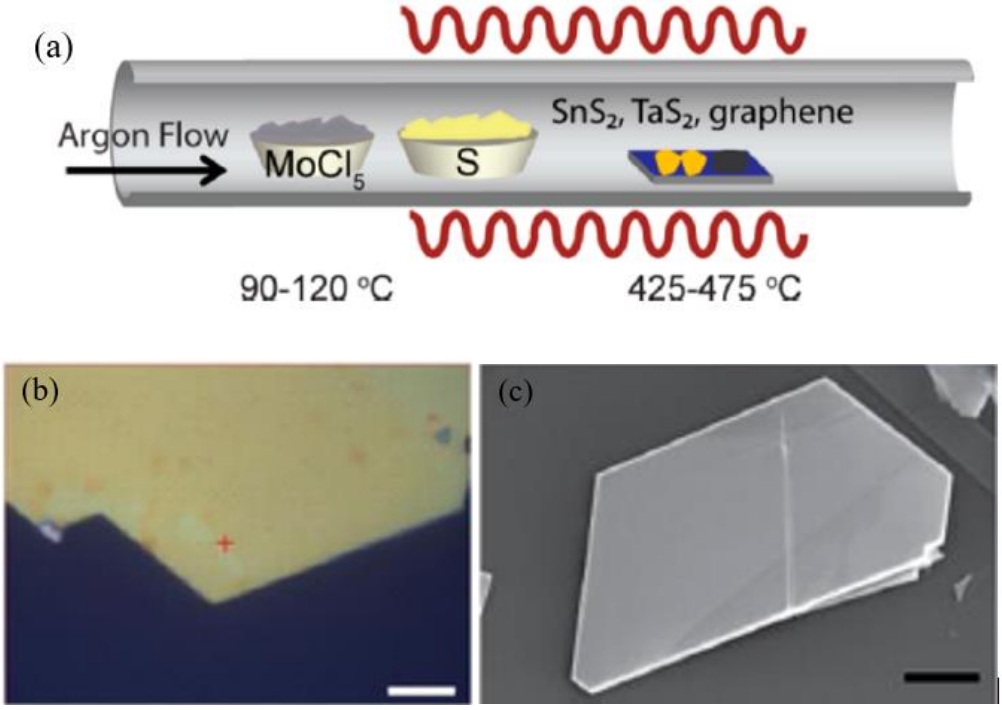

Figure 26: (a) Furnace setup for CVD growth, (b) optical image of single layer MoS_2-SnS_2 heterostructure (scale bar is 20μm), and (c) SEM image of single layer MoS_2-SnS_2 heterostructure (scale bar is 40μm). [57]

While much research has gone into the fabrication and application of MoS_2, there is still much need to study MoS_2 in order to improve process and development of the film. Researchers have been able to produce large area MoS_2 films with edge lengths as large as 50μm, however there is often still impurities across the surface of the film, such as nucleation sites for additional layers of MoS_2. Producing large area nanosheets with a thickness closer to that of bulk MoS_2 has also been achieved, however many of the electronic attributes of monolayer MoS_2 diminish with an increase in film's thickness. For these reasons, it is necessary to continue studying MoS_2 in order to produce a low impurity monolayer film at a large scale.

3 Experimental Aspects of This Study

3.1 CVD Growth

3.1.1 The CVD setup

The method used for molybdenum disulfide synthesis in this study was chemical vapor deposition. The tube furnace (Thermo Scientific™ Lindberg/Blue M™ Mini-Mite™ Model TF55030A-1) has the capability of programming a temperature profile. This is a single zone furnace, designed to hold a 1 inch diameter tube; the heated zone is 12 inches in length, with a temperature range between 100^{o}C and 1100^{o}C. [58] The tube for the furnace was 1 inch in diameter and 24 inches in length, allowing for space to place the S powder just outside the furnace block.

The precursors are molybdenum trioxide (MoO_3) powder and sulfur (S) powder. Sulfur (>99% purity) will begin to melt at a temperature of 118 ˚C and with a flash point at 207 ˚C. [59] At atmospheric pressure MoO_3 has a melting temperature of about 1250^{o}C. [60]

3.1.2 Growth Procedures

Experimentally, the predetermined amount of precursors, i.e. MoO_3 and S, were measured and placed into quartz boats upstream from the growth substrate in the quartz tube. The substrate was placed in the center of the quartz tube, where the thermocouple is located and the furnace will be at the set temperature.

The furnace was firstly purged with argon gas. The tube furnace was programmed to stay at room temperature for the time of purging and was then to increase the temperature at a rate of 15˚C per minute until it reached the growth temperature. Once the furnace reached the growth temperature, it was held at that temperature for a desired amount of

time (1-10 minutes) before being allowed to cool back down. The furnace was then allowed to cool down to a specified temperature at which point the contents of the tube furnace were removed and the substrate was analyzed. The temperature at which the furnace was opened, and the substrate and quartz boats were removed, is referred to here as the quench temperature.

The general schematic of the growth parameters can be seen Figure 27 below. MoO_3 sits upstream of the substrates which are placed at the thermocouple of the furnace. S is placed further upstream so that part of the boat is partially in the furnace block, in order to get the S to reach the appropriate temperature. The seeding promoter, when used, was placed on the substrate where the PTAS is labeled.

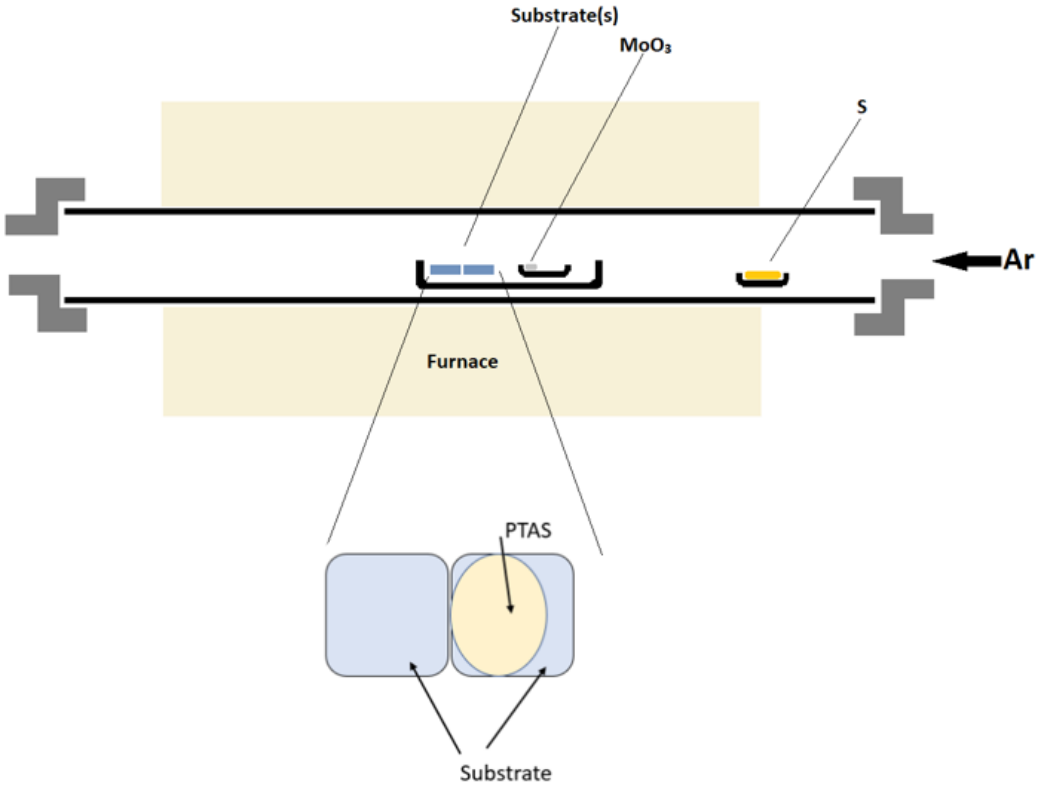

Figure 27: Schematic of growth parameters. (Top) Substrate and precursor positions inside furnace tube. (Bottom) Growth substrates and seeding promoter placement.

3.2 Growth Variables

There were a variety of variables that were considered when determining the optimal growth conditions. Such variables include position of precursors, type of substrate, substrate surface treatment, seeding promotors, promotor application method, promotor concentration, the growth time, carrier gas flow rate, quenching temperature. etc.

3.2.1 Position of Precursors

With the one-zone furnace, the tube is not heated evenly or retain the same temperature along the length of the furnace. The temperature of positions further away from the center of the furnace will gradually decrease from the setting furnace temperature. In consideration of the temperature gradient that is present within the furnace and properties of the two precursors, the sulfur powders were placed much further upstream (almost out of the tube furnace to allow it to sublime rather than burn out), whereas the molybdenum oxide was placed near the thermocouple in the furnace for its high melting temperature. Towards optimizing the growth, the exact positions of the two precursors were varied and the results of the growth were accessed.

The position of the precursor powders was altered until it seemed as though an ideal set of position parameters had been determined. For instance, the MoO_3 powder was placed in varying distances, with relation to the growth substrate, from being directly beneath the substrate to a distance of 2 inches upstream of the substrate. While the sulfur positioning was much more limited, as moving the sulfur too far into the furnace resulted in burning rather than sublimation and too far away from the furnace block presented no sulfur vapor into the chamber for growth. As a result, it was determined that placing the MoO_3 powder 1.75 inches upstream of the substrate and placing the sulfur so that the

downstream edge was ¼ inch inside of the furnace block edge while the rest of the sulfur boat rested outside of the furnace block.

3.2.2 Growth Time

Different growth times were considered ranging from 1 minute to 10 minutes, the furnace was kept at the growth temperature for the chosen duration of the growth time.

3.2.3 Carrier Gas Flow Rate

Argon was used as the carrier gas for the growths. The flow rate for the carrier gas was set at varying rates between 100sccm and 500sccm. It was decided that the optimal flow rate was between 200sccm and 400sccm.

3.2.4 Quench Temperature

Different quench temperatures were observed to determine if there was a large impact from the temperature at which the growth was ended. There was no distinct difference between the growths that were quenched at higher temperatures compared to growths that were allowed to cool down to room temperature.

3.2.5 Substrate

Lastly, a variety of substrates were used. The most common substrate used was SiO_2/Si, however sapphire was also used as was platinum and HOPG.

Sapphire substrate has a similar lattice structure as MoS_2 which made it likely to serve as a good deposition substrate.

MoS_2 is a semiconductor. It would be interesting to be able to grow MoS_2 on conductive substrates for some electrical characterization and device. In this study, growth on Pt coated on sapphire as well as HOPG substrates were explored.

Graphene and molybdenum disulfide have similar lattice structures which suggests that a film of MoS_2 might deposit on the graphene. However, due to the high temperature used for growth, the graphene did not often maintain its structure. The graphene burned off the substrate at higher temperatures.

3.2.6 Substrate Surface Treatments

Two different approaches were explored to treat the surface of the sapphire substrate which are physical scratching and plasma chemical etching. Different patterns of scratches as well as different levels of power and exposure time for the plasma etcher were tested.

Two sets of scratches were examined (see Figure 28). The first substrate has a set of three scratches around the center of the substrate. The second substrate has a set of 5 scratches with 4 on the upstream side and one near the downstream side, considering most growth nucleates at the upstream.

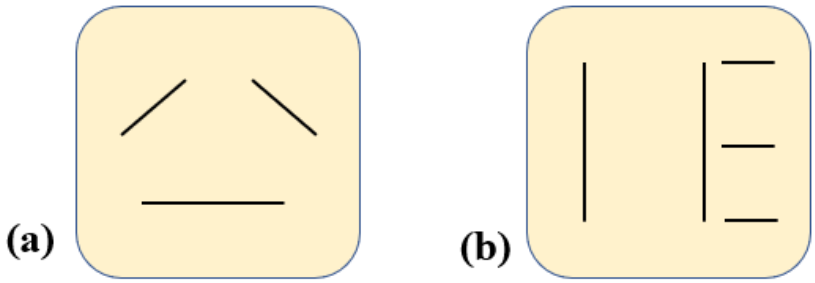

Figure 28: Scratch configuration for 3 and 5 scratch surface treatment

In this study, the substrate surface was subjected to oxygen plasma etching, which is commonly used for cleaning the surface of a substrate. At higher plasma power and exposure time plasma etching can cause small defects that remove, on an atomic scale, bits of the substrate's surface. These defects make good nucleation sites for depositing a

thin film. The O2 pressure was kept at 2 bars. Etching duration and power of plasma etching examined are at 3min at 50 W, 5 min at 50 W, as well as 30 seconds, 1 min and 5 minutes with a power of 100 watts.

3.2.7 PTAS Promotors

One major treatment is the use of a seeding promoter PTAS (perylene-3,4,9,10-tetracarboxylic acid tetrapotassium salt). This salt is known to facilitate monolayer growth via catalyzing the reduced metal oxide (molybdenum oxide) on the substrate. [61] PTAS is soluble in water. In this study, a PTAS solution was deposited on the surface of the substrate before being placed in the furnace. The experimental variables are its concentration and application method (droplet, spray, or spin coat).

The first method of application was to place a droplet of PTAS solution onto the surface. By drying the substrate with a nitrogen gun, it removed most of the PTAS that was being placed on the sample, which is not beneficial for the MoS2 growth. This method was discarded in the following experiment.

Instead, the PTAS was applied to the growth substrate and then allowed to dry on a hotplate. Water evaporated from the solution leaving the PTAS on the substrate.

This increase the amount of PTAS left on the substrate. A few different temperatures were examined. For the previous examinations the PTAS concentration was also considered by changing the number of droplets on the surface. This application created a coffee ring of PTAS on the surface which is not desirable.

In an effort to have a more uniform distribution of PTAS on the growth substrate a new mixture of the PTAS solution with isopropyl alcohol (IPA) was created to use an airbrush

spray the PTAS onto the substrate. The effect of PTAS concentration was observed by changing the number of sprays applied to the growth substrate.

To eliminate/decrease the number of defects from PTAS on the growth substrate, the last method was carried out by placing PTAS droplets on a separate substrate which was placed on the upstream side of the growth substrate.

3.3 Characterizations

3.3.1 Optical Imaging and ImageJ Quantification Analysis

Most of the growth samples were examined by optical microscopy. The images were taken using the Zeiss Axiotron microscope and the AxioVision Rel. 4.7 software. After the growth process samples were placed under the microscope for rapid assessment. Images were taken at various magnifications across the sample in order to gain the first-hand information of the size and coverage of the MoS_2 grains.

ImageJ software was used to process select images, for better quantitative analysis of the grain sizes and coverage. The basic steps of processing the images are as the following. The contrast between growth and the substrate in the image was first enhanced, and then the image was converted to a gray scale image for thresholding. Thresholding is an image segmentation technique that converts the image into a binary (black/white) image. [62] By doing this the grains can be clearly defined from the substrate. Following the thresholding, a particle analysis was done that measured the area of individual grains. This data was then able to be presented as a histogram showing the percentage of measured grains that fall into bins of specified sizes; it was also then possible to show the percentage coverage by each grain size across the surface of the substrate.

3.3.2 Scanning Electron Microscopy and Energy Dispersive X-Ray Spectroscopy

Scanning electron microscopy is another characterization technique that provides more analysis of the film's composition and a better visual of the grain topography of the sample.

In principle, the impinging electrons inelastically transfer energy to the electrons and lattice of the sample. The interaction of the primary beam with the surface of the sample creates varying excitation energies for the electrons on the surface. These energies are dependent on the penetration depth of the primary beam. A shallower penetration depth will excite a large number of low-energy electrons to be emitted from the near surface region, electrons of this nature will be called secondary electrons. While a deeper penetration of the primary beam will cause a lower number of high-energy electrons to be emitted from deeper into the sample, electrons emitted in this manner are known as back scattered electrons. An even deeper penetration could cause much higher-energy electrons to be emitted called x-rays.

In thin films, the most commonly observed electrons are secondary electrons that have been emitted from the surface or near surface area. By focusing the lens, through which the primary beam travels, the spot size on the surface can be narrowed down to about 10Å. Once the detector collects the electron energies, a topographical image for the scanned area can be formed. This topographical image can help to determine the relative thickness of nucleations and growths on the surface. In the monochromatic images, it is generally the case that the brighter regions of the image are thicker than the darker regions. [39]

While SEM can provide a good topographical depiction of the sample, energy dispersive x-ray spectroscopy (EDX/EDS), by collecting the excite x-rays from the studied sample with the help of an Si(Li) detector, is a valuable technique for identifying the chemical components of the sample. The spectrum is presented as the counts against the voltage range. [39] Each element has different counts at different voltage ranges, allowing the composition of the film to be determined by looking for the characteristic peaks of Mo and S in the spectrum.

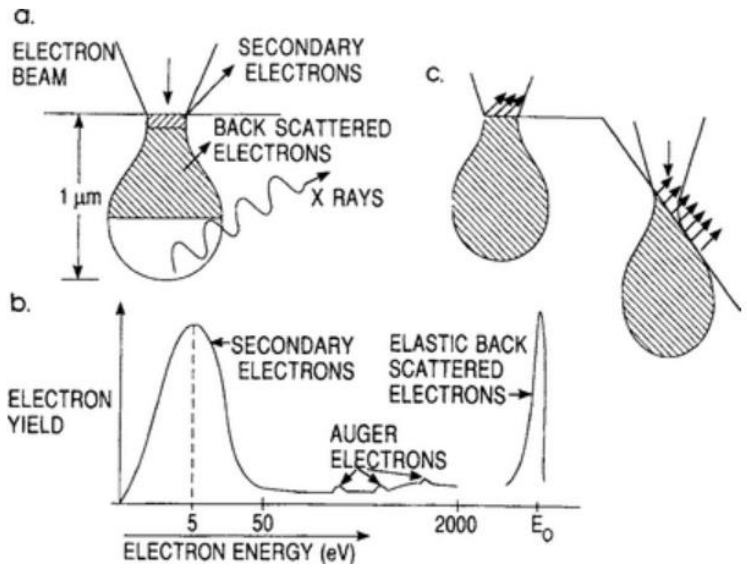

Figure 29: (a) Penetration depth profile of primary electrons on surface (b) spectrum of emitted electrons from surface (c) electron emission effected by surface topography. [39]

In this study, SEM a primary beam of electrons (1keV∼5keV) was usually used to imaging and (5-10 keV) was used for EDS analyze the MoS_2 film samples. The SEM/EDS characterization was performed on Gemini Scanning Electron Microscopy.

3.3.3 Atomic Force Microscopy

The atomic force microscopy (AFM) technique provides another opportunity to gain a topographical understanding of the sample. Using a soft spring cantilever with a sharp

tip on the end, the topography of the sample can be measured mechanically. In order for this technique to be successful it was determined that the cantilever spring constant needed to be less than the value of spring constant understood to exist between atoms. Also, the force being applied to the surface needed to be large enough to detect surface changes but no so large that it would displace any of the atoms on the surface being studied. There are two main methods of AFM, contact and non-contact. In contact AFM the tip on the cantilever comes in contact with the surface of the sample. The forces of contact AFM are typically in the range of 10^{-6} to 10^{-8} N. Non-contact AFM makes use of van der Waals forces; in this method, when the tip and the surface are widely separated van der Waals forces will weakly pull them together. Similarly, when the tip and the surface get too close together, electron clouds overlap and van der Waals forces will cause them to repulse from one another. The cantilever needs to be stiffer in non-contact AFM to prevent contact with the surface, this affects the forces applied to the surface, usually resulting in forces as low as ~10^{-12} N. [39]

In this study, AFM data and images were collected using the Agilent 5420 SPM/AFM microscope ran on contact mode.

3.3.4 Raman Spectroscopy

While the optical, SEM and AFM images can give a general idea of the size of the growth, it does not provide much information about the thickness of the growth. Raman spectroscopy was often used to assess the quality and the thickness of the MoS_2 grains/films. For this experiment the Raman equipment used was a Renishaw Raman spectrometer with 514 nm laser.

Raman spectroscopy is based on the inelastic scattering of light from a laser source in the visible or near infrared wavelength range. The light interacts with the molecular vibrations on the surface of the target, the reflected light is then collected by a detector and the change in the energy is determined. This change in energy gives a unique "fingerprint" for each element. Every material has a series of peaks correlated to the wave number of the input signal, with varying intensities. Raman spectroscopy is a tool used to observe the vibrational movement across atoms bonded together.

Every atom has three degrees of freedom; these are the directions that it can move independently of the other directions. In a cartesian coordinate system they are the x, y, and z directions. Molecules are a grouping of atoms, that are bounded to one another, representing the smallest fundamental unit of a chemical compound. The degrees of freedom of a molecule can be described mathematically by the equation $DF = 3n - 6$, where DF is the degree of freedom and n is the number of atoms in the molecule. A molecule will have the same three degrees of freedom as an atom, in which all atoms of the molecule will move simultaneously in one of the three directions of the cartesian coordinates. There are three additional degrees of freedom which describe the rotation of the molecule about principle axes of the inertial ellipsoid of the molecule. Again, the atoms in the molecule will remain unchanged with respect to each other. The remaining degrees of freedom describe the change in bond lengths and angles between the atoms of the molecule. The bonds between atoms are elastic and, as a result, allow periodic independent motion of the atoms. Vibrations among the atoms in the molecule give rise to a specific energy state. Quantum mechanics has shown that molecules will only exist

in definite energy states, and that as the energy of the molecule increases, the distance between the energy states will decrease. [63]

By exposing the molecule to light, it can absorb the energy of the light, via vibrations, and be excited from one energy state to the next. The same vibrational excitement can also be accomplished by the inelastic scattering of photons with a high energy, this is known as the Raman effect. Photons are emitted from a laser source in the direction of the specimen being studied. The electric field from the photons causes an induced dipole moment in the molecule. When the incident photons interact with the molecule those that are at the wavelength of the excitation radiation will be adsorbed. As a result, the photons emitted from the molecule will have a longer wavelength, indicating the decrease in the photon energy. Different bonds will have different energies for the excitation radiation, depending on the composition. Every bond will have a characteristic value for the excitation radiation that is specific to that particular kind of bond, this allows the decay of the photon energy to detect what chemical bonds are in the molecule. The shift in frequency, from the change in wavelength, is recorded and used to determine the composition of the molecule. [63] When the frequency shifts are plotted, peaks will be present at the frequencies representative of the excitation radiation. The Raman spectroscopy results are plotted as Raman shift / cm^{-1} vs intensity.

There are several peaks that denote MoS_2 on a Raman scattered plot, such as, 32 cm^{-1} (E^2_{2g}), 286 cm^{-1} (E_{1g}), 383 cm^{-1} (E^1_{2g}) and 408 cm^{-1} (A_{1g}). The E^2_{2g} peak comes from the vibration between multiple S-Mo-S layers, which would be a weak signal in thin films and non-existent in a monolayer film. The E_{1g} peak is not visible during backscattering and has a weak signal as well. S atoms vibrating in opposite directions

with respect to the Mo atoms in the middle causes the E^1_{2g} peak to be noticeable in all thickness of the film or bulk. Lastly, the A_{1g} peak derives from the out-of-plane vibrations of the S atoms already vibrating in opposite directions.

For thin films, the two characteristic peaks most commonly used for detecting MoS_2 are the E^1_{2g} and A_{1g} peak. These peaks are subject to shifting from different interactions within the sample and substrate. The thickness of the film affects the difference between the two characteristic peaks. It is commonly accepted that a difference of about $20cm^{-1}$ between the peaks suggests that the film is a single layer, and that a difference of $22cm^{-1}$ indicates a two-layer film, once the peak distance reaches about $24cm^{-1}$ the films is assumed to be multilayer to bulk. [64] [63]

Figure 30 is a representative Raman spectrum of MoS_2 taken with an incident laser of 488nm. Raman data collected by the 514nm laser provides similar results, however the incident laser wavelength effects the exact positioning of the resultant peaks.

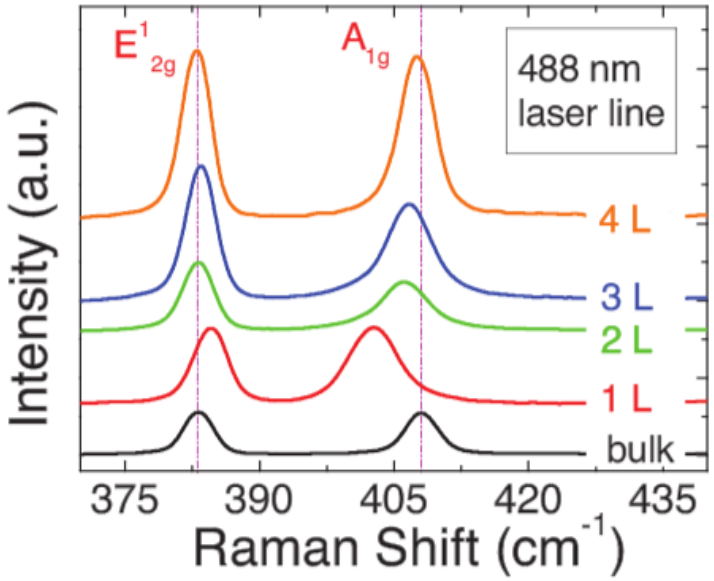

Figure 30: MoS_2 characteristic peaks of bulk, 1 layer, 2 layers, 3 layers and 4 layers. [64]

The wavelength of the incident laser will cause a slight shift in the position of the characteristic peaks along the Raman shift axis. This is to be expected, as the collected data derives from scattered light (from the incident laser) due to its interaction with the target atoms and molecules; the frequency of the scattered light is dependent on the frequency of the impinging laser light. Table 1 shows the variation in position of the peaks as a result of a change in the initial laser wavelength.

Laser	**E_{2g}^1 Mode Frequency (cm^{-1})**					**A_{1g} Mode Frequency (cm^{-1})**				
(nm)	1 L	2 L	3 L	4 L	bulk	1 L	2 L	3 L	4 L	bulk
325	384.2	382.8	382.8	382.7	382.5	404.9	405.5	406.3	407	407.8
488	384.7	383.3	383.2	382.9	383	402.8	405.5	406.5	407.4	408
514.5#	384.3	383.2	382.7	382.3	382	403	404.8	405.8	406.7	407.8
514.5*	386.1	383.1	-	383.7	383.3	404.7	406.8	-	408	408.6
532	384.7	382.5	382.4	382.4	383	402.7	404.9	405.7	406.7	407.8
632.8	385	383.8	383.3	382.9	381.5	403.8	404.8	405	406	406.6
632.8*	386.4	383.1	-	383.3	382.8	405	406.2	-	407.3	408.3

Table 1 Characteristic E_{2g}^1 and A_{1g} peaks of monolayer MoS_2 excited by lasers of different wavelengths.[65]

4 Results and Discussion

The results of MoS_2 grown at different conditions are presented here. The impacts of the growth variables on the quality of the MoS_2 films will be discussed.

4.1 Preliminary Optimization

4.1.1 Processing Settings

The first goal was to determine the optimal amount of precursor powders (MoO_3 and S) and their subsequent positions. This was determined after using a similar study as a guide for initial settings, such as the growth temperature profile and powder amounts. The temperature profile started at room temperature (~20^o C) with a 30-minute purge of the furnace by flowing the argon through the furnace at ~20SCFH (~9500 sccm). After purging the furnace, the temperature was raised to the growth temperature (typically 650^{o}C) at a rate of 14 ^{o}/min (45minutes). The temperature was held for the set growth time. Afterwards, it was allowed to cool back down naturally to the ambient temperature.

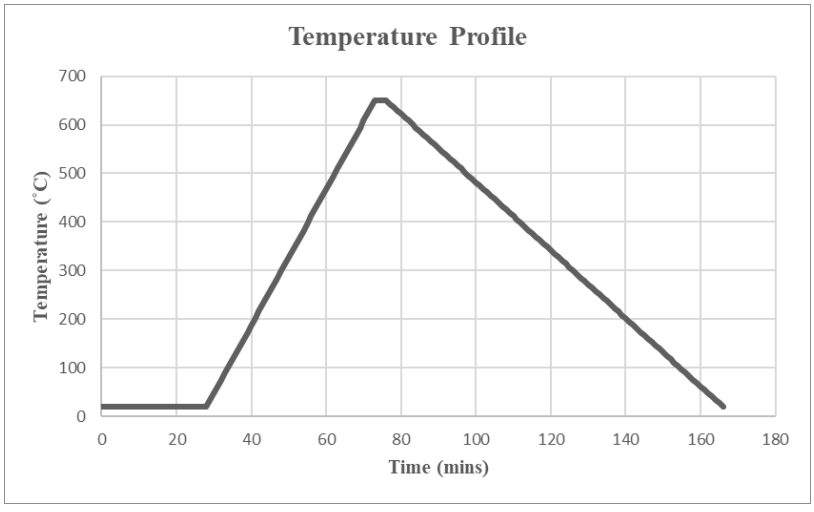

Figure 31: Typical temperature profile for growth

In an effort to determine the effect of growth temperature on the film development, a set of growths was also carried out at 750^{o}C. Different growth times were studied ranging between 1 and 10 minutes, e.g. growth time was carried out for 1, 3, 5 or 10 minutes.

4.1.2 Sulfur Position

With the growth temperature set at 650^{o}C the sulfur needed to be placed far away from the center of the furnace so as not to be burnt off before growth occurs but not too far away to have temperature below sublimation temperature. The measured S was placed with the downstream edge of the boat just inside the furnace block at distances of 4/16, 3/10, and 4/10 inches.

Experimentally, it was observed that the sulfur appears to be burned at a placement of 4/16 inches. As a result, sulfur vapor was not at a suitable concentration for growth and deposition of the film. At settings of 3/10 and 4/10 inches the sulfur did not burn and hence growth of MoS_2 grains was observed across the substrate. With the S setting at 3/10 inches the growth was substantially thicker compared to the growth carried out at a S setting of 4/10inches, as seen in Figure 32.

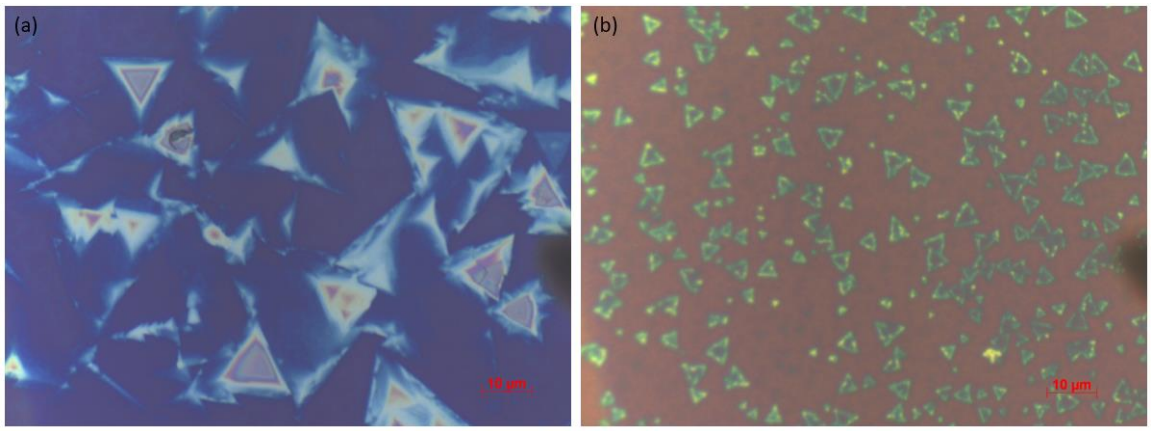

Figure 32: (a) Growth with S position at 3/10 inches and (b) 4/10 inches.

4.1.3 MoO_3 Position

Having determined the S placement at 4/10 inches, MoO_3 powder was placed at upstream of the growth substrate at distances of 1.25, 1.5, 1.75, and 2 inches to determine its ideal setting.

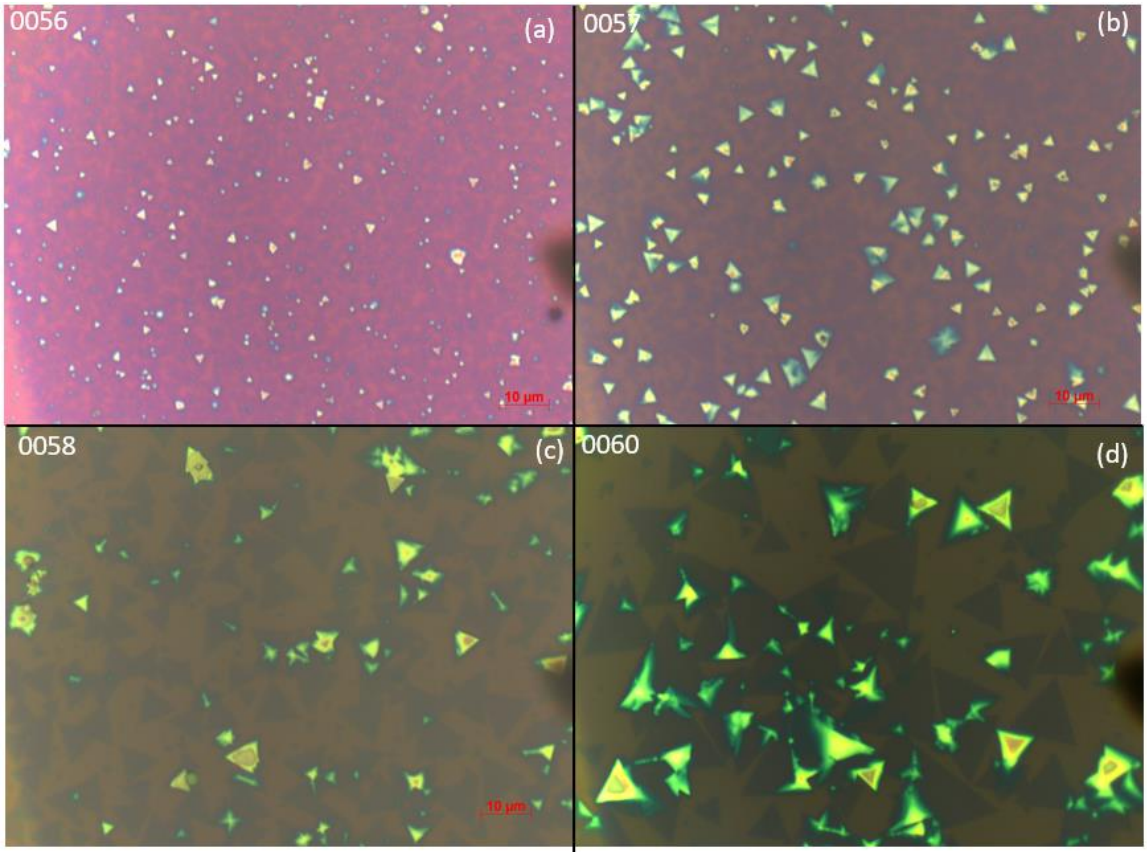

Figure 33: Growth with MoO_3 powder distances of (a) 1.25, (b) 1.5, (c) 1.75, and (d) 2 inches

Figure 33 exhibits the representative optical images obtained at these four different settings. Close to equilateral triangular shaped MoS_2 sheets were seen but the size is different obtained at different MoO_3 settings. As it can be seen in Figure 33, the grain size increased with increasing distance MoO_3 placement. The bright triangular grains on top are the thicker MoS_2 which are undesirable. Qualitatively, the sample with the MoO_3

placement of 1.75 inches upstream showed larger grain growth than the sample with MoO_3 placement at 1.25 and 1.5 inches.

Using ImageJ analysis, average grain size was measured for each setting; at 1.25 inches the average grain size was found to be about $3.5\mu m^2$, for MoO_3 placement of 1.5 inches the average grain size was about $5\mu m^2$. At a MoO_3 placement distance of 1.75 inches the average grain size increased to about $33\mu m^3$, an at a setting of 2 inches the average grain size was around $60\mu m^2$. There was larger grain growth on the sample with MoO_3 placed 2 inches upstream, however it also showed much more thick grain growth, which is undesirable. Seen from the optical images, it was determined that the ideal placement for the MoO_3 powder was 1.75 inches upstream from the substrate.

4.1.4 Substrate

Effects of substrate were also taken into consideration. Silicon dioxide on silicon (SiO_2/Si) was used for most of the growth. Sapphire (Al_2O_3) was also used due to the similarity to lattice structure of MoS_2. It was determined that there was generally larger growth on SiO_2/Si and it could also be difficult to see the growth on the sapphire substrates.

If a device were to be made from a growth it would require a conducting substrate. Having considered that, platinum and HOPG substrates were also used but not extensively studied. No growth was able to be visually detected on the surface.

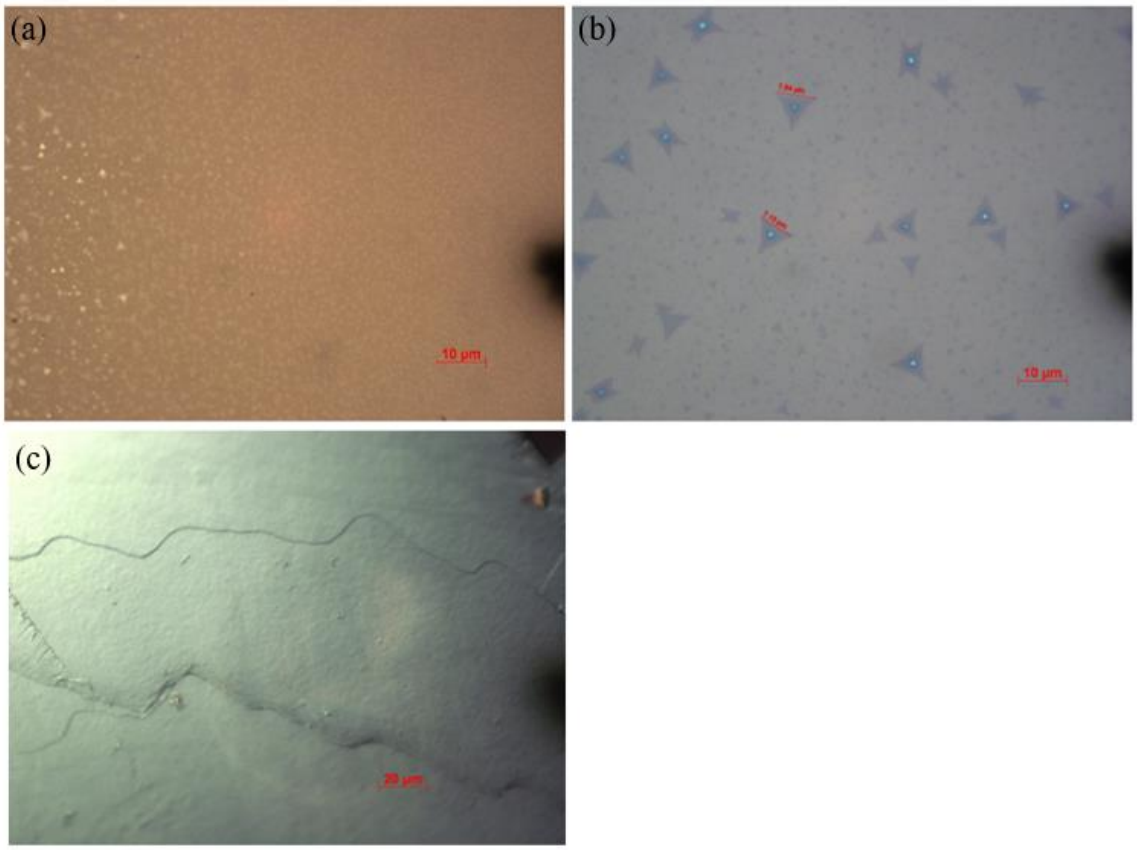

Figure 34: Substrates evaluated for growths with S at 4/10 in, MoO_3 at 1.25in and carried out at 650°C for 3mins. (a) sapphire, (b) SiO_2/Si, and (c) HOPG:

4.2 Surface Treatments on Sapphire Substrate

It was noticed that defects, either from substrate preparation or any other aspect of the growth process, often served as nucleation points for the growth. In an effort to determine the effect of defects on nucleation, a series of growths were carried out using surface defects without seeding promoters. Two methods were examined, scratching the surface of the substrate and exposing the substrate to plasma etching.

Figure 35 presents the optical images of the samples grown on the sapphire substrates with physical scratches. Either there are 3 or 5 large scratches over the substrate, there are

little or almost no triangular grain growth. The scratches did not provide the necessary nucleations points for the deposition of large area MoS_2 on the substrate. However, Raman data shows that the growth that was obtained was monolayer (see Figure 36)

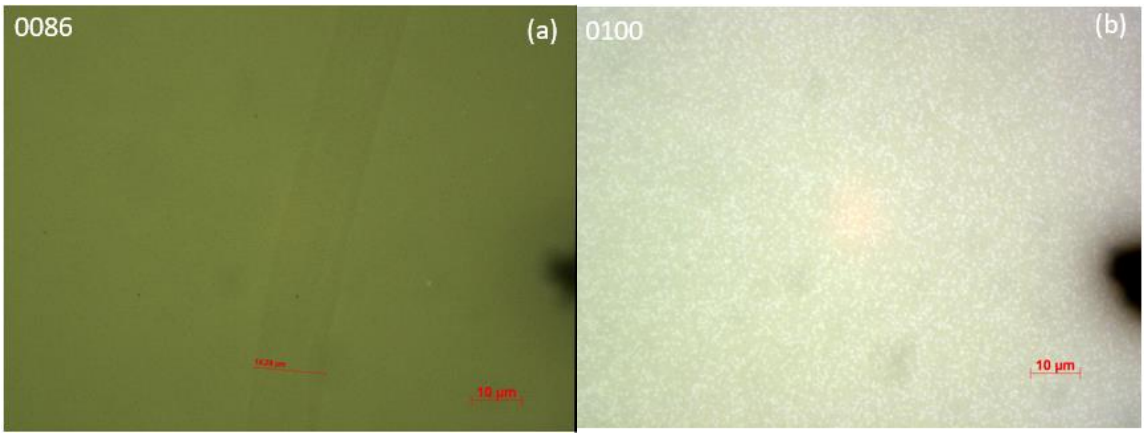

Figure 35: Growths with S at 4/10 in, MoO_3 at 1.25in and carried out at 650^oC for 3mins (a) Sample with 3 scratch surface treatment on sapphire at 100x near the center of the sample and (b) Sample with 5 scratch surface treatment on sapphire at 100x at the upstream edge

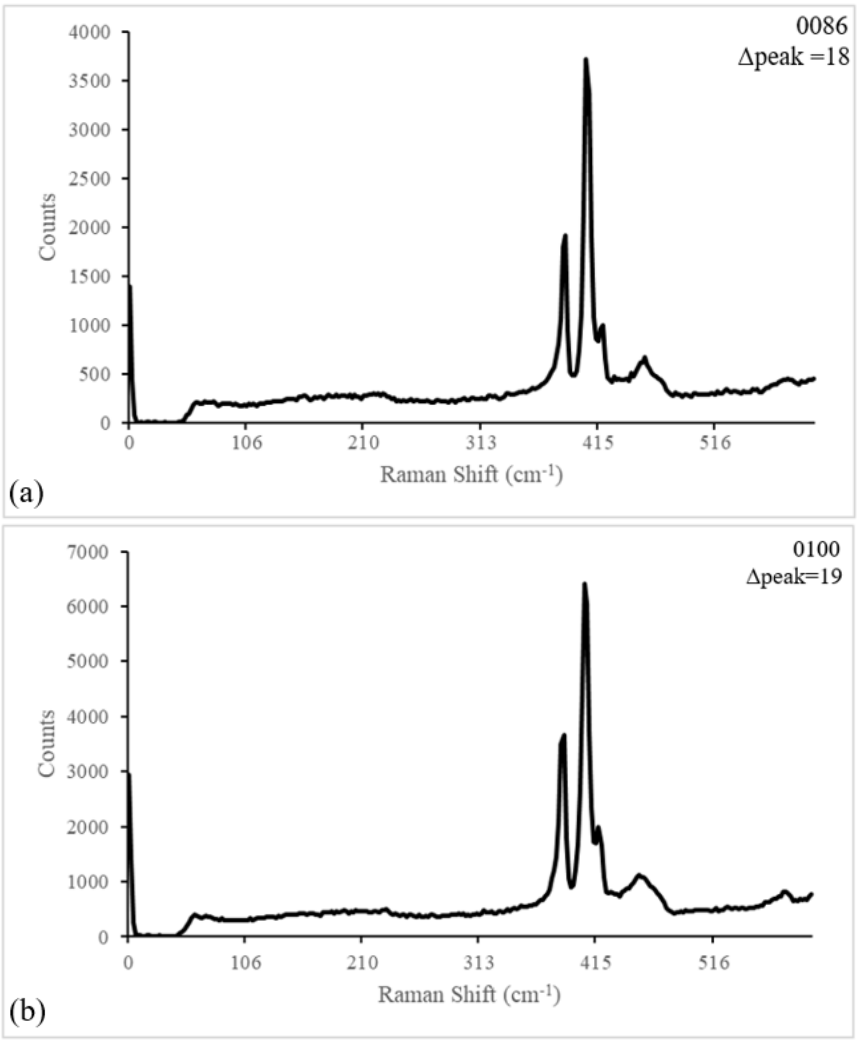

Figure 36: Raman Spectroscopy for sample (a) with 3 scratches and a peak separation of 18 and (b) with 5 scratches and a peak separation of 19, both indicating monolayer film.

Figure 37-Figure *39* presents the images of the samples grown on sapphire with O_2 plasma etching at various conditions, i.e. 50W for 3min, 50W for 5min, 100W for 30s 100W for 1min, and 100W for 3min. On the substrate etched for 3min at 50W, some areas were able to seen growing together on the sample, as seen in Figure 37 (a). However, the larger grains also had a thicker growth than the smaller grains. At the same power for 5 minutes, there are very small triangular nucleations that did not grow together seen in Figure 37 (b). It is possible that the extended exposure of plasma etching removed

enough surface material that there were less defects present than there were at the 3-minute exposure.

The substrate etched for 30 seconds at 100W, had small clusters grew on the substrate but no triangular growth could be seen across the substrate. When the exposure time was increase to 1-minute, there was almost no triangular nucleation to suggest MoS_2. Instead, the nucleation took on the appearance of deposited molybdenum bars, as seen in Figure 38, which would suggest that there was a high concentration of MoO_3 compared to S, however, precursors were measured out to be the same as past growths. It is possible that severity of deformations to the substrate, from the plasma etching, was more effective for molybdenum deposition than MoS_2. The exposure time was then increased to 5 minutes. Again, no triangular growth was able to detected under the microscope. On the upstream edge, there was growth that resembled molybdenum nucleation, however, the downstream edge did not exhibit the same nucleation patterns; this can be seen in Figure 39. On the downstream side of the substrate, individual grains could not be identified, but the growth looked similar to the clusters that can be seen on the 30-second exposure substrate. This indicates that the downstream side of the sample could have larger, or coalesced, grains of MoS_2.

Raman data collected showed that some areas of the substrate were covered in multilayers of MoS_2, with a small area on the downstream side of the sample that had a peak difference suggesting monolayer growth.

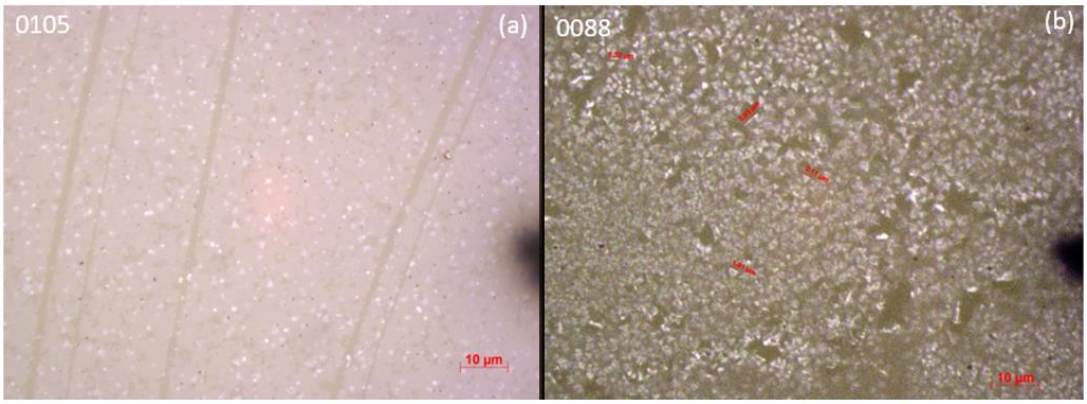

Figure 37: Growth on substrate treated with O_2 plasma etcher at (a) 50 watts for 3 minutes at 100x near the center of the sample and at (b) 50 watts for 5 minutes at 100x near the middle of the substrate

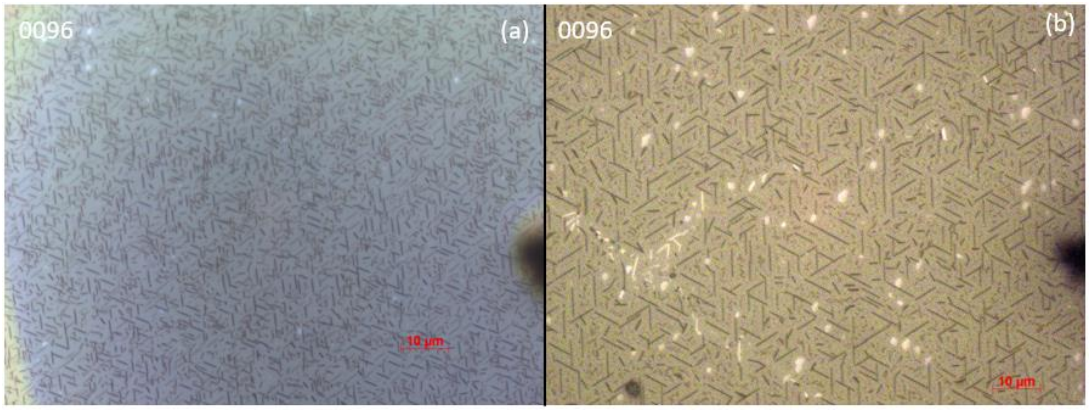

Figure 38: Growth on substrate treated with O_2 plasma etcher at 100 watts for 1 minute at 100x (a) near the center of the sample and (b) near the downstream edge

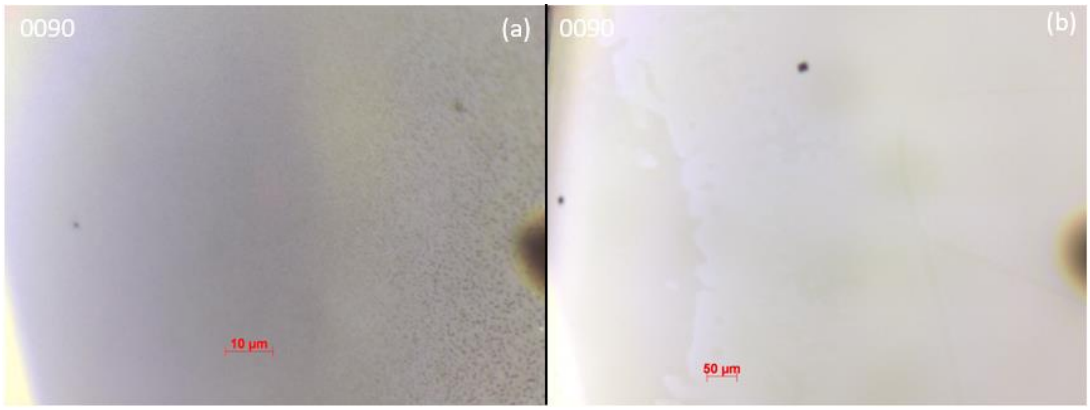

Figure 39: Growth on substrate treated with O_2 plasma etcher at 100 watts for 5 minutes at (a) 100x at the upstream edge and (b) 50x at the downstream edge

4.3 With PTAS Applied via Thermal Drying

4.3.1 Drying Temperature

PTAS droplets were placed on the substrate sitting on hotplate. Different hotplate temperatures (50^{o}C, 100^{o}C, and 250^{o}C) were tried to evaluate the impact on the PTAS drying. At 50^{o}C the evaporation of PTAS created a series of rings on the surface of the substrate. This is known as the "coffee ring" effect, where the evaporation of a liquid leaves a residue rings from the shrinking droplet during evaporation. These "coffee rings" became deformations on the surface and served as nucleation points. However, they are not controllable or tunable to serve as a repeatable seeding promoter. As the temperature of the hot plate was increased to 100^{o}C and 250^{o}C, the reduced drying time necessary at increased did not effectively suppress the ring effect. In contrast, on the substrate heat dried at 250^{o}C, the rings were worse than they had been at 50^{o}C. The "coffee rings" are prominent in each setting, but at higher temperatures there are more rings and they have a smaller separation between each ring, meaning that more surface deformations are present on the substrate

Shown in Figure 40, small grains can be seen forming on the substrate with PTAS dried at 50^{o}C, while large grains and thicker areas can be seen forming on the substrate with PTAS dried at 100^{o}C. At drying temperature of 250^{o}C, there was very little growth across the surface. It is possible that only a small portion of PTAS remained on the surface while others may be deposited.

The higher temperatures created worse coffee ring effects on the surface of the substrate, as such, it was concluded that the heat drying at 50^{o}C produced better results and was the more optimal condition.

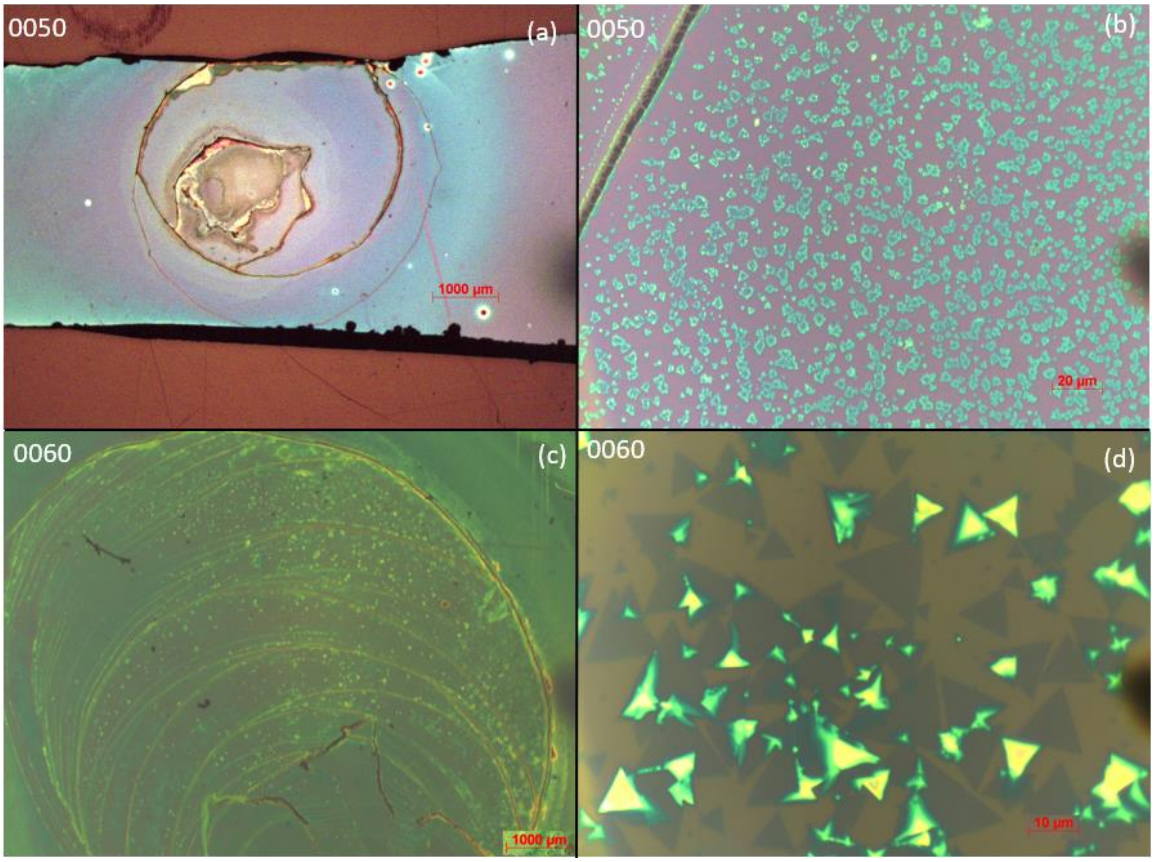

Figure 40: Sample with PTAS dried on a hotplate at a temperature of 50°C at (a) 1.25x and (b) 100x and sample with PTAS dried at 100°C at (c) 1.25x and (d) 100x. Growth settings of S at 4/10 in, MoO_3 at 1.25in and carried out at 650°C for 3mins

4.3.2 Surface Treatment

Coffee rings of PTAS make it challenging to have a uniform MoS_2 growth across the substrate. In an effort to have a more uniform distribution of PTAS solution across the sample and attempt to reduce the coffee ring effect, the substrate was treated with O_2 plasma etching to make the surface hydrophilic. This caused the PTAS solution to spread out across the entire sample, rather than sit as a droplet where it was placed on the surface.

The results of the PTAS and MoS_2 growth on the hydrophobic ad hydrophilic substrates are compared in Figure 41. Although it did not prevent the coffee ring effect, the

hydrophilic surface allowed PTAS to be more evenly distributed across the sample giving more nucleation sites for growth. However, many of the grains were much thicker than on a hydrophobic substrate. This indicated that the PTAS concentration was too high for growth of monolayer films.

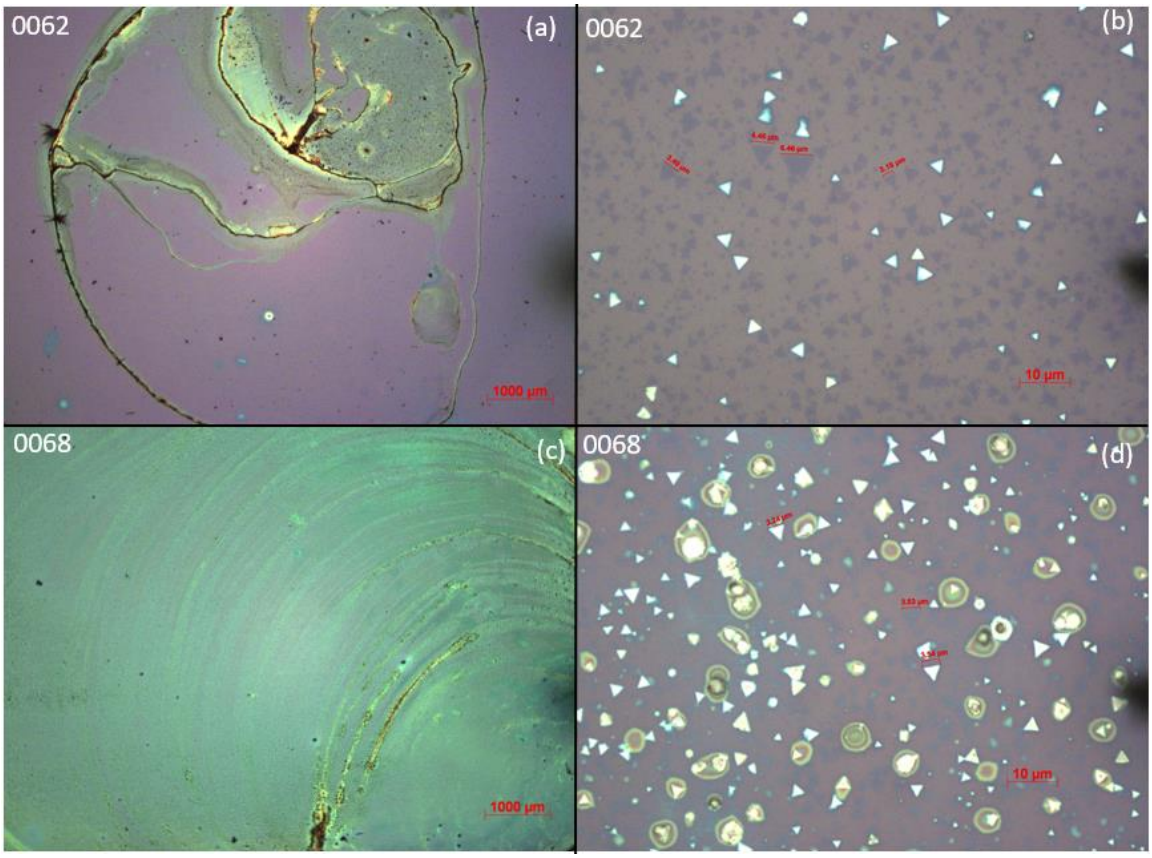

Figure 41: Growth on hydrophobic substrate at (a) 1.25x and (b) 100x and growth on hydrophilic substrate at (c) 1.25 x and (d) 100x. Growth S at 4/10 in, MoO_3 at 1.25in and carried out at 650^oC for 3mins

4.4 With PTAS Applied via Spraying

It was difficult to quantify an amount smaller than a droplet with a pipette and it was possible to finely tune the amount of PTAS deposition. A new approach was adopted via spraying PTAS solution with the help of AirBrush Sprayer.

The spraying solution contains 50 droplets of the PTAS solution and 30ml of isopropyl alcohol (IPA). The mixture of IPA allowed the solution to quickly dry on the substrate without use of a hot plate and the IPA left no additional residue, allowing the substrate to only have the PTAS deposition. The concentration of PTAS was controlled by the number of sprays. The effect of the PTAS solution was observed under four different concentrations. In this study, the concentrations studied were 5, 10, 15 and 20 sprays.

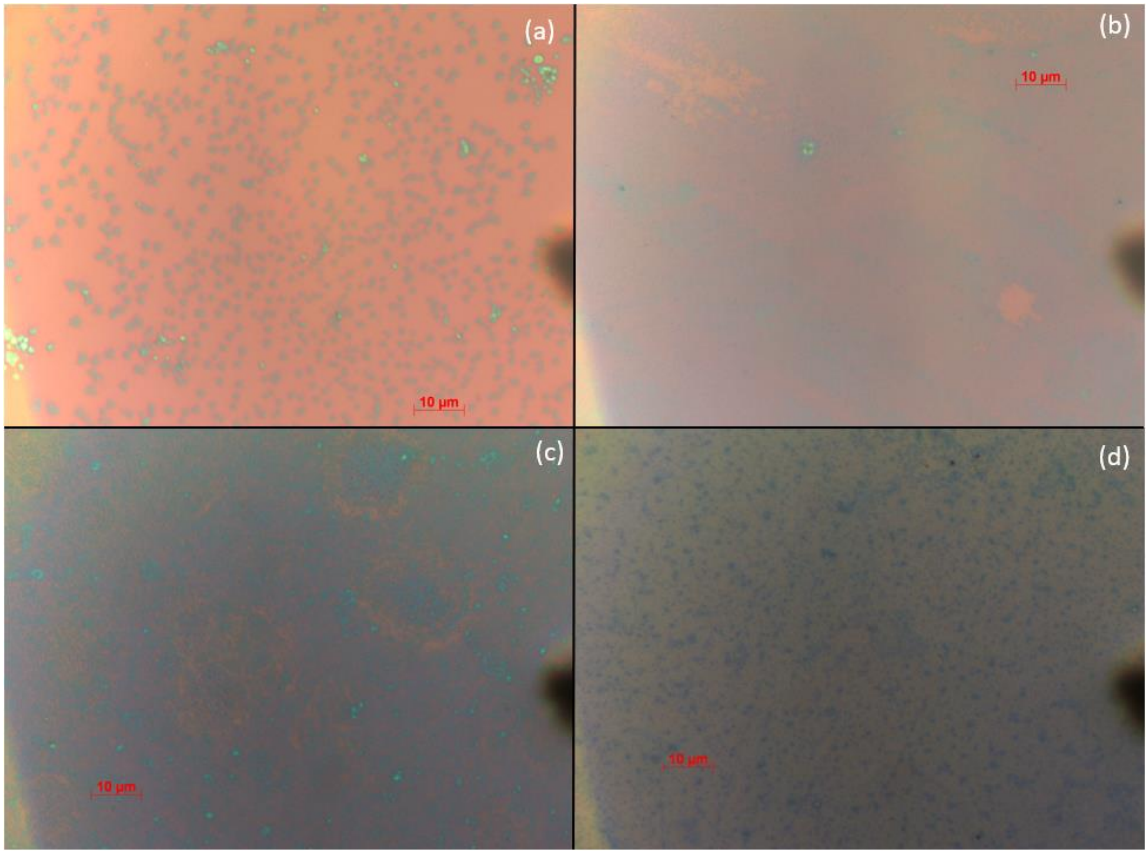

Figure 42: Optical images (100x) of growth with (a) 5 sprays, (b) 10 sprays, (c) 15 sprays, and (d) 20 sprays. Growths settings of S at 4/10 in, MoO_3 at 1.25in and carried out at 650°C for 3mins

See in Figure 42, there was small growth under all four conditions. Individual grains were no larger than a few micrometers, while some nucleation was too small to determine individual grains. With a lower concentration (5 sprays) the grains are very small and do

not begin to coalesce. The grains that appear to be a bright blue under the microscope reflect more of the incident light back to the lens; this requires a thicker sample, which indicates that the growth was at least multi-layer, even though they are small in area. When 10 and 15 sprays were used the grains began to grow together, however, they were still multilayer growths, displaying a bright blue color under the microscope that would not be suitable for devices. At a higher concentration of PTAS (20 sprays), the grains are not triangular or coalescing to form larger growth.

4.4.1 Graphene Substrate with PTAS

Graphene and a combination of graphene with PTAS droplets were also examined as seeding promoter possibilities.

Seen in Figure 43, very little growth was able to be seen on the sample using graphene as the sole seeding promoter. This indicated that under the settings being used, PTAS was necessary for deposition of MoS_2.

Growth was able to be seen using the optical microscope on the substrate using both graphene and PTAS as seeding promoters. The growth that occurred on the SiO2/Si substrate appeared to be thin growth. However, it was difficult to distinguish if any growth occurred on the graphene (see Figure 44).

Further Raman analysis confirmed the existence of the thin MoS2 nanosheet on graphene with the observation of the characteristic two peaks. In some areas the twin peaks have a peak separation of 22.94 while in other areas the separation is 24.34. These results are presented in Figure 45. All these indicate that the growth was multilayer. Additional peaks can be observed in Figure 45 (b) and (c); they are characteristic peaks of Si at

520cm^{-1} and 1000cm^{-1}; characteristic graphene peaks are at 1300cm^{-1}, 1600cm^{-1} and 2700cm^{-1}.

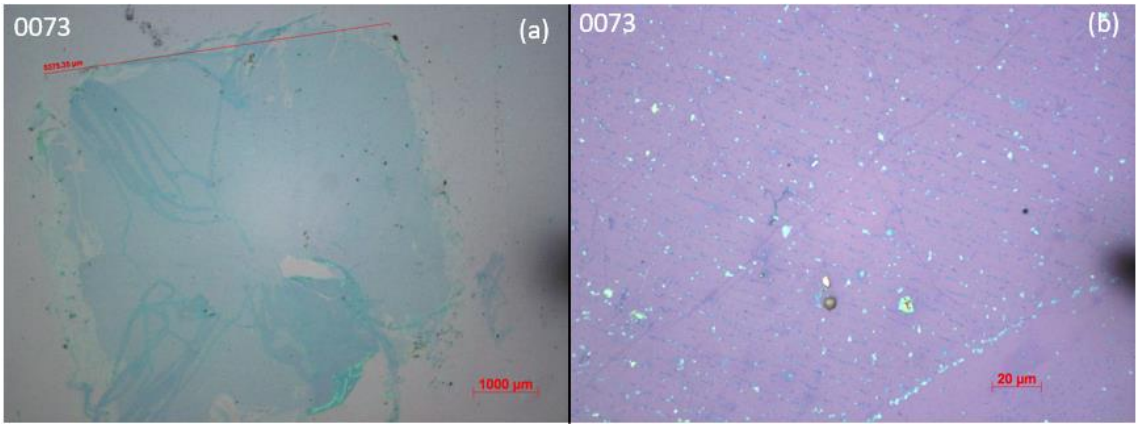

Figure 43: Sample graphene as sole seeding promoter at (a) 1.25x (b) 50x

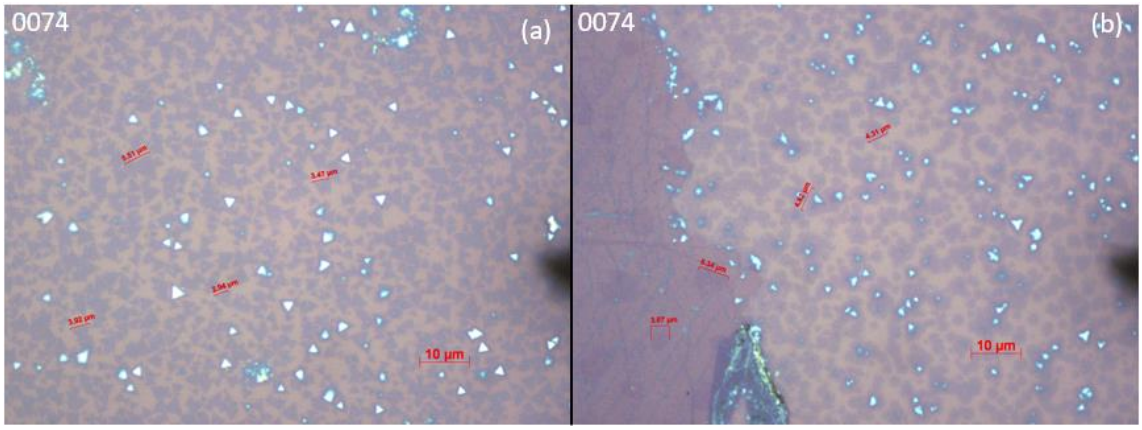

Figure 44: Sample with graphene and PTAS (a) upstream edge of sample at 100x, (b) upstream edge of graphene at 100x, and (c) Raman data growth near the graphene.

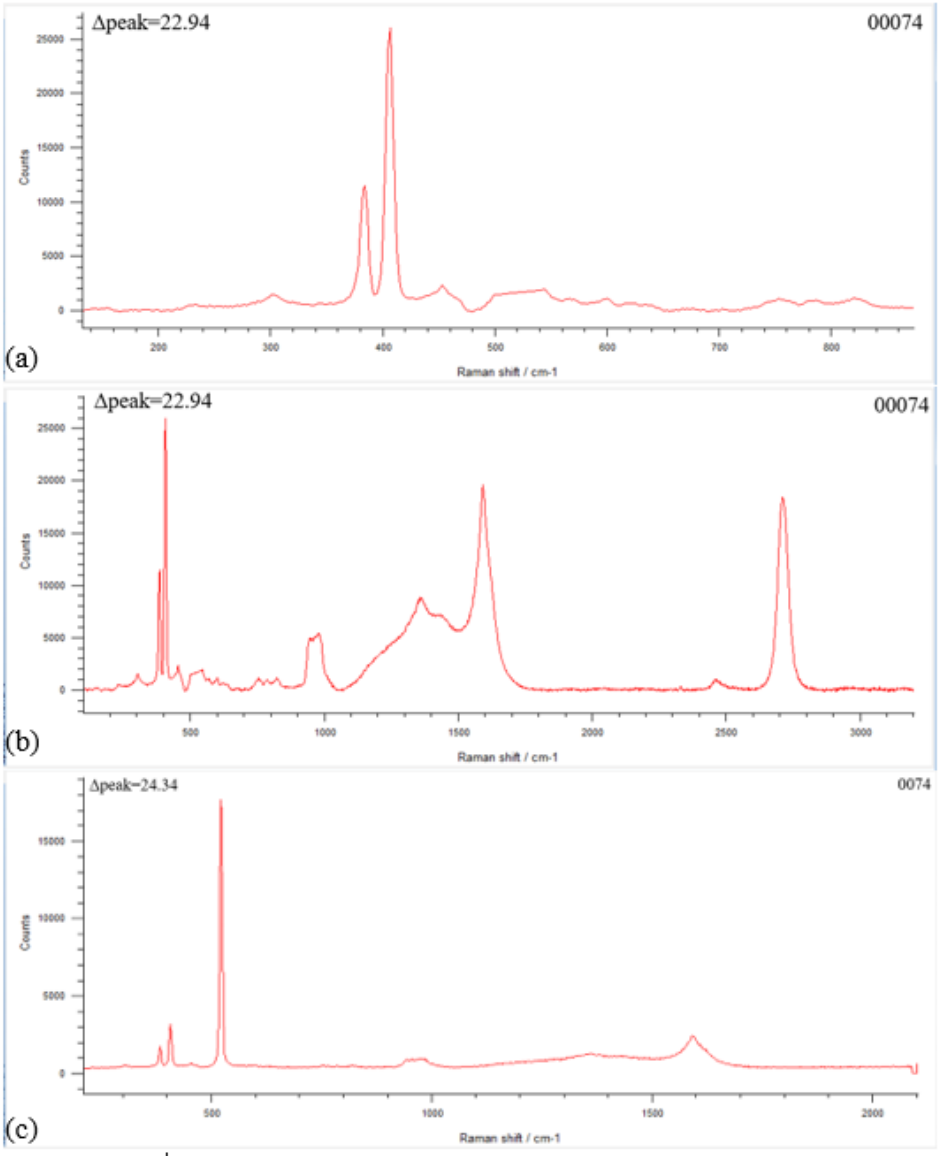

Figure 45: (a) Raman on graphene showing MoS_2 peaks, (b) extended Raman on graphene showing MoS_2 and graphene peaks, and (c) Raman of thicker growth next to graphene

4.5 PTAS Seeding Promoter on Separate Upstream Substrate

To minimize the impacts of PTAS morphology on the MoS2 growth, PTAS seeding promoter was placed on a separate upstream substrate. This approach appears to lead the best MoS_2 growth after optimizing the PTAS concentration, growth time and carrier flow rate.

4.5.1 Varying Amount of PTAS

In this series of study, the concentration of PTAS was quantified by the number of droplets placed on the upstream substrate. Concentrations of 1, 2, and 3 (samples 0130-0140) droplets placed on the upstream substrate were examined in this study. By inspecting the sample visually with optical microscopy (see Figure 46), it was able to be determined that all three concentrations were capable of producing a large area grains (~100μm). However, there were far fewer large grains on the sample grown with 1 droplet of PTAS when compared to the 2 and 3 droplet samples.

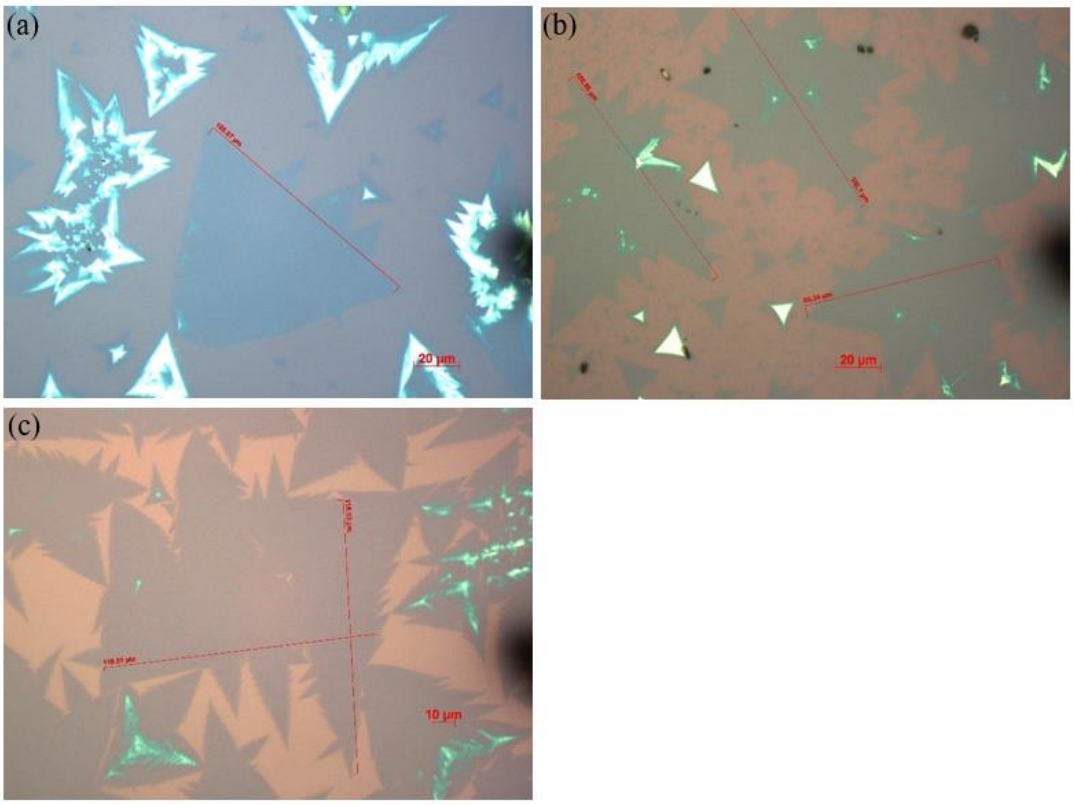

Figure 46: Large MoS_2 growth on SiO_2/Si substrate with PTAS on a separate substrate in the upper stream. (a) 1 PTAS droplet, (b) 2PTAS droplets, and (c) 3PTAS droplets

Further analysis was carried out on the samples of 2 and 3 droplet concentrations in the form of SEM and EDX.

Figure 47 presents a series SEM images of MoS_2 growth taken across the $1cm^2$ SiO_2/Si substrate with the 2 PTAS droplet substrate in the upper stream. It can be seen that an MoS_2 film is growing in many areas across the bare substrate. Large triangular grains can be seen on the on the middle to upstream side of the sample (middle to right images in set). There are also star-like grains on the sample that are likely thicker films of MoS_2. On the more downstream side of the sample (left images in set), there are areas with a more continuous film growth.

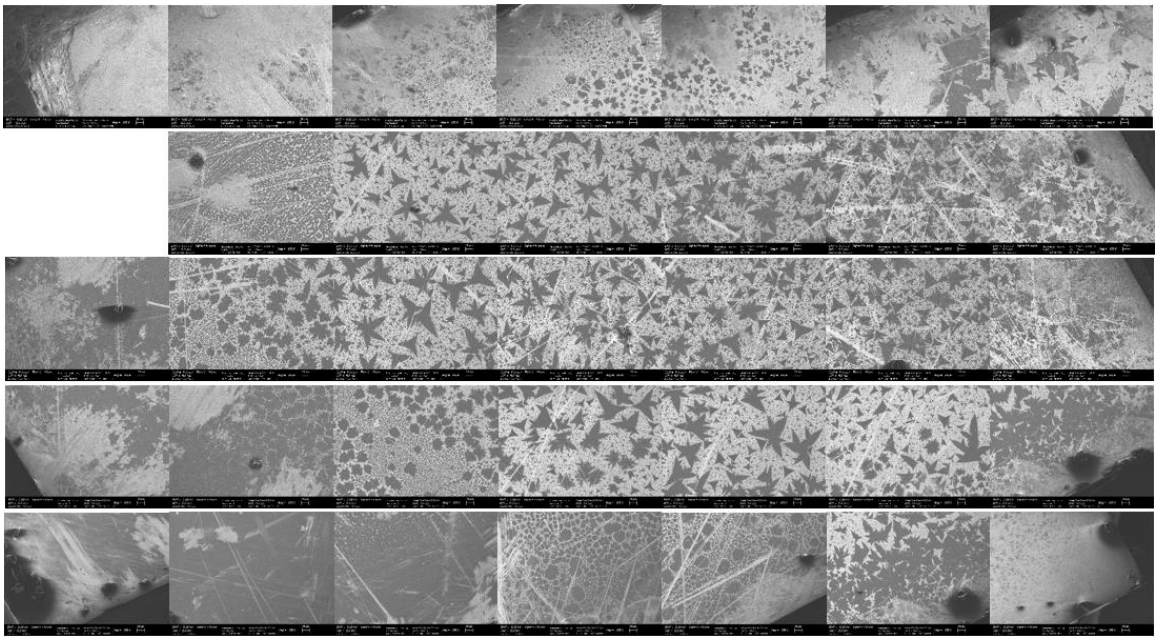

Figure 47: SEM images across the entire bare substrate in the presence of a separate PTAS substrate (2 droplet concentration) in the upper stream.

Evaluating the star-like shaped grains (Figure 48) shows that different thicknesses. Near the center (nucleation point) of the grain a thicker film can be seen, whereas closer to the edges of the grain a thinner film is present. The thicker area seen in the SEM image is

the darker area, while the thinner film has a lighter color. There are bright dots across both the thinner and thicker areas which could have been nucleation points for additional grains had the growth process been extended. The thin triangular shaped grains have a relatively more uniform thickness.

(a) 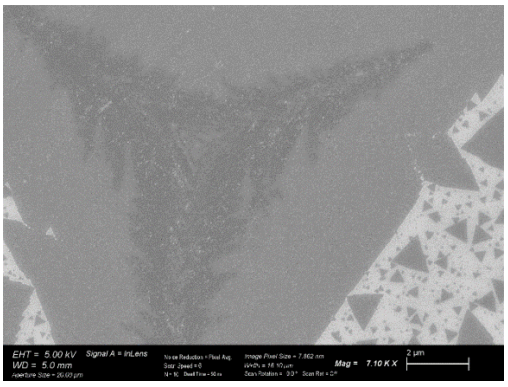 (b) 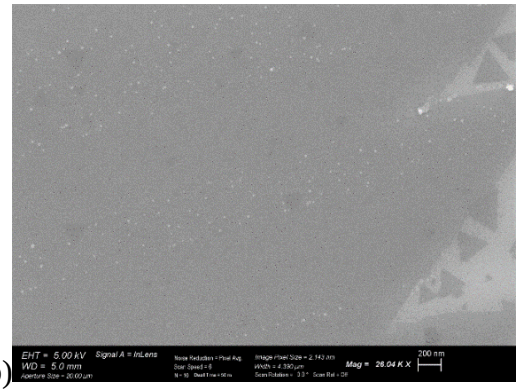

Figure 48: (a) SEM Image of star-like shape MoS_2 grain, showing the difference between thicker film (dark gray) at the center of the grain and the thinner film (light gray) near the edges. (b)Thin triangular growth, with smaller triangles and nucleating points

This area is further characterized using Raman spectroscopy, seen in Figure 49. A thickness gradient can be seen in some growths, for instance the center of the triangle is usually brighter (almost white). Moving away from the center of the triangle the thickness often decreases, and the color dims. In many cases, the grain may contain multiple layers of growth. Using a peak fitting software (Renishaw Wire), the raw Raman data is able to studied in better detail. When the spectrometer detects multiple thicknesses in the same measurement, the characteristic peaks of each thickness can appear as a wide combined peak for all range of thicknesses, as opposed to detecting each independent thickness. Therefore, peak fitting is necessary to determine if the peaks detected during the measurement are composed of one measured thickness or multiple. If multiple thicknesses are measured, then each characteristic peak can be broken down in

two or more other peaks. This can be seen in Figure 49 (b) as the measured peaks of MoS_2 (red) are each broken down into a peak representing monolayer MoS_2 (turquoise and pink) and multi-layer MoS_2 (green and dark blue). As a result, the Raman peaks often have peaks that identify both monolayer and multilayer growth. In this set of data monolayer can be detected with a peak separation as low as 20, and bulk with a separation of 25.

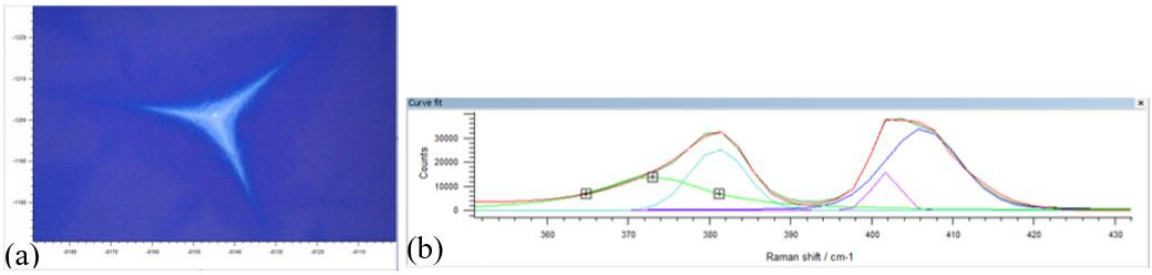

Figure 49: (a) Image from Raman and (b) Raman data for sample with a 2-droplet concentration.

On the downstream side of the sample a more continuous MoS_2 film covers a large area, as seen in Figure 50. Grain boundaries are not easily distinguishable although imperfections can still be seen on the film.

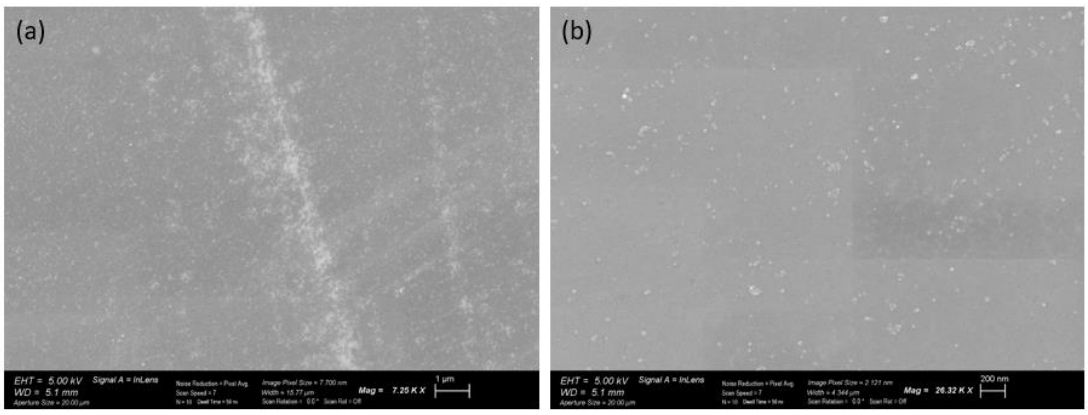

Figure 50: SEM image of continuous downstream area at (a) 7.25kX, (b) 23.63kX;

Local EDX analyses were performed in different areas, e.g. the triangular area, the star shaped area, and the downstream continuous area (see Figure 51). All the quantitative results confirmed the deposited films are composed of MoS_2.

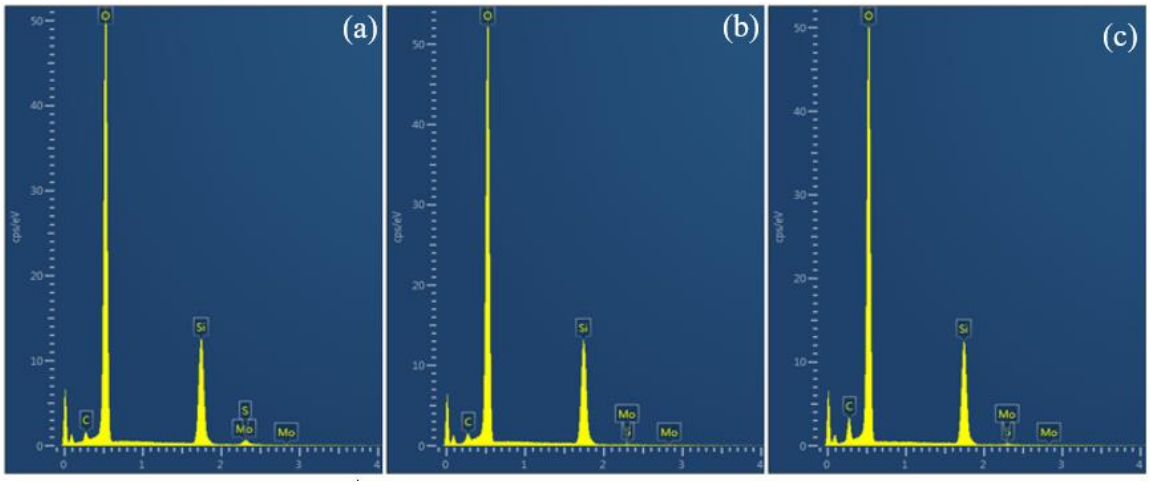

Figure 51: EDX (a) analysis of star, (b) triangular area, and (c) downstream area (0138)

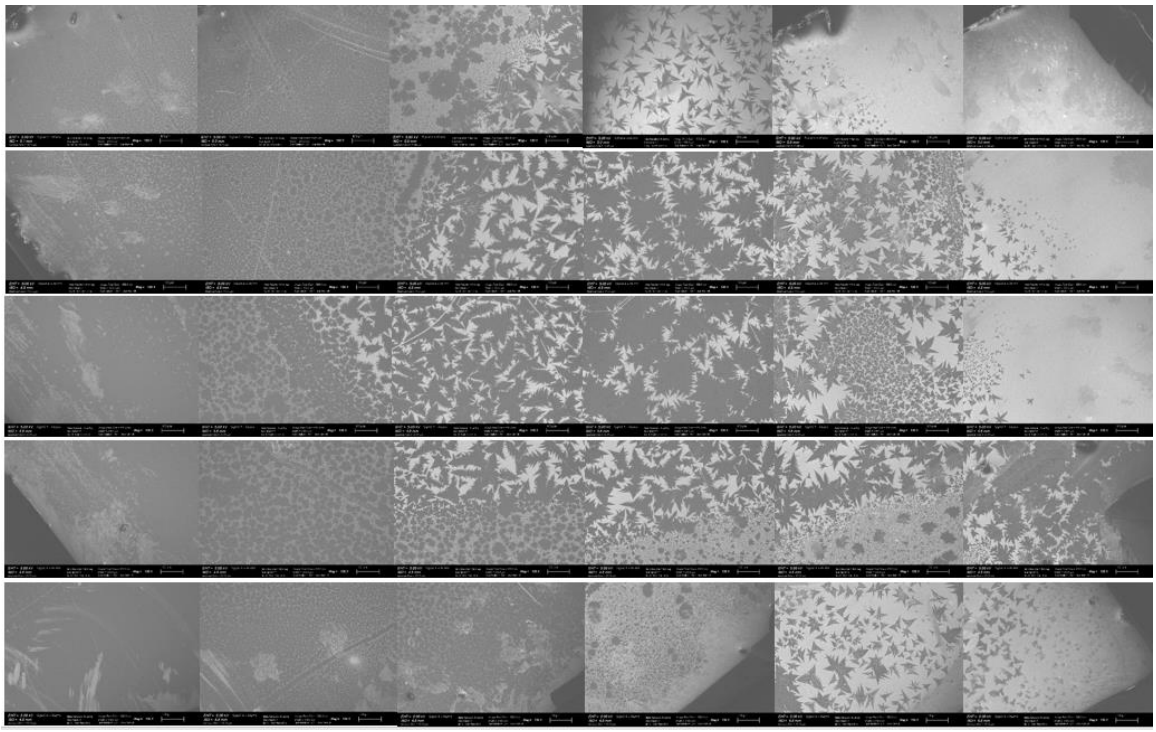

Figure 52: SEM images across the entire bare substrate in the presence of a separate PTAS substrate (3 droplet concentration) in the upper stream.

Upon evaluating the three-droplet sample (see Figure 52), it is seen that the MoS_2 film covers much of the substrate. The growth on the sample is largest (~120µm) and more continuous near the center of the sample. Upstream growth is of a smaller magnitude and less continuous, while growth that happens downstream is smaller and less triangular in shape.

Further investigation of the center area on the substrate, shows that there are grain boundaries within the large triangular growths (Figure 53). Points where the growth was starting another layer on top can also be seen scattered through the grains. It can be determined visually (Figure 49) that multiple layering of MoS_2 films has occurred, as shown by the bright (thick) growth in the center and the darker (thinner) growth near the edges of the triangle. Based on the EDX analyses, all the star-shaped and continuous downstream growth are still identified as MoS_2.

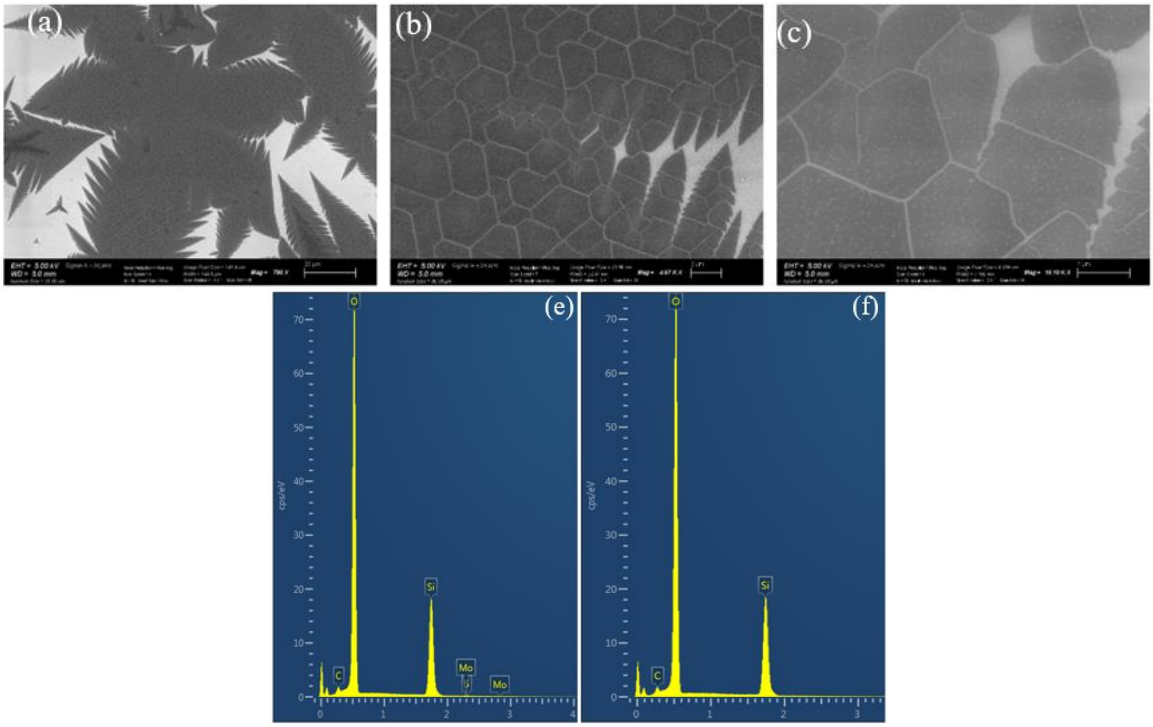

Figure 53: SEM imagines of large star/triangles in center of substrate. At (a)790X, (b) 19.42kX, (c) 4.57kX, (d) 16.10kX, (e) EDX on grain, and (f) bright substrate area (0136)

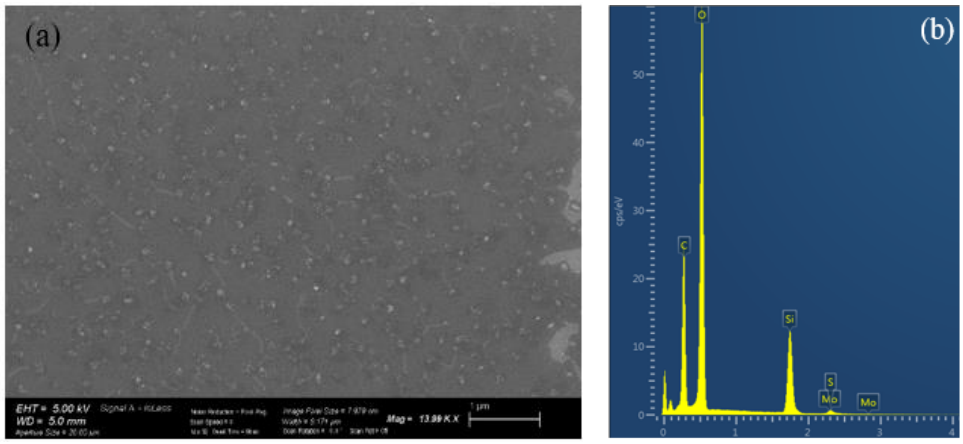

Figure 54: (a) SEM image of continuous area with (b) EDX measurement (0136)

4.5.2 Varying Carrier Gas Flow Rate

The impact of the carrier gas flow rate was studied by running growths with varying flow rates. Flow rates were set at 100, 200, 400 and 500sccm, and then the grain size of the growth was measured and compared. The optical images are shown in Figure 55. At 100sccm the growth was small with grain widths being less than 5µm; the growth that took place at 200sccm had grains that were larger, about 7µm, and growth at 400sccm was larger still at around 15-20µm, while the growth at 500sccm was much larger with areas as wide as 130µm. It was determined that 500sccm would produce the largest area grains, however it can also be seen that there are more defects across the growth due to uneven growth. Therefore, the optimized flow rate was determined to be 400sccm. While grains could be identified as thick or thin by the color of the growth, more analysis was required to determine the value of each thicknesses. For this Raman spectroscopy was used. A thickness gradient can be seen in some growths, for instance the center of the triangle is usually brighter (almost white). Moving away from the center of the triangle the thickness often decreases, and the color dims. In many cases, the grain may

contain multiple layers of growth. As a result, the Raman peaks often have peaks that identify both monolayer and multilayer growth. As can be seen in the following Raman data, monolayer can be detected with a peak separation as low as 20, and bulk with a separation of 25.

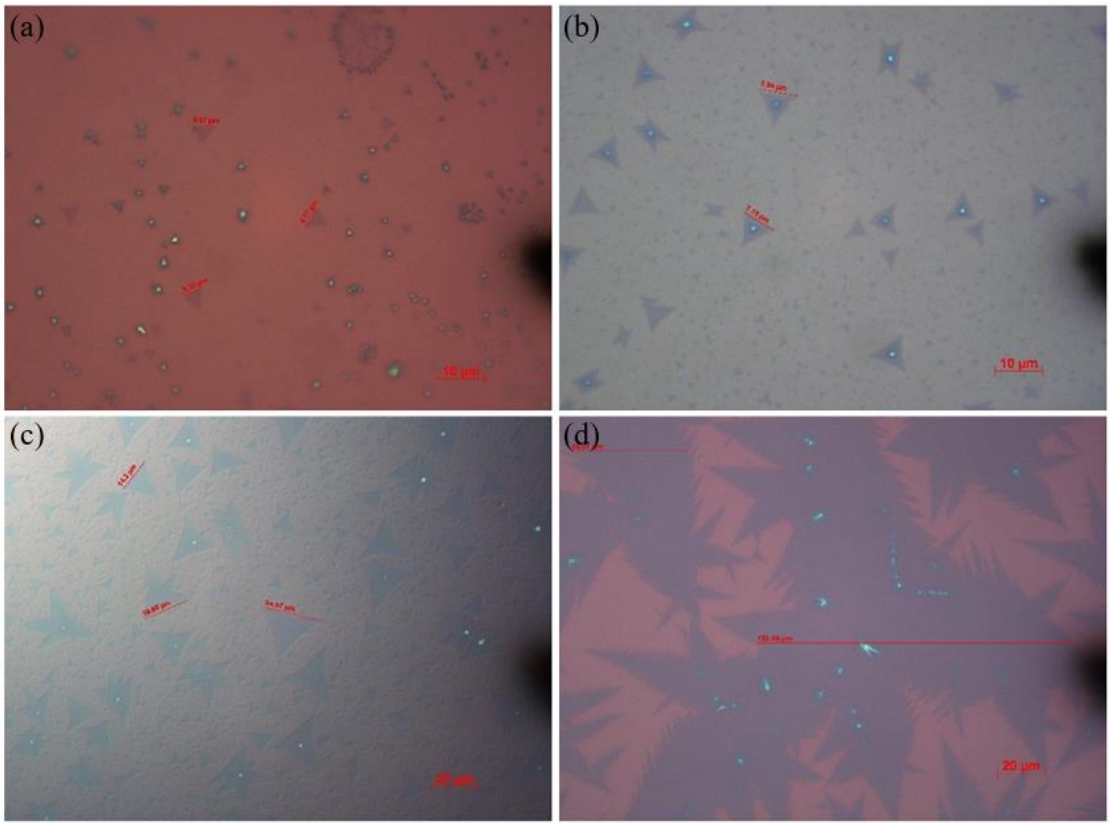

Figure 55: Optical images of MoS_2 growth with Ar flow rate of (a) 100sccm, (b) 200 sccm, (c)400 sccm, and (d) 500 sccm

4.5.3 Varying Growth Time

For systematical study, the impacts of the growth time on the film quality was evaluated with the growth temperature fixed at 650˚C. The growth times varied from 1, 3, 5, to 10 minutes. It can be seen that as the growth time increases so does the overall area of growth coverage, however there is less uniformity across the growth substrate at a longer

growth time. Upon examining the effect of time on the growth, it was determined that the 5-minute growth produced too many areas that were thicker than a monolayer film.

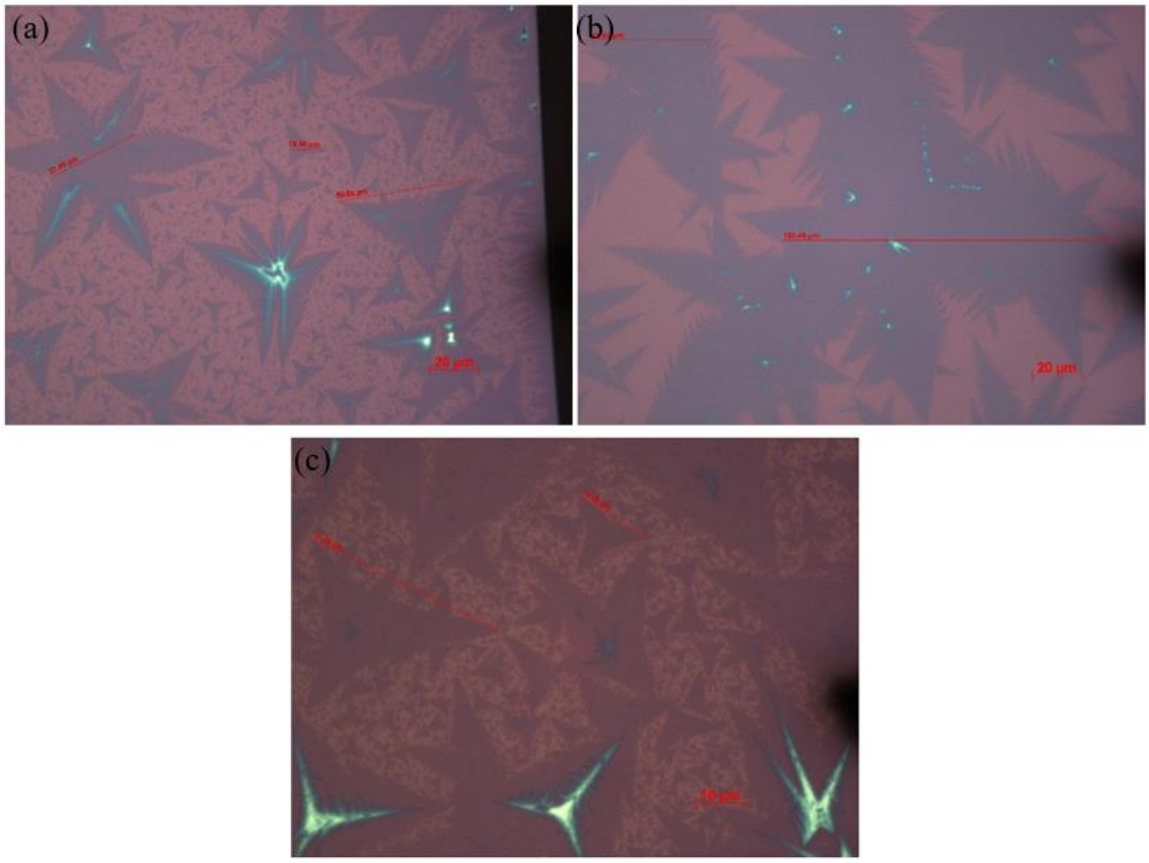

Figure 56: (a) 1 minute, (b) 3 minutes, and (c) 5 minutes with other growth settings being S at 4/10 in, MoO_3 at 1.25in and carried out at

AFM was then performed on both the 1- and 3-minute growths. As discussed previously, MoS_2 has a monolayer thickness of about 0.6nm. Monolayer grains were found on both the 1- and 3-minute samples as seen below in Figure 57. Line scans were taken on both samples as depicted in Figure 57 (a) and (c) with the maximum thickness being measured between 0.4 and 0.6nm for both samples, shown in (b) and (d).

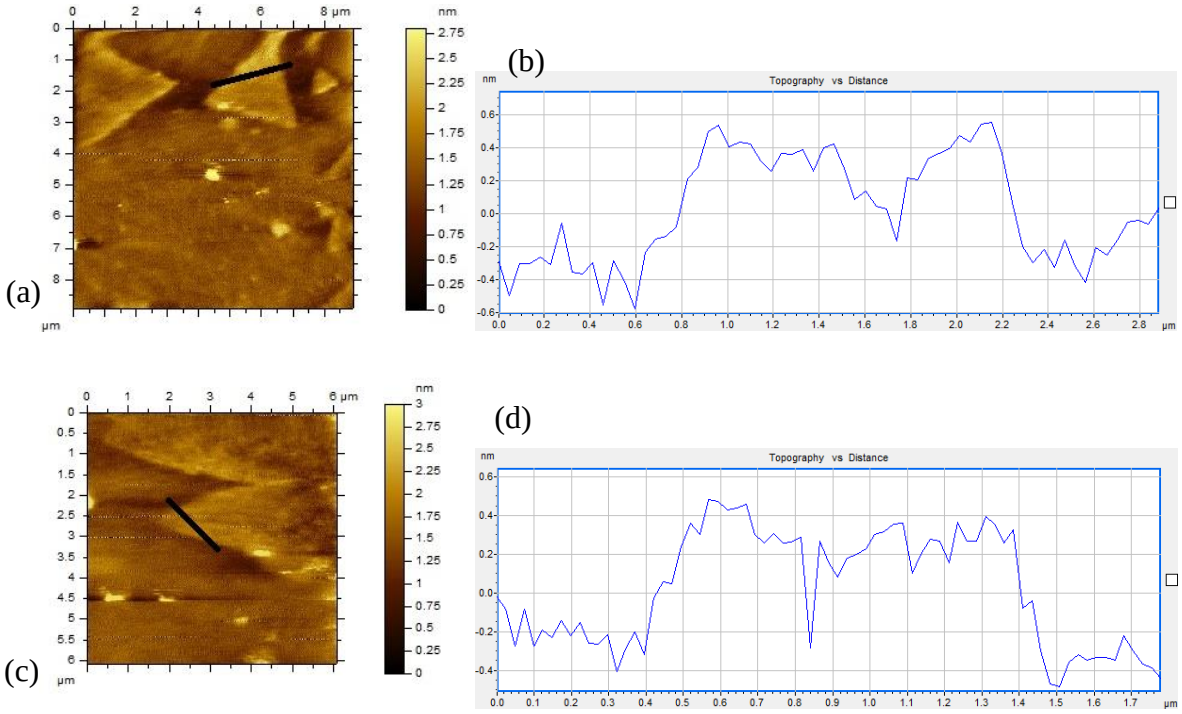

Figure 57: (a) AFM image of 1 min growth, (b) topography measurement for 1 min growth, (c) AFM image for 3 min growth, (d) topography measurement of 3 min growth

4.6 Quantitative Analysis

Images of the grains from growths at different times were further evaluated using ImageJ. About 95% of the grains from the 1-minute growth were less than 200μm^2 with a few outliers as large as 3200μm^2. The 3-minute growth was determined to be the largest film coverage, with a grain size of about 24,500μm^2. This grain was however an outlier, as the majority of the grains measured were less than 6500μm^2. The grains grown during the 5-minute conditions were the smallest with the largest grains being around 650μm^2. It can then be determined that the three-minute growth provides a more optimal time for the grains to grow laterally across the sample to form larger grains.

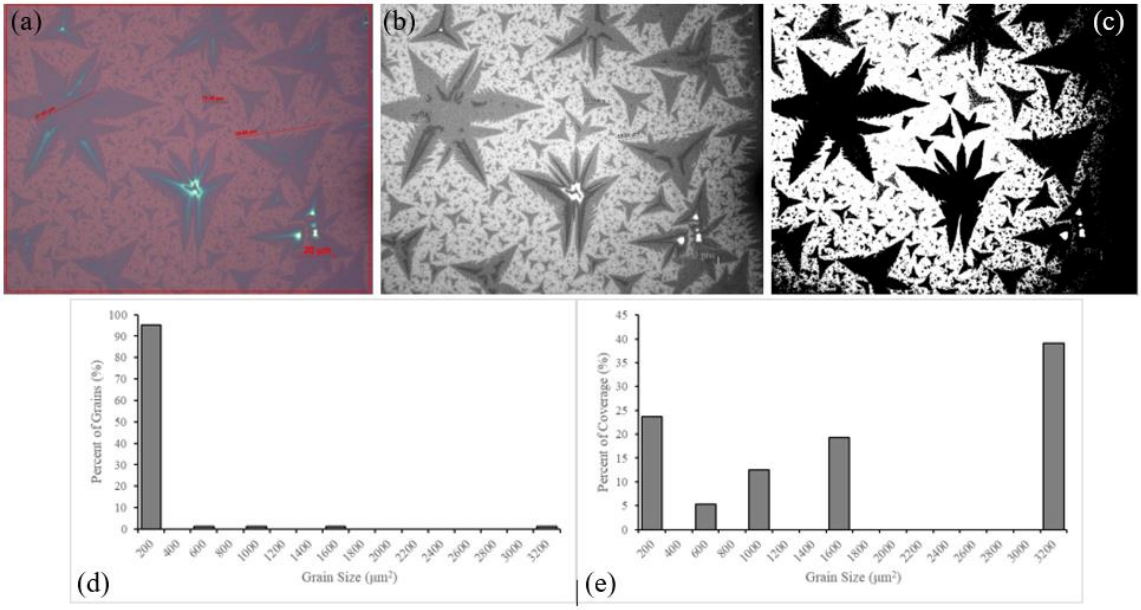

Figure 58: ImageJ Analysis of 1-minute growth (0153). (a) Original microscope picture, (b) edited picture for measurement, (c) digital picture from thresholding measurement; ImageJ output measurement (0153) (d) the percentage of grains at different sizes, and (e) the total coverage by the grains of different sizes

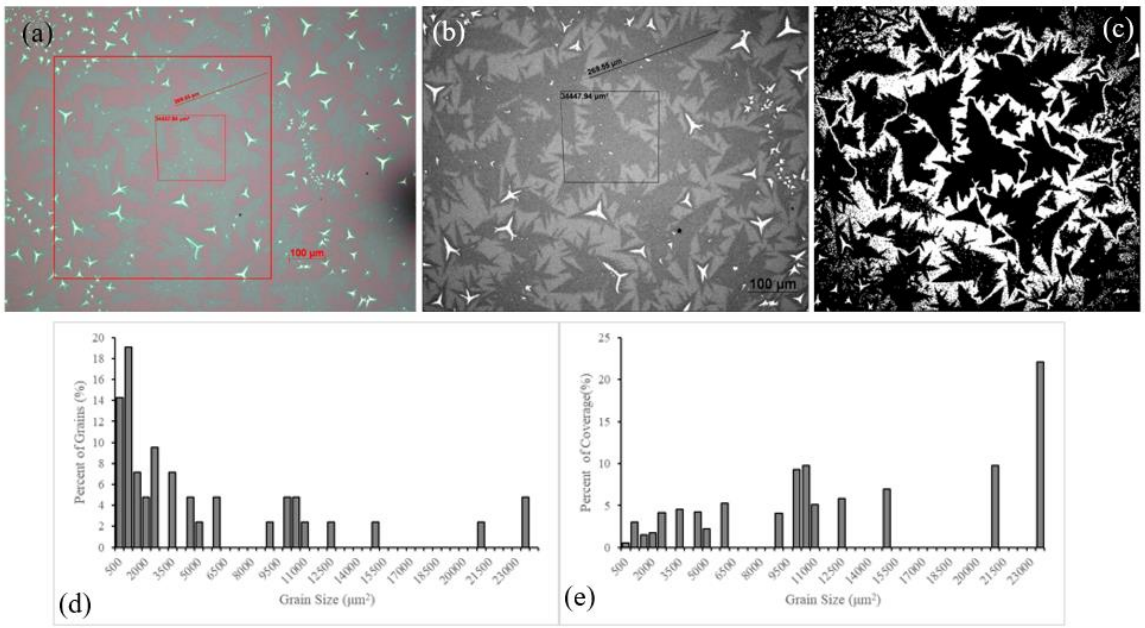

Figure 59: ImageJ Analysis and measurements of 3-minute growth (0151). (a) Original microscope picture, (b) edited picture for measurement, and (c) digital picture from thresholding measurement. (d) The percentage of grains at different sizes and (e) the total coverage by the grains of different sizes.

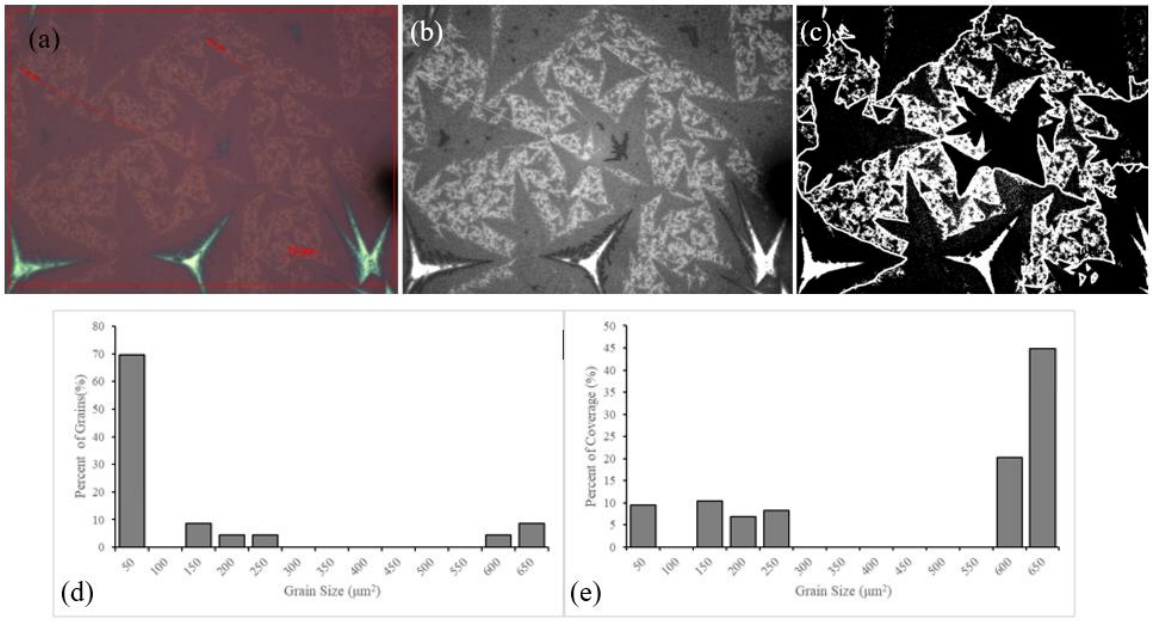

Figure 60: ImageJ Analysis and measurement of 5-minute growth (0154). (a) Original microscope picture, (b) edited picture for measurement and (c) digital picture from thresholding measurement. (d) The percentage of grains at different sizes and (e) the total coverage by the grains of different sizes.

To minimize the impacts of PTAS morphology on the MoS2 growth, PTAS seeding promoter was placed on a separate upstream substrate. This approach appears to lead the best MoS2 growth after optimizing the PTAS concentration, growth time and carrier flow rate. For instance, Table 1 summarize the quantitative results showing the impacts of growth time on the percentage of small and large grains, the largest grain size, and total coverage.

Growth time	region	Grain size info			Large grain (>100 μm^2) coverage
		Percentage (<100 μm^2)	percentage >100 μm^2	Largest grain (μm^2)	
1min	Down	90%	10%	400	45%
	Mid	82%	18%	900	78%
	Upper	62%	38%	1100	87%
	Upper	92%	8%	1900	77%
3min	Upper	50%	50%	1300	95%
	Upper	90%	10%	7200	90%
5min	Upper	70%	30%	700	90%
	Upper	86%	14%	4000	95%

Table 2: Summary of the quantitative analytical results showing the percentage of smaller grains (<100 μm^2), the percentage of larger grains (>100 μm^2), the largest size of the grain, and the total coverage of larger grains within the image.

5 Conclusion

Transition metal dichalcogenides (TMDs), represented by molybdenum disulfide (MoS_2), are promising and emerging in power electronics due to their large direct bandgap and other electronic properties. Much research has demonstrated that 2D MoS_2 can be fabricated by chemical vapor deposition (CVD). However, the processing is very sensitive to experimental settings for different CVD system. Many factors affect the growth process of thin film MoS_2. As discussed, the seeding promoter and application, growth time, temperature, quenching temperature, carrier gas flow rate, precursor position and amount can all make vast changes in the growth of the film. In order to define a reliable and repeatable method, all factors needed to be studied independently.

This thesis study has determined key important experimental factors for the designated CVD system. The most optimal precursor amount and positions, as well as the growth time and carrier gas flow rate have been able to be determined. The most reproduceable and repeatable larger grain size has been a result of precursor of 0.03g MoO_3 powder placed 1.75 inches upstream of the growth substrate, with 0.54g of S powder placed 4/10 of an inch inside the furnace edge. While the precursor powder was in this position, it is found that 1) MoS_2 growth is sensitive to the carrier flow rate and temperature; and 2) 2D MoS_2 grain size and areal coverage are correlated with grow time as well as the distance from the PTAS (perylene-3,4,9,10-tetracarboxylic acid tetrapotassium salt) resource. A growth time of 3 minutes and a carrier gas flow rate of 500 sccm has provided the largest grain size of MoS_2 films. Existence of large-area (that have an edge length of

over one hundred up to several hundreds of micrometers) monolayer and multilayer MoS_2, in the presence of PTAS promotor, have been successfully grown on clean Si substrate in the presence of PTAS promotor vapor in the vicinity.

Future work should be focused on maintaining a monolayer film deposition and impact of MoS2 nucleation on different substrates. Factors likely to affect include the use two or three zone CVD system to better control the growth temperature, capable of inserting precursor to control the growth time well, alternative seeding promoters and their appropriate applications.

In the field of thin film electronics, other 2D materials could be studied using a similar process as the optimized CVD setup used in this study. As previously discussed, advancements in electronics will derive, at least, partially from the advancement in the electronic materials and their capabilities. Further studying of these materials and methods of synthesizing will create the possibility to make many advancements in electronics and technologies that are used in day to day lives.

6 Bibliography

[1] L. I. Berger, *Semiconductor Materials*. Boca Raton, Florida: CRC Press, Inc., 1997.

[2] B. G. Yacobi, *Semiconductor Materials: An Introduction to Basic Principles*. New York, New York: Kluwer Academic/Plenum Publishers, 2003.

[3] A. K. Geim and K. S. Novoselov, "The rise of graphene," *Nat. Mater.*, vol. 6, no. 3, pp. 183–191, 2007.

[4] R. J. Lambert, "Graphene The University of Manchester." [Online]. Available: http://www.graphene.manchester.ac.uk/. [Accessed: 10-Jul-2017].

[5] F. Schwierz, "Two-Dimensional Electronics — Prospects and Challenges," *Electronics*, vol. 5, no. 2, p. 30, 2016.

[6] S. Najmaei *et al.*, "Vapor Phase Growth and Grain Boundary Structure of Molybdenum Disulfide Atomic Layers," *arXiv.org*, vol. cond-m, no. 8, pp. 754–759, 2013.

[7] J. A. G. Sheneve Z. Butler, Shawna M. Hollen, Linyou Cao, Yi Cui, "Progress, Challenges, and Opportunities in Two-Dimensional Materials Beyond Graphene," *ACS Nano*, vol. 7, no. 4, pp. 2898–2926, 2013.

[8] M. Zeng, Y. Xiao, J. Liu, K. Yang, and L. Fu, "Exploring Two-Dimensional Materials toward the Next-Generation Circuits: From Monomer Design to Assembly Control," *Chem. Rev.*, p. acs.chemrev.7b00633, 2018.

[9] A. N. Enyashin and A. L. Ivanovskii, "Graphene allotropes : stability , structural and electronic properties from DF-TB calculations," *Phys. Status Solidi B*, vol. 7, no. 343, pp. 1–12, 2011.

[10] H. Zhu, A. T. Balaban, D. J. Klein, and T. P. Živković, “Conjugated-circuit computations on two-dimensional carbon networks,” *J. Chem. Phys.*, vol. 101, no. 6, pp. 5281–5292, 1994.

[11] F. Iacopi, J. Boeckl, and C. Jagadish, *Semiconductors and Semimetals: 2D Materials*, 1st ed. Amsterdam: Academic Press, 2016.

[12] J. M. D. Coey and M. Venkatesan, “Half-metallic ferromagnetism: Example of CrO2(invited),” *J. Appl. Phys.*, vol. 91, no. 10 I, pp. 8345–8350, 2002.

[13] L. M. Yang *et al.*, “Revealing unusual chemical bonding in planar hyper-coordinate Ni<inf>2</inf>Ge and quasi-planar Ni<inf>2</inf>Si two-dimensional crystals,” *Phys. Chem. Chem. Phys.*, vol. 17, no. 39, pp. 26043–26048, 2015.

[14] F. F. Zhu *et al.*, “Epitaxial growth of two-dimensional stanene,” *Nat. Mater.*, vol. 14, no. 10, pp. 1020–1025, 2015.

[15] Z. Zhu and D. Tománek, “Semiconducting layered blue phosphorus: A computational study,” *Phys. Rev. Lett.*, vol. 112, no. 17, pp. 1–5, 2014.

[16] X. Wang, C. Zhi, Q. Weng, Y. Bando, and D. Golberg, “Boron nitride nanosheets: Novel syntheses and applications in polymeric composites,” *J. Phys. Conf. Ser.*, vol. 471, no. 1, 2013.

[17] J. Zhao *et al.*, “Rise of silicene: A competitive 2D material,” *Prog. Mater. Sci.*, vol. 83, pp. 24–151, 2016.

[18] K. Kalantar-zadeh, J. Z. Ou, T. Daeneke, A. Mitchell, T. Sasaki, and M. S. Fuhrer, “Two dimensional and layered transition metal oxides,” *Appl. Mater. Today*, vol. 5, pp. 73–89, 2016.

[19] B. M. Radovic and M. W. Barsoum, “MAX phases : Bridging,” *Am. Ceram. Soc.*

Bull., vol. 92, no. 3, pp. 20–27, 2013.

[20] Y. Gogotsi, "Chemical vapour deposition: Transition metal carbides go 2D," *Nat. Mater.*, vol. 14, no. 11, pp. 1079–1080, 2015.

[21] H. Zhang, G. Yang, X. Zuo, H. Tang, Q. Yang, and G. Li, "Computational studies on the structural, electronic and optical properties of graphene-like MXenes (M_2CT_2, M = Ti, Zr, Hf; T = O, F, OH) and their potential applications as visible-light driven photocatalysts," *J. Mater. Chem. A*, vol. 4, no. 33, pp. 12913–12920, 2016.

[22] D. Jariwala, V. K. Sangwan, L. J. Lauhon, T. J. Marks, and M. C. Hersam, "Emerging Device Applications for Semiconducting Two-Dimensional Transition Metal Dichalcogenides," *ACS Nano*, vol. 8, no. 2, pp. 1102–1120, 2014.

[23] R. Lv *et al.*, "Transition metal dichalcogenides and beyond: Synthesis, properties, and applications of single- and few-layer nanosheets," *Acc. Chem. Res.*, vol. 48, no. 1, pp. 56–64, 2015.

[24] Y.-H. Wang, K.-J. Huang, and X. Wu, "Recent advances in transition-metal dichalcogenides based electrochemical biosensors: A review," *Biosens. Bioelectron.*, vol. 97, no. May, pp. 305–316, 2017.

[25] U. of Cambridge, "DoITPoMS." [Online]. Available: https://www.doitpoms.ac.uk/tlplib/semiconductors/direct.php. [Accessed: 15-Nov-2017].

[26] F. Schwierz, R. Granzner, and J. Pezoldt, "Two-dimensional materials and their prospects in transistor electronics," *Nanoscale*, vol. 7, pp. 8261–8283, 2015.

[27] Q. H. Wang, K. Kalantar-Zadeh, A. Kis, J. N. Coleman, and M. S. Strano,

"Electronics and optoelectronics of two-dimensional transition metal dichalcogenides," *Nat. Nanotechnol.*, vol. 7, no. 11, pp. 699–712, 2012.

[28] N. Response and M. Nanosheet, "Strain Induced Optimization of Nanoelectromechanical Energy Harvesting Article Strain Induced Optimization of Nanoelectromechanical Energy Harvesting and Nanopiezotronic Response in MoS Monolayer Nanosheet," no. September, 2017.

[29] I. Song, C. Park, and H. C. Choi, "Synthesis and properties of molybdenum disulphide: from bulk to atomic layers," *RSC Adv.*, vol. 5, no. 10, pp. 7495–7514, 2015.

[30] H. Zeng, J. Dai, W. Yao, D. Xiao, and X. Cui, "Valley polarization in MoS2 monolayers by optical pumping," *Nat. Nanotechnol.*, vol. 7, no. 8, pp. 490–493, 2012.

[31] T. G. Council, "Two-Dimensional Materials Make 'Valleytronics' Possiblee." [Online]. Available: http://www.thegraphenecouncil.org/?page=Valleytronics. [Accessed: 20-Aug-2017].

[32] W. Wu *et al.*, "High mobility and high on/off ratio field-effect transistors based on chemical vapor deposited single-crystal MoS_2 grains," *Appl. Phys. Lett.*, vol. 102, no. 14, p. 142106, 2013.

[33] Y. Tong, Y. Liu, D. S. H. Chan, J. Thong, and C. Zhu, "MoS2based photosensor detecting both light wavelength and intensity," *Sensors Actuators, A Phys.*, vol. 266, pp. 205–210, 2017.

[34] D. Chimene, D. L. Alge, and A. K. Gaharwar, "Two-Dimensional Nanomaterials for Biomedical Applications: Emerging Trends and Future Prospects," *Adv.*

Mater., vol. 27, no. 45, pp. 7261–7284, 2015.

[35] H. Li *et al.*, “Fabrication of single- and multilayer MoS 2 film-based field-effect transistors for sensing NO at room temperature,” *Small*, vol. 8, no. 1, pp. 63–67, 2012.

[36] J. Sun *et al.*, “Synthesis Methods of Two-Dimensional MoS_2: A Brief Review,” *Crystals*, vol. 7, no. 7, p. 198, 2017.

[37] K. K. Amara, L. Chu, R. Kumar, M. Toh, and G. Eda, “Wet chemical thinning of molybdenum disulfide down to its monolayer,” *APL Mater.*, vol. 2, no. 9, 2014.

[38] C. M, “Photoluminescence from Chemically Exfoliated MoS2,” *Nano Lett.*, vol. 12, no. 12, p. 526, 2012.

[39] M. Ohring, *Materials Science of Thin Films*, 2nd ed. Academic Press, 2002.

[40] I. Bilgin *et al.*, “Chemical Vapor Deposition Synthesized Atomically Thin Molybdenum Disulfide with Optoelectronic-Grade Crystalline Quality,” *ACS Nano*, vol. 9, no. 9, pp. 8822–8832, 2015.

[41] D. Zhou, H. Shu, C. Hu, L. Jiang, P. Liang, and X. Chen, “Unveiling the Growth Mechanism of MoS2with Chemical Vapor Deposition: From Two-Dimensional Planar Nucleation to Self-Seeding Nucleation,” *Cryst. Growth Des.*, vol. 18, no. 2, pp. 1012–1019, 2018.

[42] S. J. Kim *et al.*, “Large-scale Growth and Simultaneous Doping of Molybdenum Disulfide Nanosheets,” *Sci. Rep.*, vol. 6, no. October 2015, pp. 24054–60, 2016.

[43] Y. H. Lee *et al.*, “Synthesis of large-area MoS 2 atomic layers with chemical vapor deposition,” *Adv. Mater.*, vol. 24, no. 17, pp. 2320–2325, 2012.

[44] X. Ling *et al.*, “Role of the seeding promoter in MoS2 growth by chemical vapor

deposition," *Nano Lett.*, vol. 14, no. 2, pp. 464–472, 2014.

[45] W. Chen *et al.*, "Oxygen-Assisted Chemical Vapor Deposition Growth of Large Single-Crystal and High-Quality Monolayer MoS2," *J. Am. Chem. Soc.*, vol. 137, no. 50, pp. 15632–15635, 2015.

[46] S. Inguva, J. Cai, C. Hu, J. Wu, Y. Lu, and X. Liu, "Effect of substrate angle on the growth of MoS 2 vertical nanosheets using a one-step chemical vapor deposition Effect of substrate angle on the growth of MoS 2 vertical nanosheets using a one-step chemical vapor deposition."

[47] W. Wang *et al.*, "Effect of Mo concentration on shape and size of monolayer MoS_2 crystals by chemical vapor deposition," *J. Phys. D. Appl. Phys.*, vol. 50, no. 39, p. 395501, 2017.

[48] X. Wang, Y. P. Zhang, and Z. Q. Chen, "Effect of MoO_3 constituents on the growth of MoS_2 nanosheets by chemical vapor deposition," *Mater. Res. Express*, vol. 3, no. 6, p. 065014, 2016.

[49] W. Wang *et al.*, "Investigation of the Growth Process of Continuous Monolayer MoS2 Films Prepared by Chemical Vapor Deposition," *J. Electron. Mater.*, vol. 47, no. 9, pp. 5509–5517, 2018.

[50] X. Wang, H. Feng, Y. Wu, and L. Jiao, "Controlled Synthesis of Highly Crystalline MoS 2 Flakes by Chemical Vapor Deposition," *J. Am. Chem. Soc.*, vol. 135, no. 14, pp. 5304–5307, 2013.

[51] A. Zafar *et al.*, "Probing the intrinsic optical quality of CVD grown MoS2," *Nano Res.*, vol. 10, no. 5, pp. 1608–1617, 2017.

[52] W. Zheng, Y. Qiu, W. Feng, J. Chen, and H. Yang, "Controlled growth of six-

point stars MoS 2 by chemical vapor deposition and its shape evolution mechanism," 2017.

[53] D. Dumcenco, D. Ovchinnikov, K. Marinov, O. Lopez-sanchez, A. Radenovic, and A. Kis, "Large - area Epitaxial Monolayer MoS 2," pp. 1–11.

[54] S. Guo, A. Arab, S. Krylyuk, A. V. Davydov, and M. E. Zaghloul, "Fabrication and characterization of humidity sensors based on CVD grown MoS<inf>2</inf>thin film," *2017 IEEE 17th Int. Conf. Nanotechnology, NANO 2017*, pp. 164–167, 2017.

[55] M. Wen, J. P. Xu, L. Liu, X. Zhao, P. T. Lai, and W. M. Tang, "Fabrication and electrical performance of CVD-grown MoS 2 transistor," pp. 3–5.

[56] S. Wang, X. Wang, and J. H. Warner, "All Chemical Vapor Deposition Growth of MoS 2 : h-BN Vertical van der Waals Heterostructures," *ACS Nano*, vol. 9, no. 5, pp. 5246–5254, 2015.

[57] L. Samad *et al.*, "Layer-Controlled Chemical Vapor Deposition Growth of MoS2 Vertical Heterostructures via van der Waals Epitaxy," *ACS Nano*, vol. 10, no. 7, pp. 7039–7046, 2016.

[58] "Lindberg/Blue M^{TM} Mini-Mite^{TM} Tube Furnaces," *ThermoFisher Scientific*. [Online]. Available: https://www.thermofisher.com/order/catalog/product/TF55035C-1?SID=srch-srp-TF55035C-1.

[59] S. D. Sheet, "SIGMA-ALDRICH," pp. 1–8, 2018.

[60] "Vapor Pressure Chart," *Luxel*. [Online]. Available: https://luxel.com/wp-content/uploads/2013/04/Luxel-Vapor-Pressure-Chart.pdf.

[61] "PTAS (Solid)," *2D Semiconductors*. [Online]. Available: https://www.2dsemiconductors.com/perylenae-3-4-9-10-tetracarboxylic-acid-tetrapotassium-salt-ptas/.

[62] P. K. Sahoo, S. Soltani, A. K. C. Wong, and Y. C. Chen, "A Survey of Thresholding," *Comput. Vision, Graph. Image Process.*, vol. 41, pp. 233–260, 1988.

[63] B. Schrader and D. B. . . . [et al. . Contributors, *Infrared and Raman spectroscopy : methods and applications*. Weinheim ; New York: VCH, 1995.

[64] H. Li *et al.*, "From bulk to monolayer MoS 2: Evolution of Raman scattering," *Adv. Funct. Mater.*, vol. 22, no. 7, pp. 1385–1390, 2012.

[65] M. Ye, D. Winslow, D. Zhang, R. Pandey, and Y. K. Yap, "Recent Advancement on the Optical Properties of Two-Dimensional Molybdenum Disulfide (MoS2) Thin Films," pp. 288–307, 2015.